THE UNIVERSITY OF MICHIGAN

INDUSTRY PROGRAM OF THE COLLEGE OF ENGINEERING

AN EXPERIMENTAL STUDY OF SWITCHING IN A BISTABLE FLUID AMPLIFIER

Sudhir D. Savkar

A dissertation submitted in partial fulfillment
of the requirements for the degree of
Doctor of Philosophy in the
University of Michigan
Department of Mechanical Engineering
1966

December, 1966

IP-764

ACKNOWLEDGMENTS

The author is very appreciative of the following gentlemen who served on his doctoral committee:

Professor Arthur G. Hansen (Former Chairman)
Associate Professor Robert B. Keller (Chairman)
Assistant Professor Poul S. Larsen
Assistant Professor Ward O. Winer
Associate Professor Wen J. Yang
Professor Vi-Cheng Liu

In particular gratitude is extended to Professors Hansen, Keller and Larsen for their encouragement, assistance and patient understanding throughout the period of research and writing.

Sincere thanks are extended to Mr. Ronald Lane who constructed a major portion of the experimental apparatus and Messrs Bruce Pomeroy, John Tichy, and Richard Klein who assisted in taking data.

The financial assistance of the National Science Foundation to the project under which this research was conducted is gratefully acknowledged.

Finally the author wishes to thank his wife, Leela, who was a constant source of encouragement through all his trying moments.

TABLE OF CONTENTS

TABLE OF CONTENTS (CONT'D)

LIST OF FIGURES

LIST OF FIGURES (CONT'D)

LIST OF FIGURES (CONT'D)

LIST OF FIGURES (CONT'D)

NOMENCLATURE

b_c in.	Control Nozzle Width
b_s in.	Main jet nozzle width
C	A constant
D	A constant
D in.	Offset
E	The Eüler number $\left(\begin{matrix}\text{ratio of control} \\ \text{to main jet momentum,}\end{matrix} \quad \frac{\rho A_c U_c^2}{\rho A_s U_s^2}\right)$
J $\frac{\text{lbm.ft.}}{\text{sec}^2}$	The jet momentum
K	A constant
l_b in.	Setback
l_s in.	Splitter location
l_w in.	Distance from the main nozzle to the angled walls of the bistable fluid amplifier
L ft.	A reference length to be specified
Q_c gpm	Control jet flow rate
Q_e gpm	Flow rate of the fluid entrained from the separation bubble by the main jet
Q_n gpm	Differential flow rate into the separation bubble
Q_r gpm	Flow rate of the fluid returned to the separation bubble from the reattachment point
Q_s gpm	Main jet flow rate
P_∞ psi	Ambient pressure
P_c psi	Control jet plenum pressure
P_s psi	Main jet plenum pressure
R	Reynolds number defined as $\rho Q/t\mu$
R ft.	Radius of curvature of the axis of the curved jet
R_T ohms	Electrical resistance
t in.	Depth of the amplifier model

T °F	Temperature
T sec.	Transport time
U_c ft/sec	Average control jet velocity
U_s ft/sec	Average main jet velocity
U_{ref} ft/sec	Reference velocity to be specified
u ft/sec	Axial velocity component in the free jet
v ft/sec	Transverse velocity component in the free jet
w ft/sec	Transformed axial velocity component in the curved jet
ΔV m-ft.	Change in the volume of the separation bubble
X_R inches	Reattachment distance from the main nozzle
α °F^{-1}	Temperature coefficient of resistivity
σ	A free parameter used in jet analysis
Θ	Angle contained by the vertex of the splitter
ρ lbm/cu ft	Density of water
τ_1 sec	Minimum pulse to switch
τ_a sec	Maximum switching time
τ_b sec	Minimum switching time
τ_1^*	Non-dimensionalized minimum pulse to switch
τ_a^*	Non-dimensionalized maximum switching time
τ_b^*	Non-dimensionalized minimum switching time
μ $\frac{\text{lbf.sec}}{\text{ft}^2}$	Viscosity
μ_Q	Dynamic flow gain defined as the ratio of the main jet to control jet flow rate
$\mu_{Q_{max}}$	Maximum dynamic flow gain
ν ft^2/sec	Kinematic viscosity
ϵ ft^2/sec	Turbulent kinematic viscosity
ψ	Stream function

CHAPTER I

INTRODUCTION

Following the announcement by Diamond Ordinance Fuse Laboratory of the United States Army (now known as Harry Diamond Laboratories, (HDL)) in 1960 of their turbulent reattachment fluid amplifier, considerable interest was aroused among various university and industrial research groups in the "Coanda effect" and "pure fluid amplifiers". The Coanda effect is named after Henri Coanda, a Rumanian engineer who, in 1933, first made use of the effect in several inventions after accidently discovering the effect while experimenting with an early model jet engine. In practice there are several different versions of "pure fluid amplifiers", that is, devices utilizing only fluid elements without any mechanical parts, each performing a different type of function. The most common units are the wall reattachment, proportional, and vortex amplifiers, although only the first of these really makes use of the Coanda effect.

A common illustration of the Coanda effect is seen when a stream of water from a tap played on a finger adheres to the finger and is effectively deflected in a direction different from the original. This deflection results from the curvature of the streamlines and the resulting transverse pressure gradient. This is illustrated schematically in Figure 1.

A simple explanation of the Coanda effect is as follows: When a (turbulent) jet is ejected near an offset wall, the jet entrains fluid from either side of the jet (Figures 2a, 2b), but due to the constriction effect of the side wall the pressure on that side drops slightly

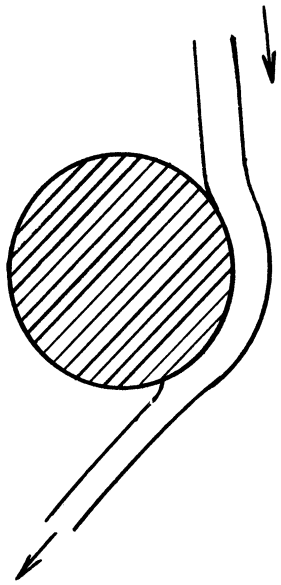

Figure 1. Deflection of a Jet by an Obstacle.

through the acceleration of the fluid contained between the wall and the jet. Thus, the resulting pressure differential induces the jet to curve towards the wall causing further reduction in pressure. This process continues until the jet attaches to the wall, forming a trapped pocket of fluid, with the state of equilibrium reached when both the curvature of the jet is sufficient to balance the pressure differential and the fluid returned to the pocket, called the separation bubble, is equal to that absorbed by the jet on the pocket side of the jet. Thus the Coanda effect is primarily a geometric effect.

The wall reattachment fluid amplifier (or the bistable flip-flop unit) is therefore a (turbulent) jet confined within a geometry not unlike that illustrated in Figure 3 . The jet, due to the Coanda effect, attaches to one or another wall, the stable mode of the jet then being attached to one of the two walls. The jet may be disturbed from one given stable mode (on one wall) to the other (on the opposite wall)

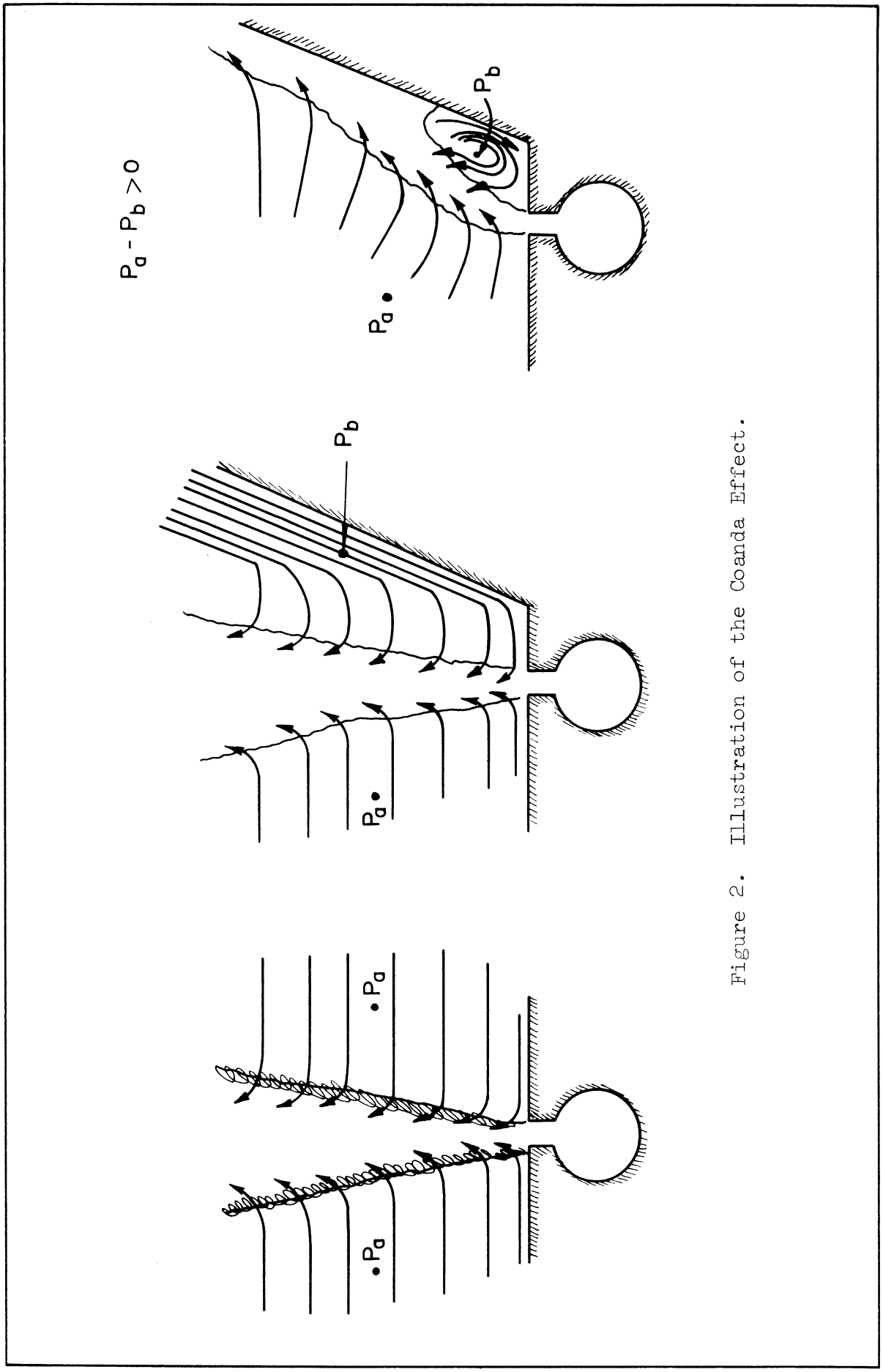

Figure 2. Illustration of the Coanda Effect.

by the application of a proper control signal, in our case this is simply accomplished by a second jet acting at right angles to the axis of the main jet. The notion of amplification then being served by the fact that in terms of either flow rates or total pressures the ratio of control signal strength to the main jet strength is less than one.

In the "momentum exchange" or "proportional fluid amplifier", as depicted in Figure 4, the deflection of the main jet is proportional to the momentum differential of the relatively weaker control jets, the output signal down a given channel being proportional then to the deflection. In this type of unit, the wall effects, which give rise to the Coanda attachment, are minimized. As a result of its relative simplicity, most of the analytical progress is associated with the proportional fluid amplifiers. In other areas of fluid devices mathematical analysis has resulted in very little that is conclusive.

1. Literature Survey

a. Review of the Static Characteristics

The first successful analysis of the Coanda effect is that due to Bourque and Newman.[7] Their initial analysis dealt with the offset parallel wall as shown in Figure 5.

The analysis assumed a turbulent, incompressible jet with the following additional assumptions:

1. The pressure in the separation bubble is constant.
2. Centerline of the jet is a circular arc up to the point of reattachment.
3. The velocity distribution is the same as that in a free jet, as per Goertler's analysis (See Reference 1, p. 605).
4. Shear force due to the wall is neglected.

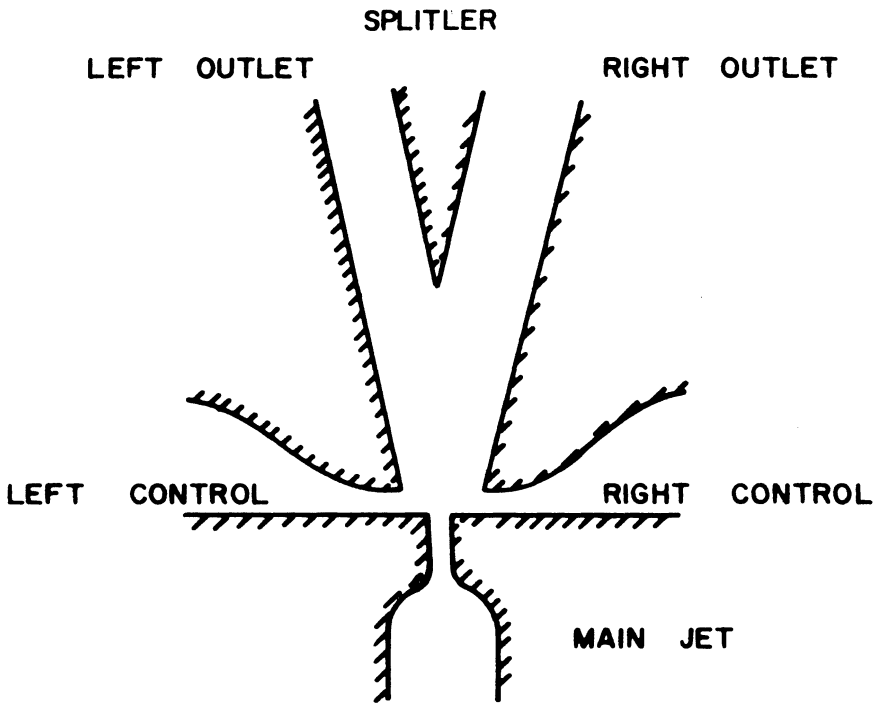

Figure 3. Schematic of a Bistable Fluid Amplifier

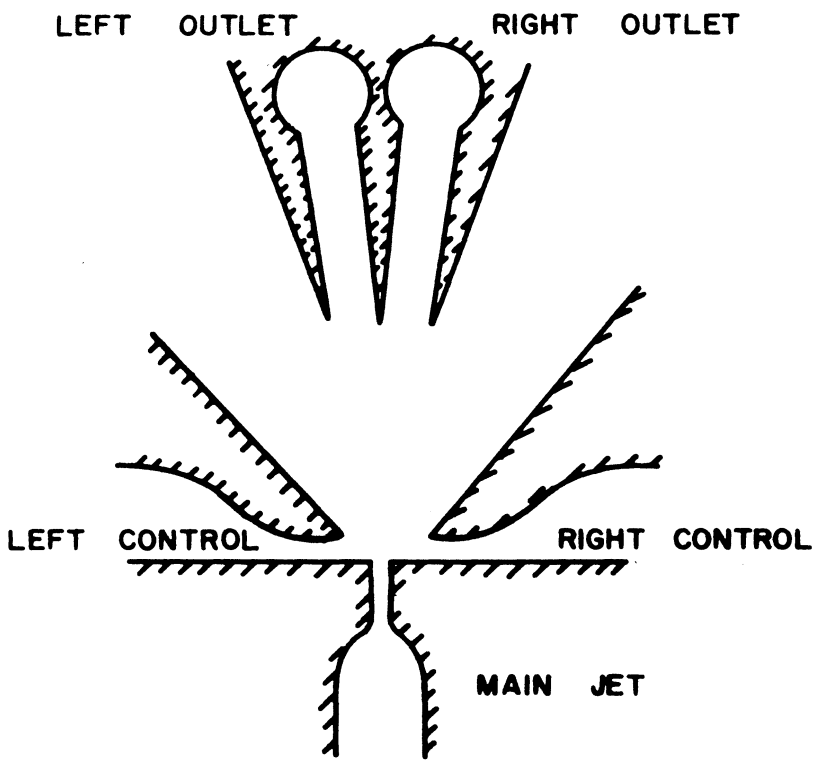

Figure 4. Schematic of a Proportional Fluid Amplifier.

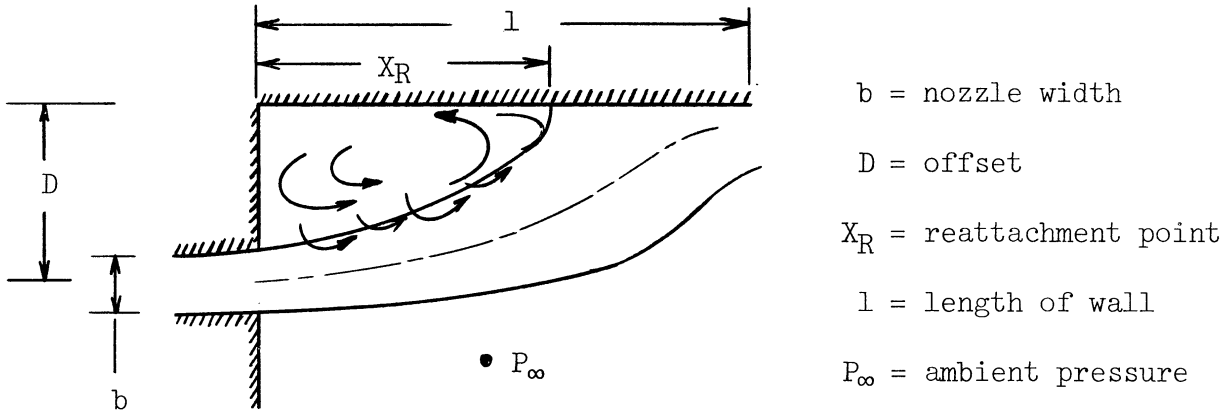

Figure 5. Mathematical Model for Reattachment to an Offset Parallel Wall.

The resulting theory, although based on a grossly simplified analysis involving the momentum balance of the flows in a direction parallel to the wall at the point of reattachment, gave a good representation of the experimental data. The analysis predicted and the experiments verified the functional relationship:

$$X_R/b = f(D/b)$$

That is to say, that the reattachment distance is essentially independent of Reynolds number of the jet. These results are given in Figure 6. Bourque and Newman also used the same approach to an angled plate, with no offset, but the correlation with experiments was less satisfactory.

An improved version of Bourque and Newman's work was detailed by Sawyer,[9] who took into account the variation in entrainment rate with curvature and reported an improved correlation of his theory with the experimental results of Bourque and Newman. Sawyer's results are shown in Figure 7. Further effort along the same lines is represented by the

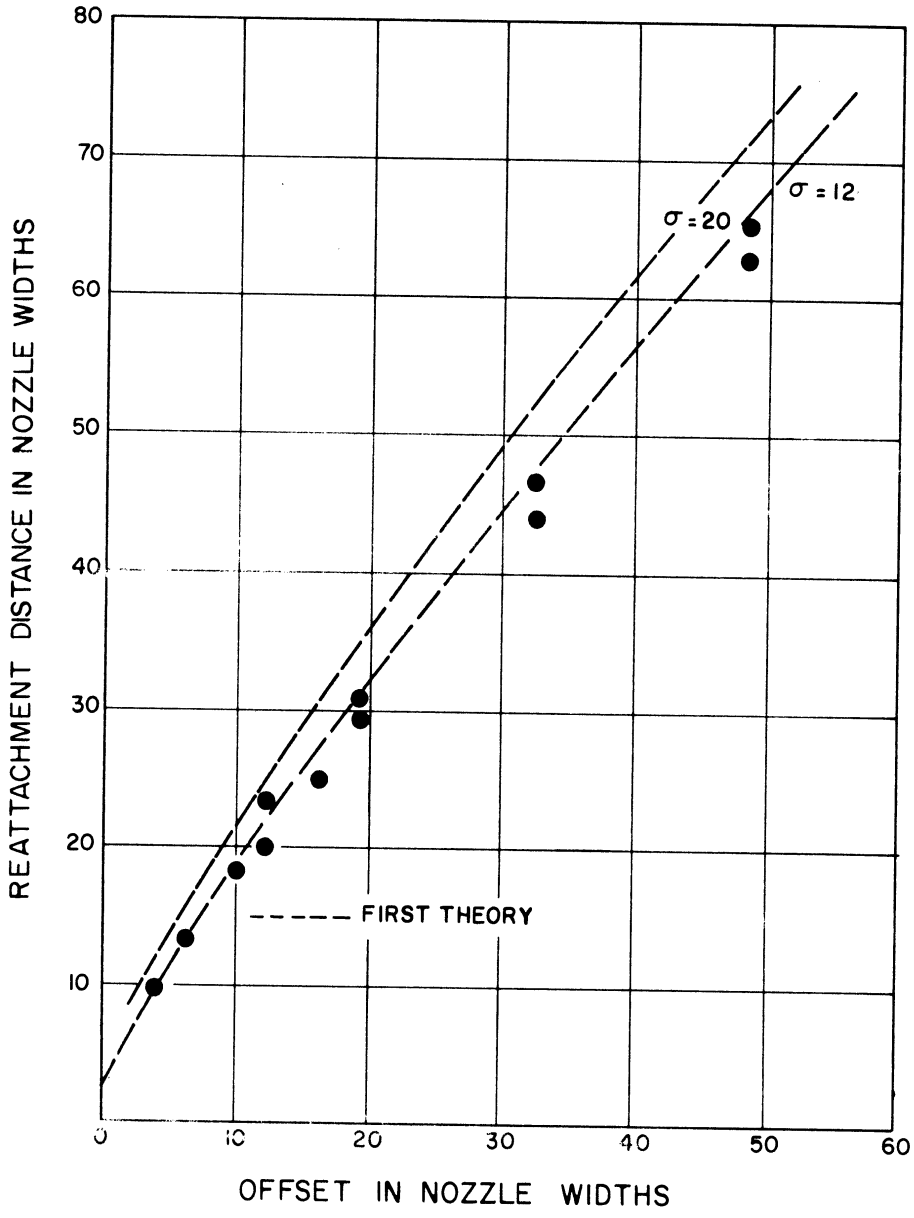

Figure 6. Reattachment Distance for the Offset Parallel Plate. (From Reference 7)

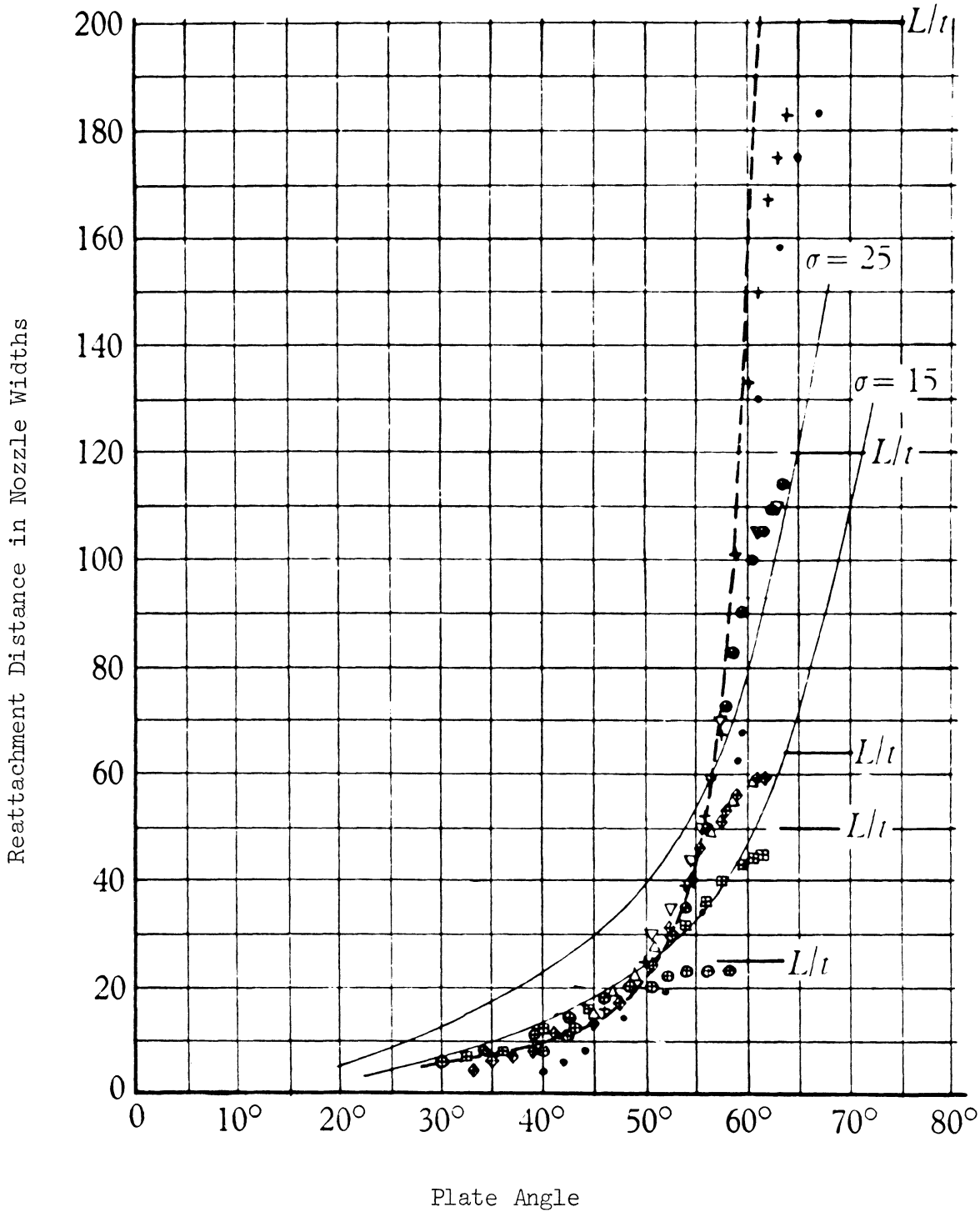

Figure 7. Comparison of Sawyer's Theory (broken line) With Theoretical (Solid lined) and Experimental Results of Bourque and Newman. (From Reference 9)

papers of Sher,[22] Levin and Manion[13] (See Figure 8), who dealt with the case of the offset inclined wall, and Brown[14] who included the effects of control flow on the attachment point location.

After these, what may be termed as more fundamental studies, the work became more directly oriented towards the fluid amplifier and the investigators began defining and studying the effects of various parameters on the static characteristics. Comparin, et.al.[20] in their extensive study of the effects of geometry indicate the existence of a minimum Reynolds number (defined with respect to the nozzle width and average nozzle velocity), for attachment in a given configuration, below which the jet does not "attach". This critical Reynolds number they found was related to the aspect ratio of the main nozzle (ratio of the depth of the nozzle to the width of the nozzle) and surface roughness of the elements and may therefore be taken as indicating the effect of the boundary layer. Their studies indicate that for aspect ratios three and greater the critical Reynold's number does not change greatly, allowing a criterion to experimentally reduce the three-dimensional effects to a minimum. Also presented are some arguments relating flow gain to pressure gains with Strouhal number (based on main nozzle velocity and width) as a parameter. This would be of use in interpreting data which presents say only the flow gain data. Their results are given in Figures 9 and 10. Figure 11 summarizes some qualitative observations of the effects of geometry as compiled by Warren.[16]

b. Review of Available Dynamic Results

While the static characteristics of the fluid amplifiers have been extensively studied, as the selected references above indicate, the

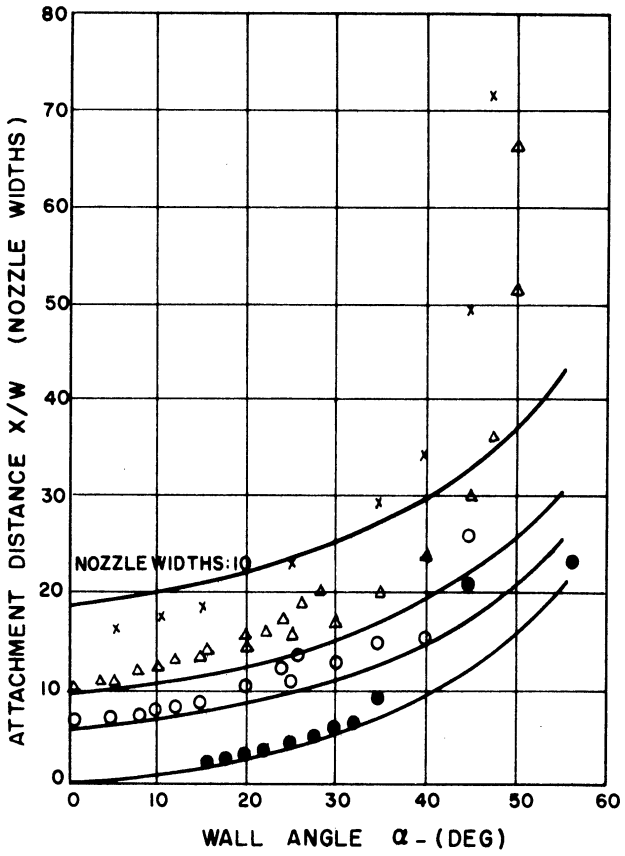

Figure 8. Attachment to an Offset Angled Wall. (From Reference 13)

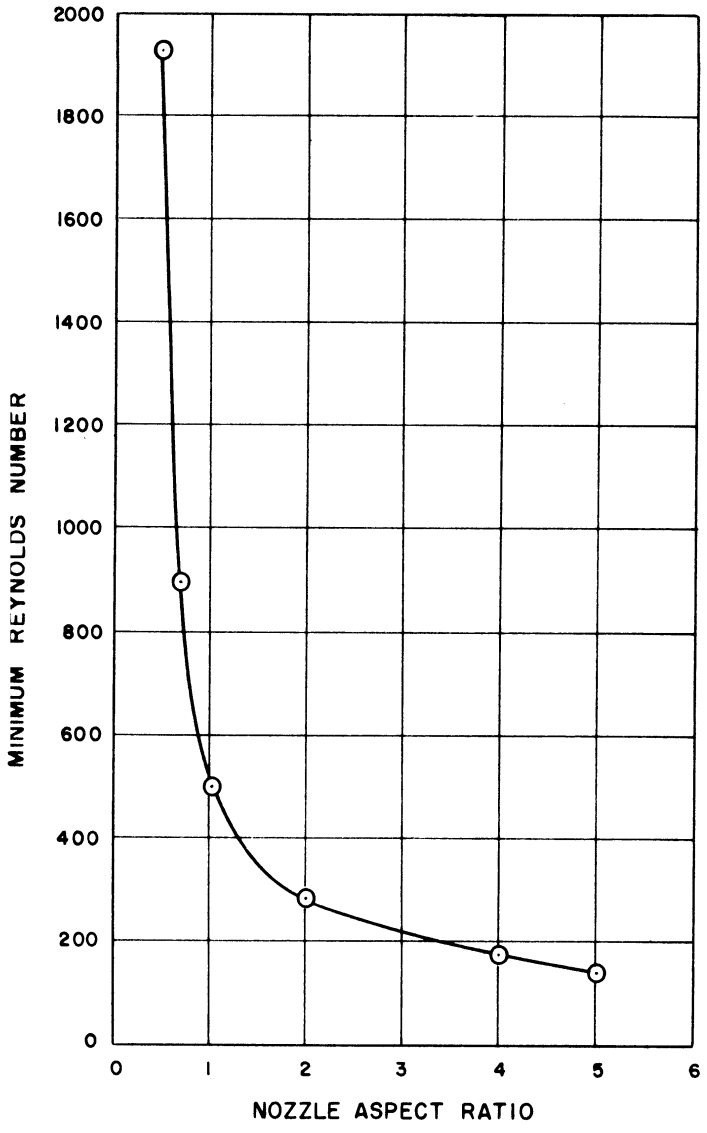

Figure 9. Variation of Minimum Reynolds Number with Nozzle Aspect Ratio for a Double Sided Element. (From Reference 15)

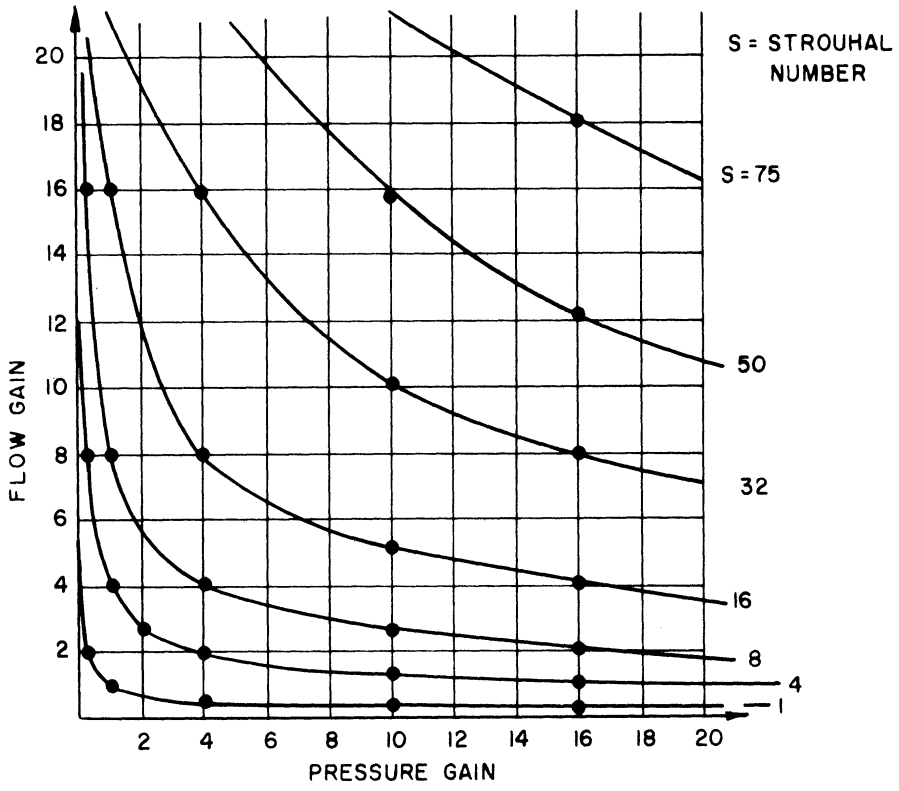

Figure 10. Relationship Between Pressure Gain (μ_P) and Flow Gain (μ_Q) with Strouhal Number as Parameter. (From Reference 20)

Muller[8,19] conducted several studies into the switching of fluid amplifiers and concluded that the total response time is not significantly increased when the control pulse is shortened and further that the control pulse is independent of the wall length. Muller's studies use a mathematical model for prediction of the time "to release" the separation bubble using essentially the principle of conservation of mass. This model is unsatisfactory since it is based only on continuity and the transient interaction of the momentum of the two jets is handled empirically. Yet, this interaction of the jets plays an important role in the switching and is also very difficult to analyze. Portions of Muller's results are indicated in Figures 12 and 13.

Olson and Stoeffler[12] studied both analytically and experimentally what may be termed as the response of the reattachment location in a bistable fluid amplifier to a step change in control flow at a level below the critical value required to complete switching (that is the jet does not flip over to the opposite wall). Their analysis was based on a quasi-steady flow model for the separation bubble which has similar to that proposed by Korst[26] for the calculation of two-dimensional base pressures with a base bleed. Poor agreement was achieved between their theory and experiment. The reason given for this poor agreement was the fallacy of the assumption that the jet spread in the device was the same as that in a free jet in view of the finite velocities in the separation bubble. Their experiments revealed the following:

1. The plate angle increases the effectiveness of the control flow as the angle is increased.

2. The separation bubble pressures at first increase and then decrease as the control flow is increased beyond a certain limiting value.

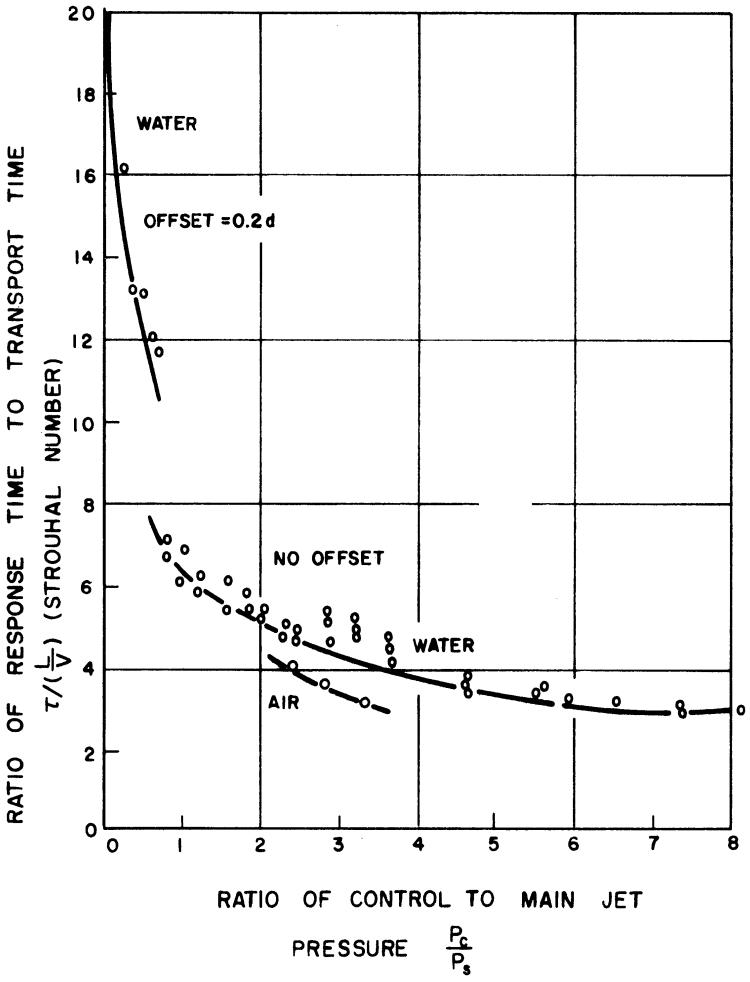

Figure 12. Variation of Response Time with Control Pressure. (From Reference 8)

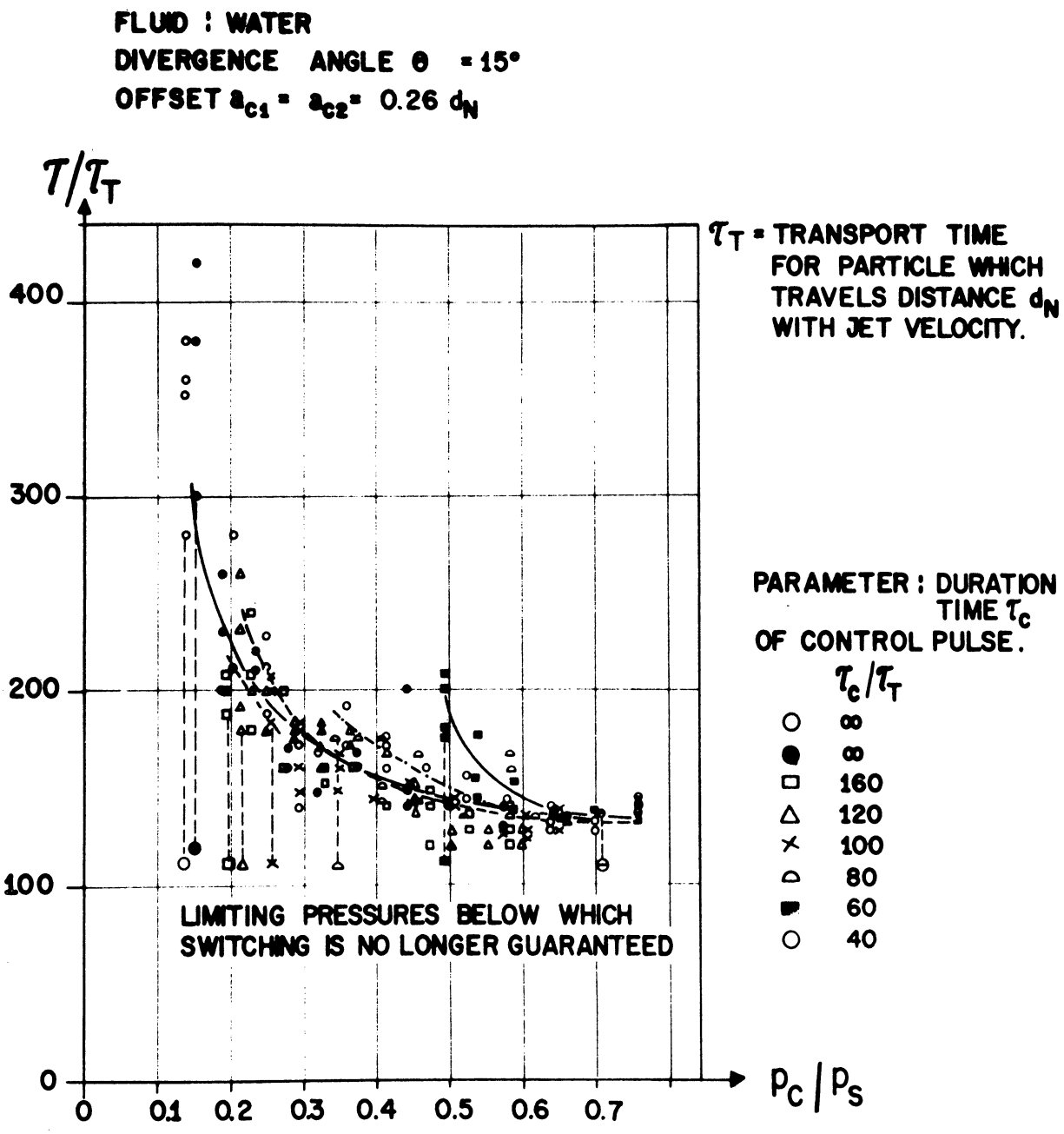

Figure 13. Response Time Versus Control Supply Pressure. (From Reference 19)

3. The control flow "effectiveness" increases as the offset is decreased.

It should be mentioned that Olson and Stoeffler worked with air in the range of Mach numbers from 0.66 to 1.5 and observed that at the higher Mach number the behavior of the separation bubble is different from the lower Mach number.

Johnston[17] conducted studies into the switching mechanism of a bistable fluid amplifier without a splitter and concluded that Strouhal number was relatively independent of changes in the main jet Reynolds number. His definition of the Strouhal number was based on the average velocity of the main jet at the nozzle exit and the width of the nozzle. Johnston further concluded from a "top injection" fluid amplifier, where the control pulse was introduced in a direction perpendicular to the plane of the fluid amplifier, that the primary switching mechanism is that due to the mass flow rate, a conclusion contrary to that of Keto. Also, Johnston developed a separation time model based on the continuity equation which yielded good correlation with experiment (See Appendix D). It should be noted however, that the mathematical model used required two experimentally determined constants, while the experimental model was one sided, lacked a splitter, and a definite separation of the main jet occurred due to the relatively short length of the wall. These features do not describe a true operational bistable or flip-flop device.

Katz, et.al.[18] studied the switching times of two configurations of bistable fluid elements at various main and control jet pressures. The units differed mainly in the ratio of control to main jet nozzle widths, having values 1 and 0.67. For a given ratio of control to main jet pressures switching times were longer for the smaller control orifice

and they assigned the difference to the relatively smaller size of the control orifice. It was concluded, from the data, that switching is due to momentum interaction of the control and main jets. Their results showed a very large spread in the data and also identical tests sometimes produced results that differed by as much as a factor of two. This inconsistency was attributed to the difficulty of reading the pressure transducer output signal.

Several other papers which describe the transient phenomena in a bistable fluid amplifier are those of Hrubecky,[21] Harvey[32] and Sarpkaya.[31] Sarpkaya's paper is perhaps the most informative in that the importance of the role played by the vortices in the fluid amplifier through the interpretation of photographic and pressure data is clearly presented. The experimental model used a splitter cusp to aid in producing an accentuated recirculation vortex.

2. Scope and Objectives of this Study

There are two major problems in the area of dynamics of fluid amplifiers. The first problem involves the dynamic behavior of a given fluidic component. The second is the dynamic behavior of a system built up from several fluidic components. The progress in the second problem, both on the theoretical plane and in the art of synthesizing circuits from component units, although considerable, is hampered by insufficient knowledge of the dynamic behavior of the fluidic components. So far, most of the work in synthesis has tried to build up on the steady state characteristics or by adaptations based on the transmission line theory as represented by the papers of Brown[25] and Belsterling.[38] The method based on steady

state characteristics is inadequate when the dynamics of the situation are involved as pointed out by Muller[8] and Kirshner[37] and the systems approach is as yet in its early stages of development (Brown[25]). Moreover the systems approach, as mentioned earlier, depends heavily on the available data on the dynamics of the components to generate the required transfer functions. Therefore, there is, as seen by the brief survey in the section (b) of the Literature Survey and as brought out in the survey paper by Kirshner,[37] a considerable need to conduct parametric studies into switching performance of fluid amplifiers.

The aim of this study is to shed some further insight into the mechanism of switching in a bistable fluid amplifier by conducting a systematic experimental study of switching and the effect of varying a given set of geometric parameters. The geometric parameters involved in a bistable fluid amplifier are numerous and may be deduced both by the inspection of a typical geometric layout of the amplifier and by reference to the studies of Muller,[8,19] Warren,[16] Comparin[20] and Kirshner.[37] Kirshner in his paper details a complete list of parameters involved in a bistable fluid amplifier. The parameters are:

1. Location, size and shape of control nozzles and the angle they make with the main jet.
2. Offset
3. Angle, and/or curvature of the walls
4. Location and shape of the splitter (with and without a cusp)
5. Location, shape, size and angle of bleeds
6. Aspect ratio
7. Size of device

8. Effect of loading

9. Various combinations of the above parameters.

Within the scope of this study is to be included a comparative parametric study of switching under no load conditions; the following are the parameters to be included in this study:

1. Ratio of control to main nozzle area, as this would isolate the effects of mass flow rate from momentum.

2. The setback

3. The offset

4. Location of the splitter

5. The effect of changing scales.

These parameters are diagramatically defined in Figure 14.

Additionally, the study presents some results of qualitative photographic studies together with an analysis of the steady, incompressible, curved jet included with the appendix, as the theory presented was not experimentally verified.

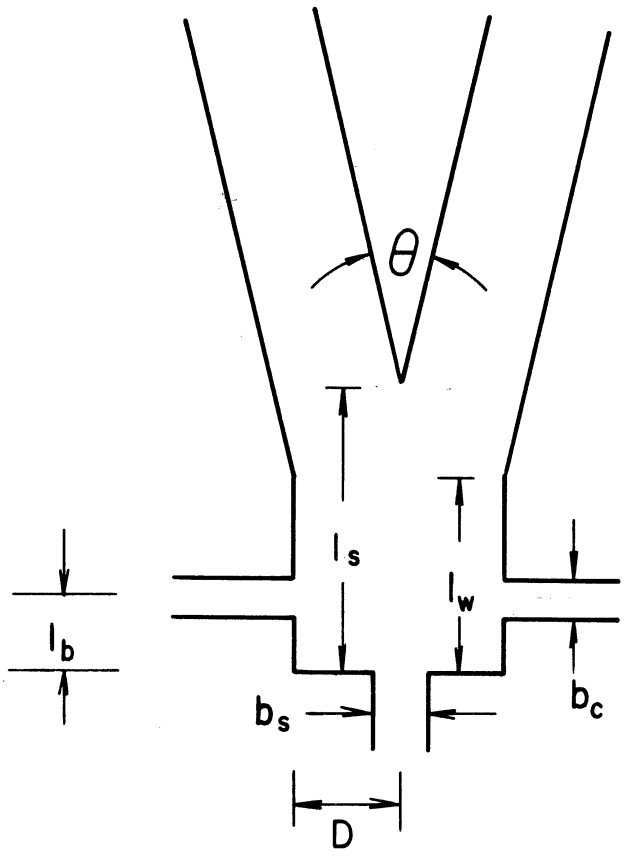

Figure 14. Schematic Arrangement of the Amplifier Used in this Study.

b_s - Main Nozzle Width

b_c - Control Nozzle Width

l_b - Setback

l_s - Splitter Location

l_w - Distance to Angled Wall

D - Offset

Θ - Splitter Angle

CHAPTER II

EXPERIMENTAL EQUIPMENT

The experimental equipment consisted of a water tunnel with plenum chambers, nozzles and ducting to simulate a bistable fluid amplifier, instrumentation to measure flow rates into the various nozzles and a thermistor probe to sense the location of the jet, together with supporting devices. Dye injection and flow tracer equipment was also incorporated.

1. The Water Tunnel and the Amplifier Model

The chief reasons for modeling the amplifier in large scale in a water tunnel were: (a) to slow the whole switching process down to a point where complete switches could be identified and switching times easily measured, (b) to be able to conduct visual studies under conditions as nearly identical to the measurements as possible, (c) to reduce to a minimum the effects of wall boundary layers and roughness of the walls of the element.

The water tunnel was constructed of aluminum with a useful test section of dimensions 15 inches wide by 26 inches long by 3 inches deep. The top and bottom cover plates of the test section were made of plexiglas to allow visual and photographic observation. The plates were held in place by means of "C" clamps and one inch square steel load distribution bars which clamped down the edges of the plates uniformly through aluminum pressure pads, the load being transferred to the pads by means of 1/8 inch set screws dispersed at one inch interval around the edges of both plates. This arrangement had the advantages of

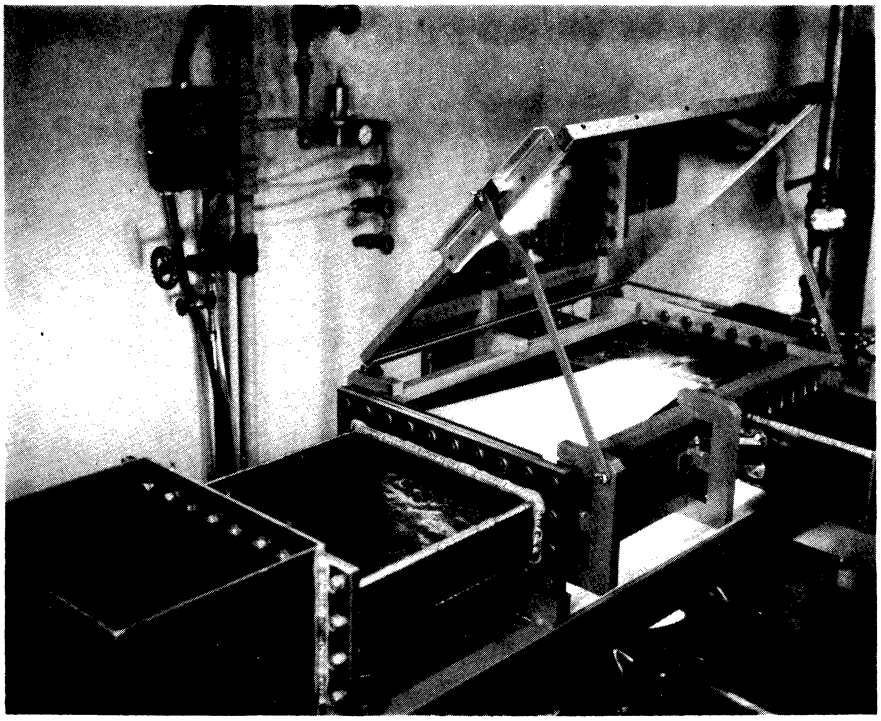

Figure 15. A View of the Water Tunnel, Test Section, Downstream Plenum and Front Silvered Mirror.

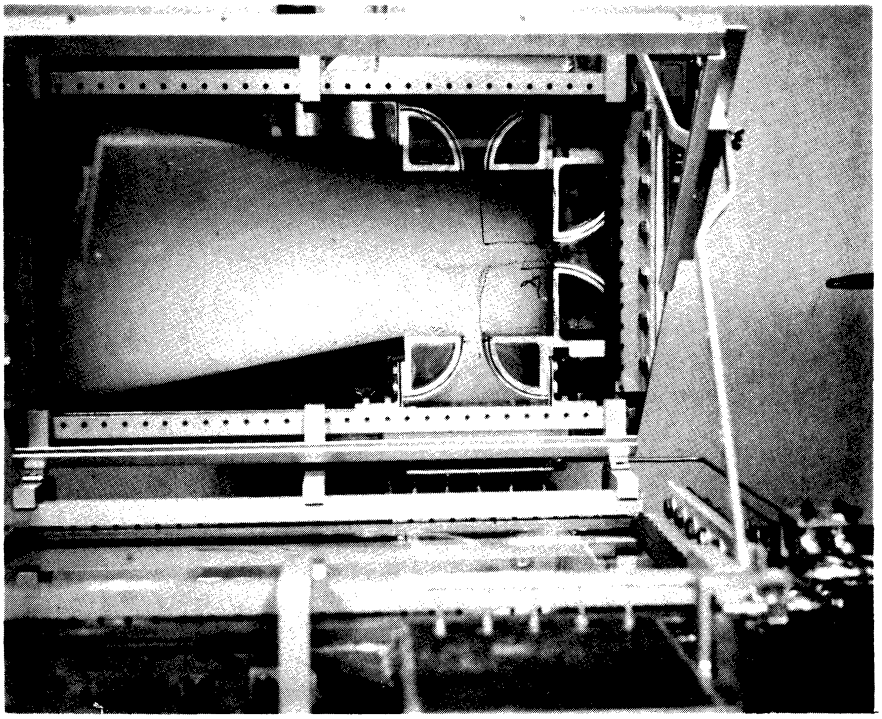

Figure 16. A View of the Test Section Through the Front Silvered Mirror Showing a Configuration of the Fluid Amplifier Studied.

being both leakproof as well as affording the ease of removal of the top and/or the bottom plate. The amplifier was modeled within the tunnel, the nozzles of which were made in the shape of quarter arcs of circles with radius of 4 inches for the main nozzle and 3 inches radius for one of the two instrumented control nozzles. These two nozzles were supplied with water from individual constant head tanks through plenum chambers of 11 1/2" x 9 1/2" x 3" . The water for the plenum chambers was brought in by brass tubing of 1.5 inches internal diameter, the flow then being evenly distributed by an arrangement of perforated plates and screens as follows: Two perforated plates 1/8" thick with 1/8" holes and 3/16" spacing giving 40% open area. These were used to distribute the flow. The plates were followed by three successive sets of two screens each with the first set of 16 mesh, 0.018" diameter wire cloth 51% open, second set of 24 mesh, 0.014" diameter wire cloth, 41% open area, and the third set of 50 mesh, 0.009" diameter wire cloth, 30% open area. The screens served to reduce the scale of turbulence entering the nozzle so that its effect on the mixing action of the interacting jets could be minimized. With the arrangement described it is estimated, using the relation of Dryden and Schubauer as reported by Pope,[35] that under the most adverse conditions the ratio of the level of turbulence after the last screen as compared to the level before the first screen is less than 1/40. A low turbulence level is further insured by a maximum velocity of less than 0.2 ft/sec in the plenum chamber. The turbulence level was checked operationally by observing the smoothness of dye traces through the nozzle section for the range of nozzle velocities used.

A second control nozzle was provided opposite the first but without a plenum chamber and was supplied by a 3/4" I.D. flexible tubing from the city water supply controlled by a hand operated valve. The distribution of the fluid in this nozzle was accomplished by means of a splash plate and two perforated plates. The primary function of this jet was to return the main jet to the other side.

The remaining portions of the fluid amplifier, the side walls and splitter were largely fashioned out of 1/2" thick plexiglas painted over in flat black paint except for narrow slits of 1/2" used for tracer photography to be described below. Amplifier geometry changes could be readily accomplished by replacing the plastic parts.

At the downstream end of the tunnel was a plenum chamber with a discharge tube capable of maintaining about a one inch head of water depending on the flow rate.

Since the transient phenomena of switching were to be measured using the best experimentally available square wave pulse, it was desirable to reduce to a minimum the effects of the transient flows within the piping, plenum chamber, nozzle and the turbine meter. In order to do this, a continuous flow system was devised whereby the flow transient was allowed to affect only a short length of piping. To do this, the water from the head tank, after passing through the set of coarse and fine rotameters was brought to a T junction with two ASCO quick acting 3/4 inch solenoid valves (See Figures 17 and 18) one of which, acting as a bypass to the control nozzle, always remained open until it was required to introduce a pulse of fluid into the control nozzle, when, by using a single pole double throw microswitch the bypass was closed and the valve connecting

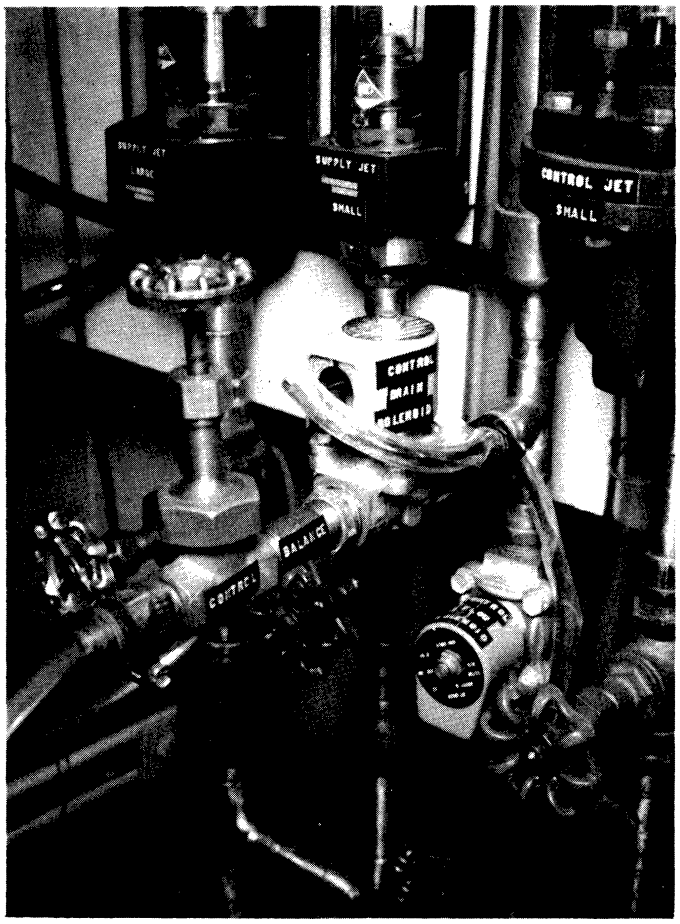

Figure 17. A View of the Continuous Flow System and the Control Balance Resistance.

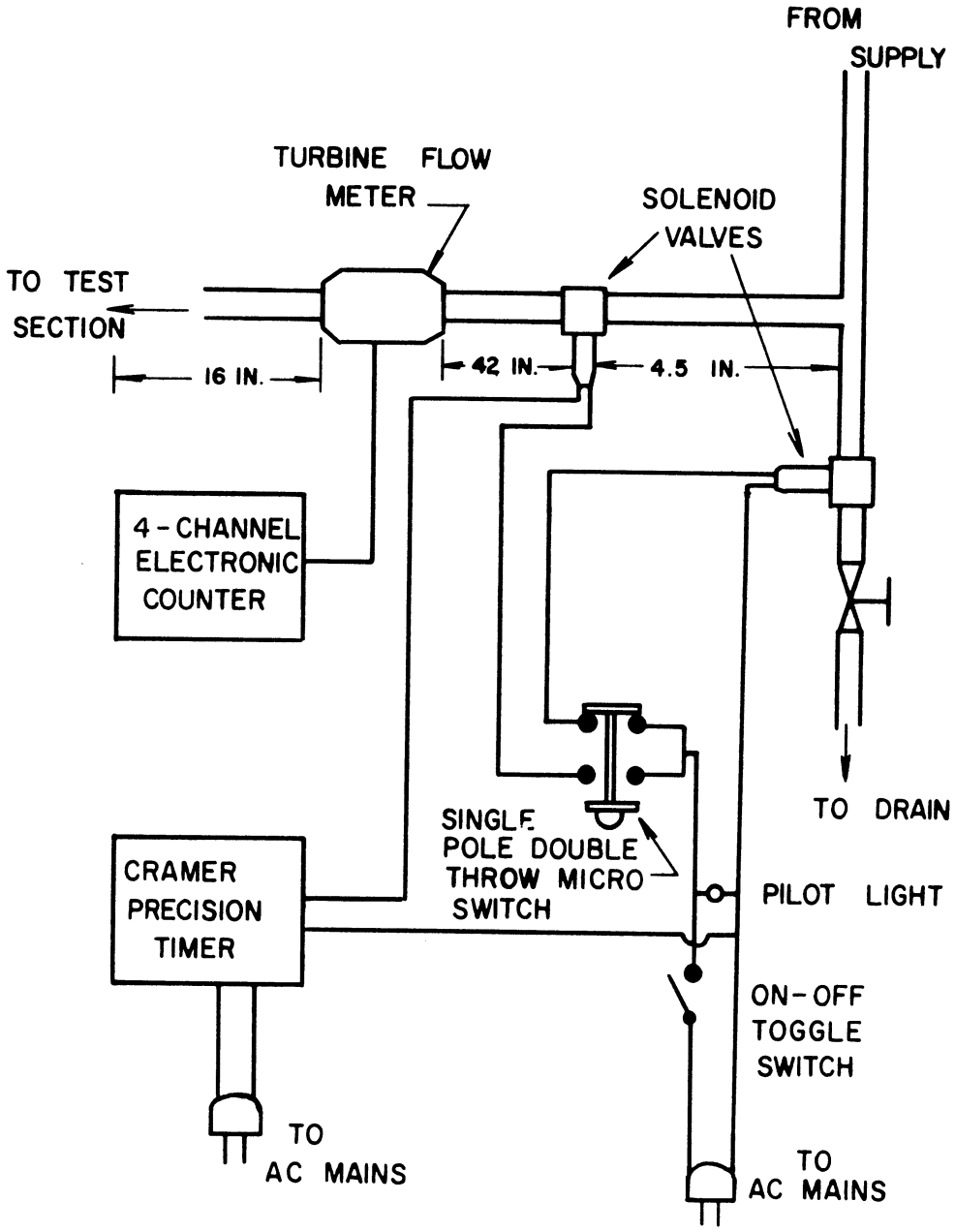

Figure 18. Schematic of the Continuous Flow System.

the control nozzle was opened. Downstream of the bypass solenoid valve was placed a needle valve as a "control balance resistance", that had the same resistance as the turbine meter and control nozzle piping resistance.

2. Equipment for Qualitative Studies

One of the prime objects of this study was to conduct qualitative photographic studies of the flow fields. In order to do this the water tunnel was fitted out with a capability of defining the flow patterns with both dye and tracers and a means of photographing the resulting flow patterns.

For the studies using dyes, the dye was injected into the main and primary control nozzle through either five horizontal or vertical ejectors as shown schematically in Figure 19. The resulting flow patterns were photographed through the front silvered mirror seen in Figure 16, the test channel being illuminated from beneath. In addition to the dye ejectors in the nozzles, another ejector was provided which would allow dye to be injected at any desired point in the test section to study localized flow effects. This movable ejector was manually located.

The dye for the control and main nozzles was supplied from separated pressurized bottles with a different color dye being used in each nozzle. The dyes used were generally red and green food coloring dyes. In practice, in order to inhibit fungus formation, a few drops of tincture of iodine were also added to each dye bottle.

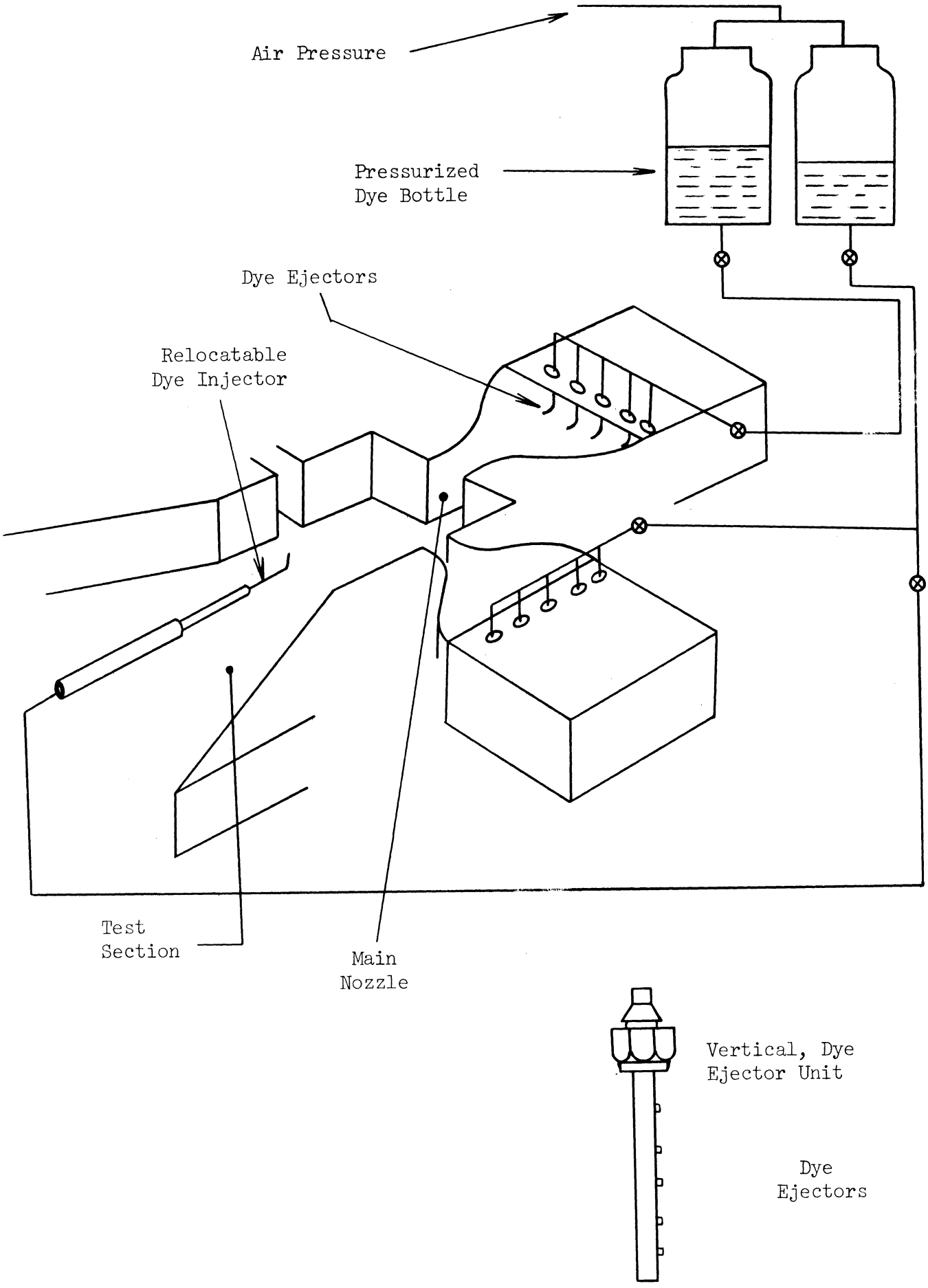

Figure 19. Schematic Drawing of the Dye Injection Unit.

To complement the work with dyes the apparatus was provided with a capability of taking time exposure photographs of light scattered from tracer particles illuminated by a narrow beam of high intensity light. For this purpose particles of Goodyear plastic plyolite material, whose density is near that of water, were carefully injected into the desired plenum chamber by a plastic squeeze bottle containing the particles in suspension in a weak solution of soap and water. The particles were then illuminated by means of eight 500 watt bulbs set up in a bank whose light was collimated by means of a set of collimating slits to provide a beam of light roughly 1/2" deep in the middle plane of the test section. The resulting flow patterns were recorded on polaroid film using a Graflex camera viewing through the front silvered mirror. Exposures for the photographs generally ranged from 1/10 sec. to 1 sec. A schematic of the above arrangement is shown in Figure 20.

There is always some question, when interpreting tracer photographs, as to what is being viewed. This becomes even more critical in low velocity flows where the effect of too large or too small a particle and density mismatch becomes even more pronounced and there is a danger of settling or rising of the particles. Additional difficulty arises from the non-uniformity of the particles. It is for this reason that the plyolite particles were selected as they had desirable optical properties and density. Further, to obtain a more uniform particle size, the particles were differentially sifted through #30 and #50 mesh screens. This when coupled with turbulent mixing and short exposures lends confidence in the approximate streamline pattern depicted in the photographs. The plastic particles, were not recycled.

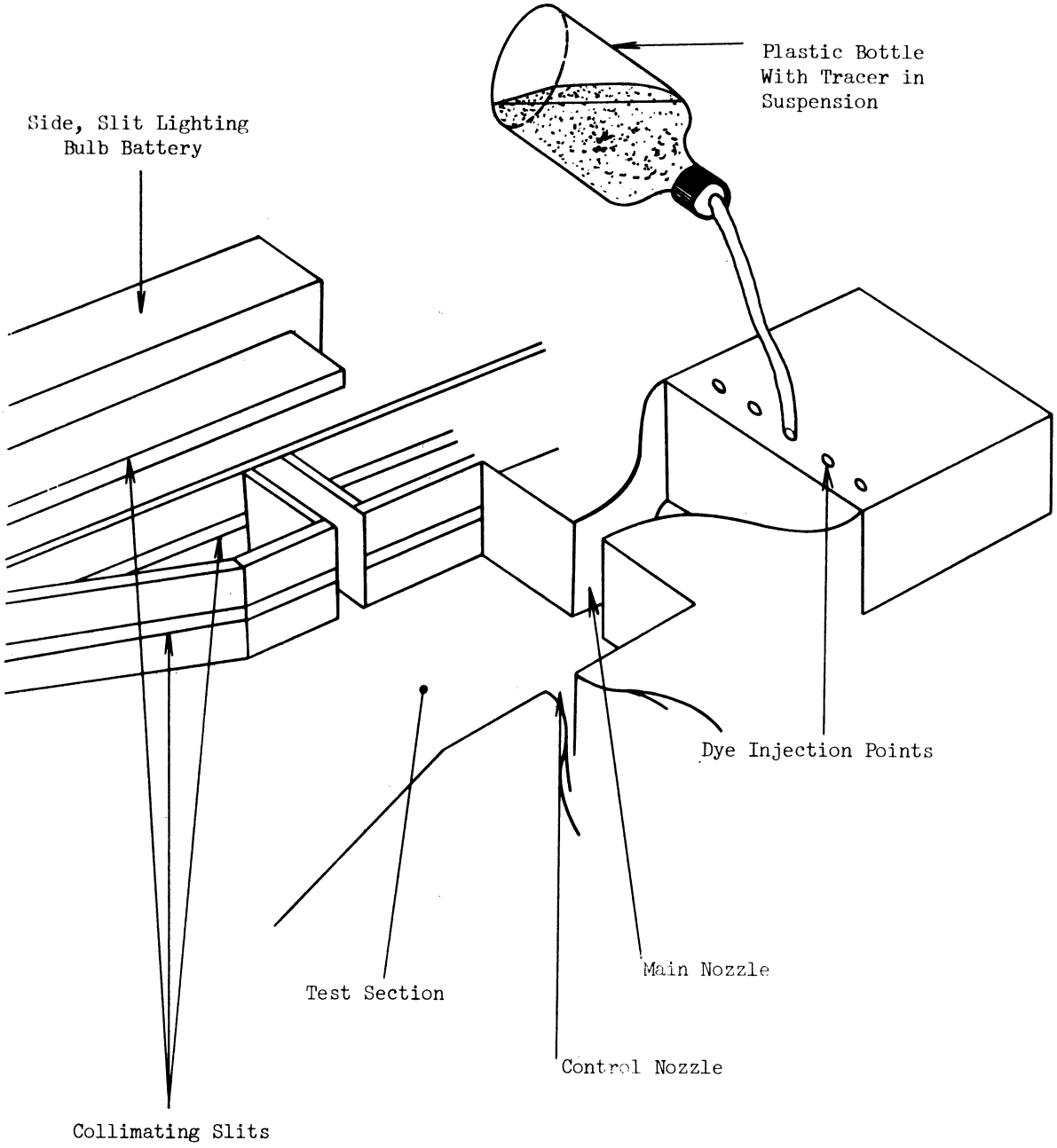

Figure 20. Schematic Drawing Showing the Method of Using Tracers.

3. Instrumentation

For the quantitative study the primary measurements were those of time and flow rates.

a. Flow Measurement

The flow rates to the main and control nozzles were measured. The flow rate of the main nozzle was measured by means of two calibrated Fischer and Porter Series 3000 and series 10A2700C variable area flowrators set in parallel to measure flow rates respectively over the ranges 0-24 gal./min and 0 to 5 gal./min. A similar arrangement was set up for the active control nozzle using Schutte and Koerting series 53-4-538T and series 53-4-544T variable area flowrators, capable of measuring flows over the ranges 0-7 gal./min and 0-1.5 gal./min. In addition, in the circuit of the active nozzle was inserted in series, after the solenoid valve arrangement described above, a Cox Model AN10, 3/4" turbine flow meter with a linear response in the range 1.5 gal./min to 7 gal./min. The signal from the turbine meter was fed through an amplifier to a four channel Hewlett Packard Model 521A electronic counter. In addition to providing a measurement of the flow rate to the control nozzle, the signal from the turbine meter was fed through a Pottermeter Model 3C-2 frequency converter to a six channel Minneapolis-Honeywell Model 1406-5KFH visicorder to provide a starting signal for the measurement of switching times.

In order to calibrate the flow meters, the outlet of the flowmeter to be calibrated was connected to a large drum on a dead weight type weighing scales. The flowmeter was then adjusted to a desired setting and the time required for the weight of the drum to change by a convenient

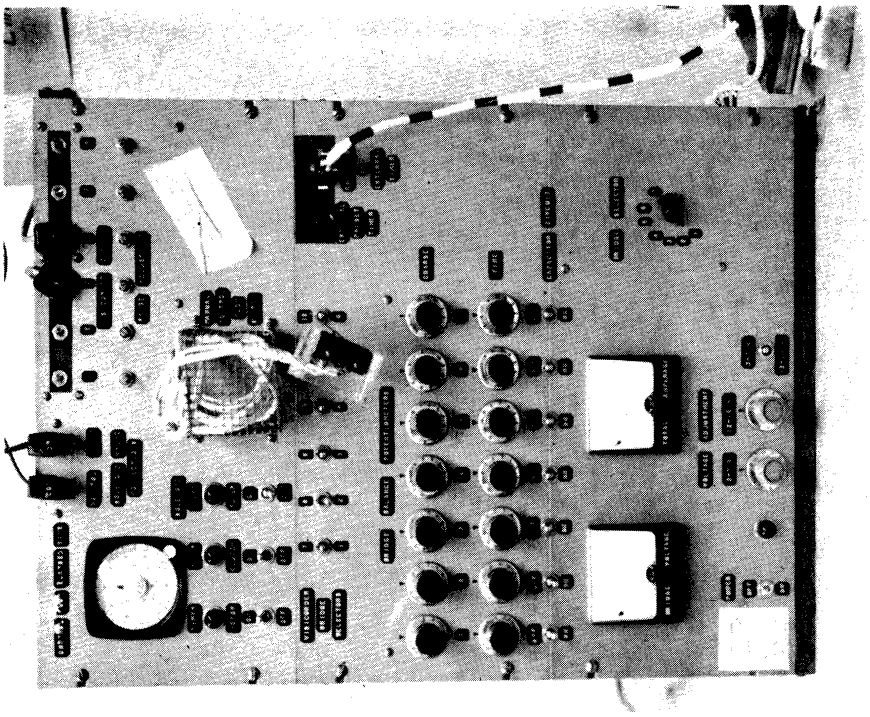

Figure 22. Control Panel.

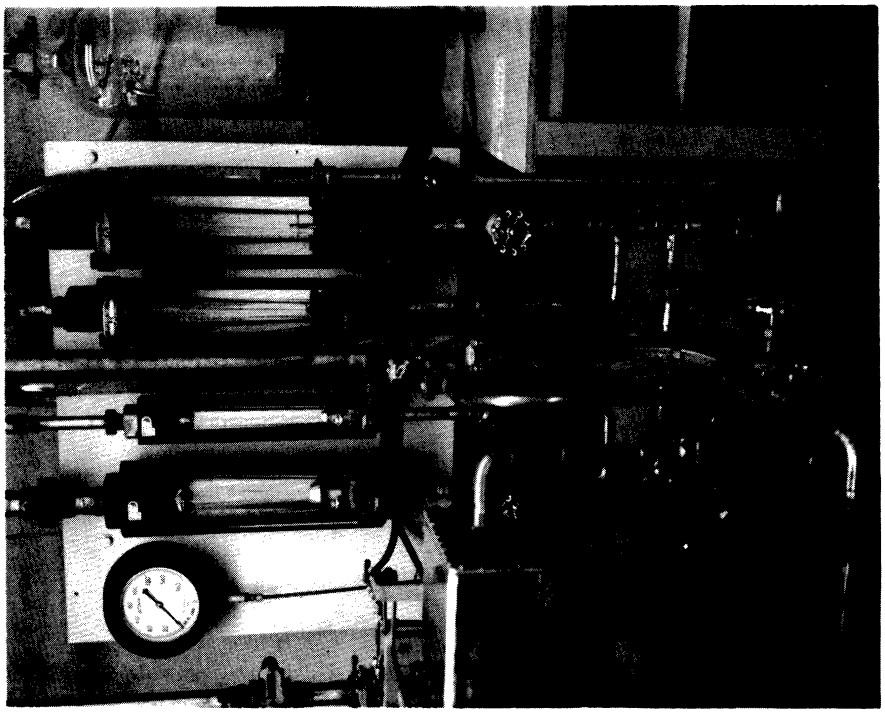

Figure 21. A General View of the Arrangement of the Flowmeters, and Solenoid Valves.

amount between 100 to 500 lbf. was repeatedly recorded. The flowrate was then calculated in terms of gallons per minute from an average value of the above readings. This was then repeated at another flowmeter setting until the range of the flowmeter was covered. The data spread during calibration was generally less than 0.5% of full scale reading. An additional check on the calibration of the turbine meter was provided by the manufacturer supplied calibration curve. The error in calibration of the turbine meter was less than 0.5% of the full range of use.

b. Time Measurement and Interval Preset Cam

In order to measure the elapsed time intervals in the switching process a Cramer type 691 interval timer accurate to 0.01 sec. with a capability of measuring intervals from 0.01 sec. to 60 sec. was incorporated into the solenoid circuit as shown schematically in Figure 18. The clock was mounted on the control panel shown in Figure 22 together with the switches for the solenoid valves. The clock was actuated by the same microswitch which operated the solenoid valve arrangement discussed above, thus measuring the actual intervals for which the control valve was open.

The opening and the closing of the solenoid valves was accomplished manually through the interval ranges of 0.5 sec. and greater. For intervals shorter than 0.5 it was found that some automatic means was required especially to repeat the same interval. For this purpose an adjustable motor driven knife edge cam actuating a single pole double throw microswitch was devised. The cam was mounted on a turn table rotating at a maximum speed of two revolutions per sec. being driven by a motor through a reduction gear arrangement. The motor speed was

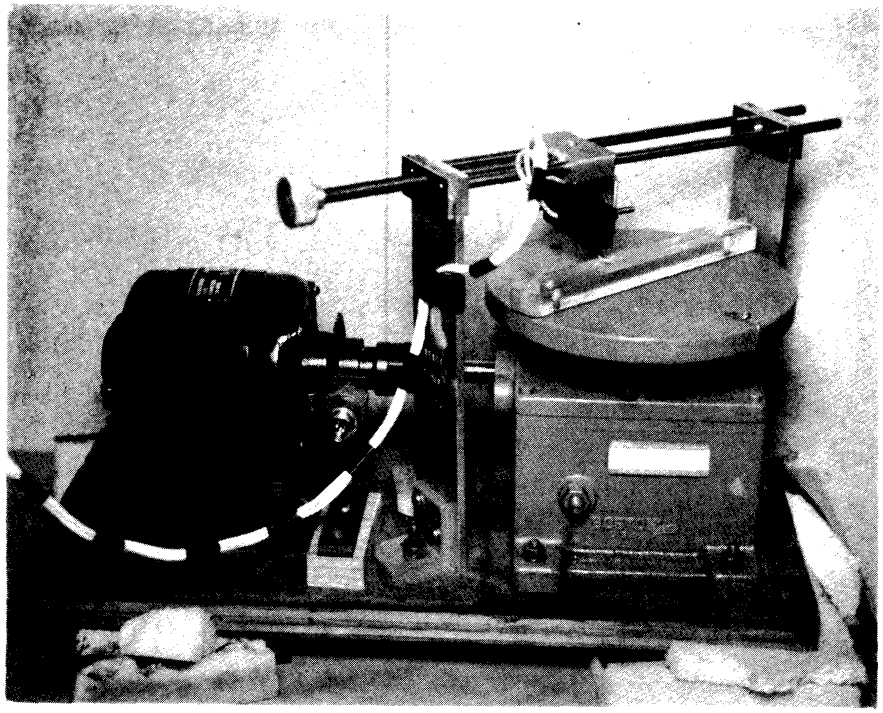

Figure 23. Interval Preset Cam.

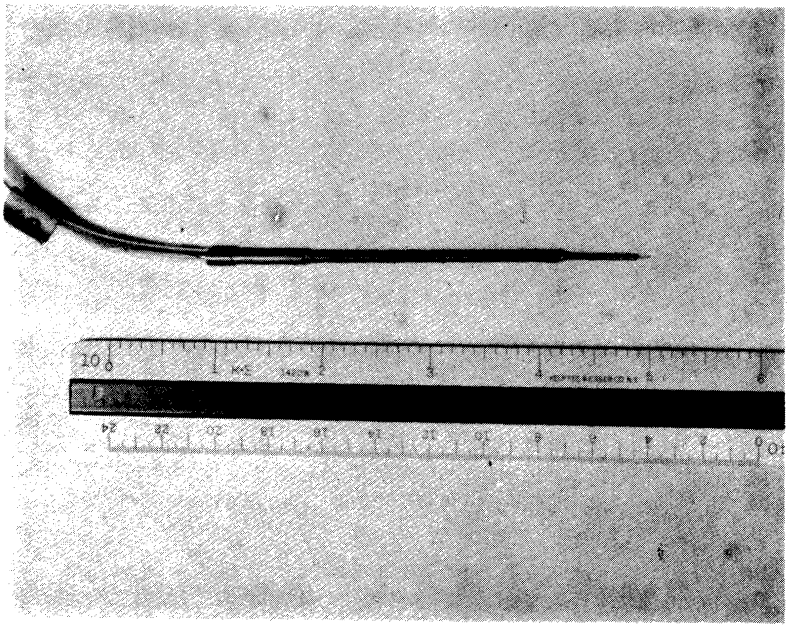

Figure 24. The Thermistor Probe.

controlled by a Variac and the desired interval was then set through trial and error by traversing the microswitch radially on a carriage driven by a traversing screw and mounted over the turntable. The cam operated microswitch, which was normally inactive through manual operations, was activated by depressing a single-pole double-throw push button switch, which then automatically deactivated the manual switch. The above arrangement is seen in Figures 22 and 23.

c. Thermistor Probe

During the switching studies, it was required, as will be pointed out more clearly in Chapter III, to sense the location of the jet. This problem posed several difficulties in that the flows involved would be of an electrically conducting fluid at low velocity and low pressure. The low velocity and low pressure ruled out the use of the pressure transducer, while the electrical nature of the fluid ruled out the use of the hot wire anemometer. In place of the hot wire, based on the work of Lane,[23] a decision was made to use a thermistor probe as an anemometer. According to Lane, the thermistor as an anemometer is especially attractive as it has a satisfactory response time, although much poorer than the hot wire, together with the major advantages of inexpensive and convenient electronics. Furthermore, the glass encased thermistor can be readily used in a liquid or otherwise conducting environment.

A thermistor is an oxide semi-conductor. It is generally made by sintering powdered metallic oxides in combinations such as CuO or NiO and Mn_2O_3 or Co_2O_3 in a bead form encased in a glass housing. Unlike an ordinary resistance wire, the temperature coefficient of resistivity is negative, thus an increase in temperature results in a drop

in resistance. Mathematically this effect can be approximately expressed by the relationship.

$$R_T = R_{T_o} e^{\beta(\frac{1}{T} - \frac{1}{T_o})}$$

where T denotes temperature, T_o a reference temperature, R_T a resistance at temperature T and R_{T_o} the reference resistance at T_o. Thus, the temperature coefficient defined as

$$\alpha = \frac{1}{R} \frac{dR}{dT}$$

becomes

$$\alpha = - \beta/T^2$$

A typical range of values, for comparison, of the thermistor and platinum wire are respectively -3 to -6% per degree centigrade and +0.36% per degree centigrade. It is this high value of α which allows the signal from a thermistor anemometer to be of an order of magnitude larger than the hot wire thereby requiring only the simplest of circuitry to measure and record the signal.

During operation as an anemometer, the thermistor formed one leg of a wheatstone bridge with the other three legs containing respectively 2,1000 Ω ± 0.1% resistors and one variable resistor. A 0 to 20V D.C. power supply was used to supply the power to the wheatstone's bridge. The signal picked up was that of the voltage unbalance resulting between the two nodes of the bridge due to the change caused in the resistance of the thermistor by the high speed jet of water flowing by it when compared to the stagnant water at the same temperature; this voltage unbalance being proportional to the velocity of the surrounding fluid through heat transfer and temperature resistance characteristics of the thermistor.

Despite the simplicity it may be noted that, for water at a temperature of about 70°F, the voltage unbalance between no flow and flow of 1 fps was on the order of magnitude of 1 volt. Due to the simplicity of the backup circuitry, the thermistor may be used in banks, hence the control panel was designed to accommodate seven wheatstone bridges (See Figure 25) with a set of selector switches to allow the use of 12 thermistors in a bank although in this study only one thermistor was used. Also, due to the calibration drift of the thermistor it was merely used to sense the location of the jet and no velocity profile studies were conducted.

The thermistors used in this study were commercially obtained. Initially Fenwal GC-32J3 thermistors were used although later discarded in favor of VECO ZA-32-A91. Both these thermistors are formed into glass enclosed ellipsoidal beads with the major axis of less than 0.015 inches. The advantage of the VECO thermistor was that it came mounted in a 1/16 inch diameter by 1 inch stainless steel tube with the thermistor protruding about 1/8 inch from the tube at the end of a glass stem of less than 0.01 inch diameter. These thermistors were then made up into probes such as that for the VECO thermistor shown in Figure 24 and mounted at a desired point in the test section using a mount made of a Swagelok fitting as shown in Figure 26.

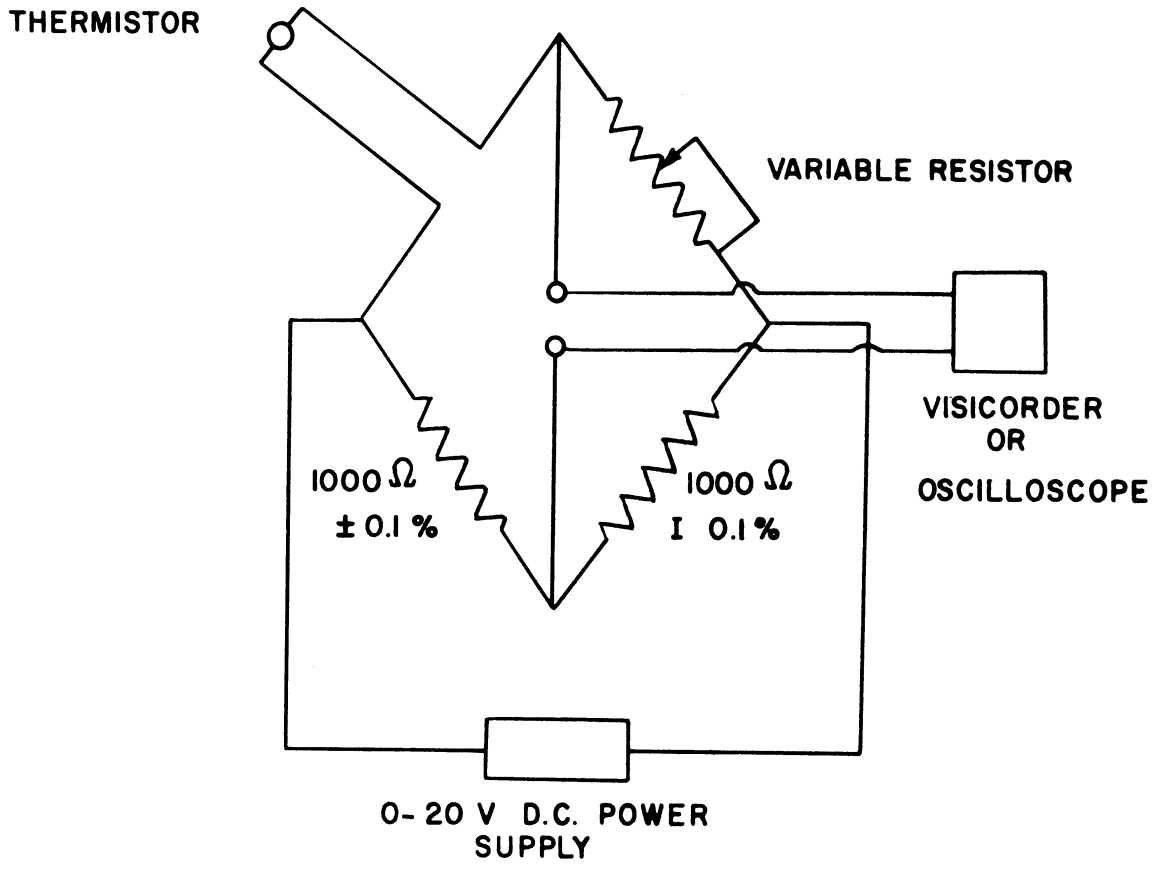

Figure 25. Schematic Diagram of the Thermistor Bridge.

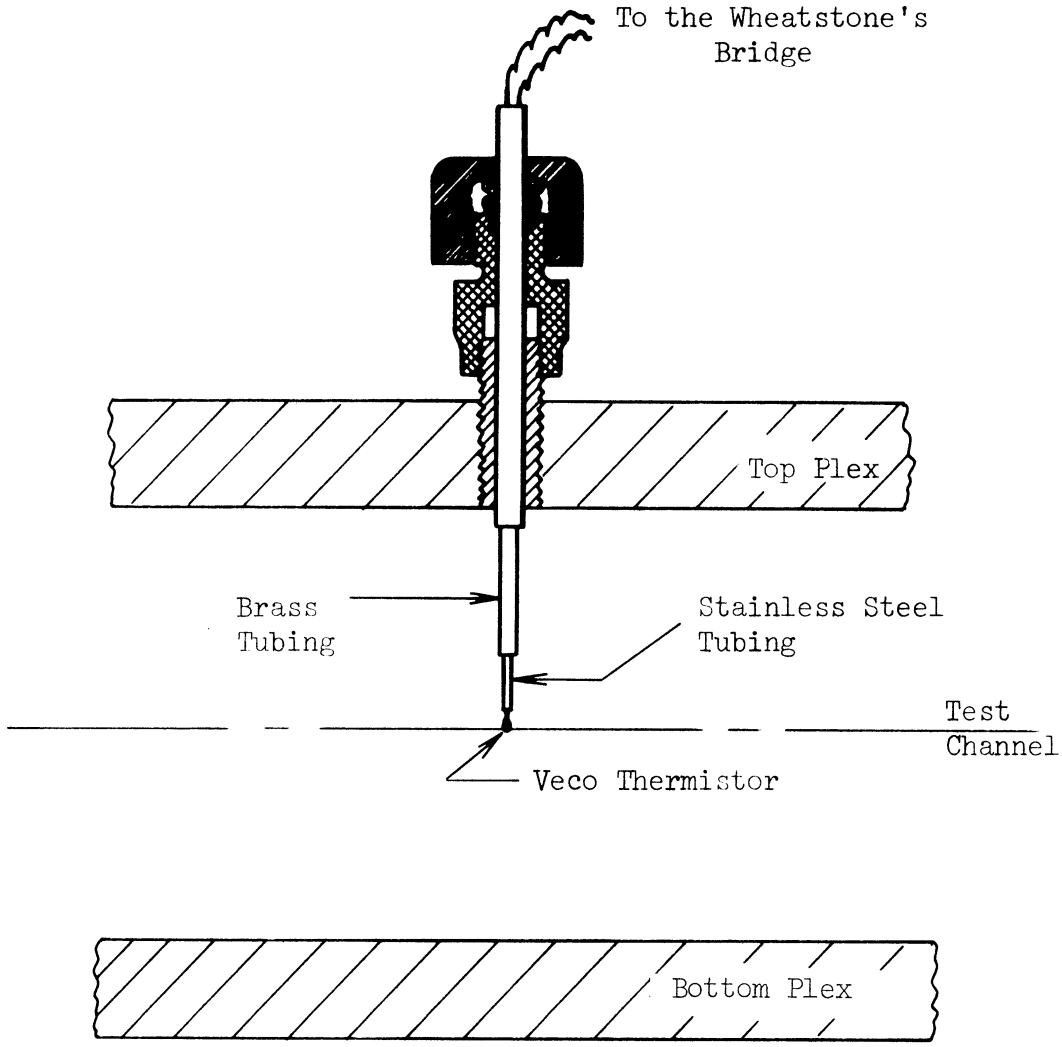

Figure 26. Thermistor Probe Mount.

CHAPTER III

THE EXPERIMENTAL PROGRAM

The experimental program consisted of modeling several geometries of a bistable fluid amplifier and measuring their effect on the switching times. Tracer photographs were also taken to augment the quantitative data.

1. Definitions of Switching Times

As the primary objective of this study was the comparative parametric study of switching in a bistable fluid amplifier, an operational definition of the switching time or times, as used in this study, should be given. Experiments reveal that switching time may be broken up into two major components. The first component is the minimum pulse length of the control jet to initiate switching, which is a threshold value below which switching will not occur. In this study the minimum pulse to switch is referred to as τ_1 and is shown in Figure 27 plotted against the ratio of control to main jet flowrates. The second component of switching time is the time required beyond τ_1 to receive a signal down the inactive channel. This time is dependent on the time beyond τ_1 for which the control jet is retained on, and varies inversely to it. Thus, if a control pulse of only τ_1 is applied, the complete switching time curve labeled τ_a in Figure 27 results. If, instead, the control jet is retained through the complete switching process a locus disposed inbetween τ_1 and τ_a results and is shown as the curve labeled τ_b in Figure 27. For a control pulse greater than τ_1 but less than τ_b the switching time falls between the values for τ_a and τ_b. Hence, two distinct switching times (in the bistable mode

τ_1: The Minimum Pulse Required to Initiate Switching

τ_b: Minimum Complete Switching Time- Time Required for a Complete Switch with the Control Jet on Continuously Until the Switch is Completed.

τ_a: Maximum Complete Switching Time - Time Required for a Complete Switch Using a Control Pulse of τ_1

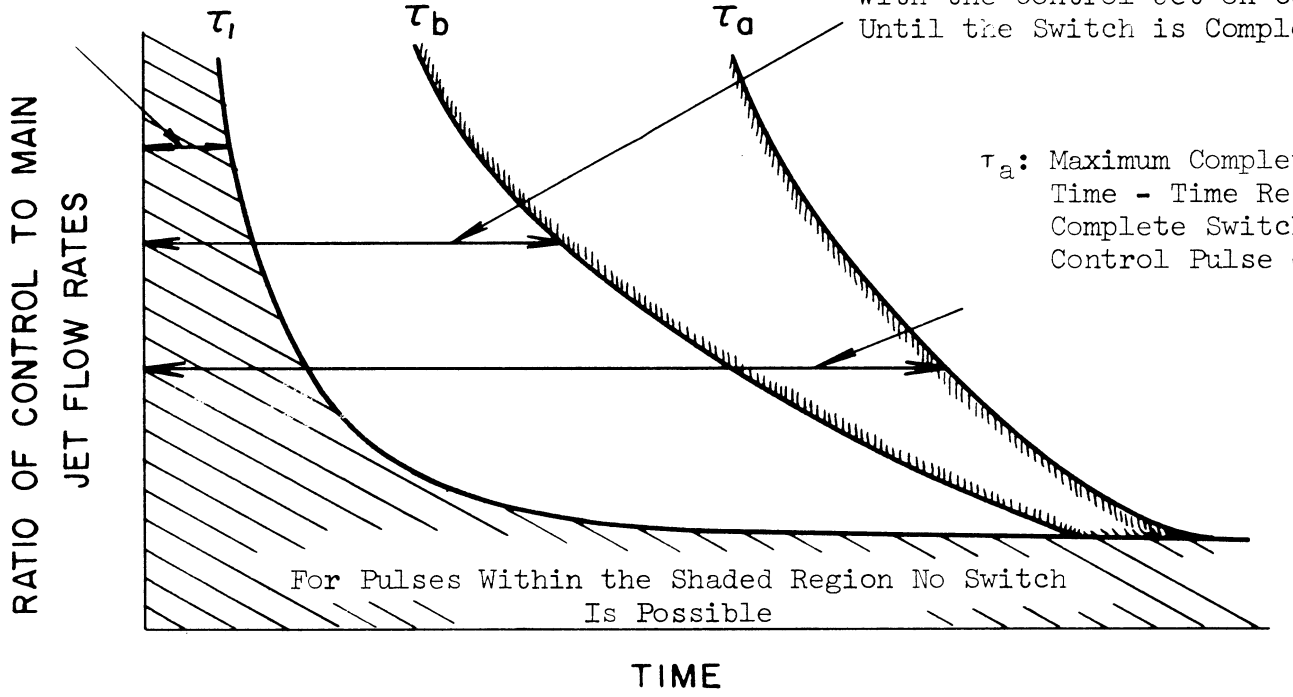

Figure 27. Schematic Diagram of the Switching Times Definitions.

with complete reattachment of the main jet), τ_a the maximum time and τ_b the minimum, may be defined.

A complete switch has not been defined yet. A definition is necessary since several different definitions are used by various workers. One definition is that switching is complete when the total head in the inactive channel, into which the main jet is switched, reaches a maximum. A second definition says that a switch is complete when the jet reaches a given location in the inactive channel. For example, a hot wire could be used in a fixed location on the receiver wall, then the switching is complete when the velocity measured by the hot wire is a maximum and/or steady. In this study the second definition proved more convenient as the pressures involved were of a very low order. In practice, however, a thermistor probe was used in place of a hot-wire to perform the same function.

A thorough definition of switching must include both the initiation of switching and also the completion of switching. The initiation of switching will be arbitrarily taken as the instant, insofar as it is recordable with the turbine flow meter, the control jet solenoid valve is opened. Summarizing, switching is initiated when the turbine flow meter shows a perceptible flow change and is completed when the main jet has moved to a given final position.

2. The Effect of the Starting Transient in the Control Nozzle Piping on the Switching Times

Ideally, the input control pulse is a square wave, but due to the inertia of the fluid in the piping and the resistance of the piping, a pulse which has s shaped ramps results. In order to minimize the

effects of fluid inertia and pipe resistance the flow path over which the starting transient were imposed were reduced by using the continuous flow system described in Chapter II. The problem was further complicated by the insertion of the turbine flow meter after the solenoid valve. In order to smooth the turbulent flow fluctuations in the wake of the solenoid valve a 42 inch length of 3/4 inch flexible tubing was inserted between the solenoid valve and the turbine flow meter, nullifying some of the advantage gained by the continuous flow system. Thus the experimentally measured times would have to be corrected using some experimentally verifiable criterion. The criterion chosen was the total mass of fluid injected, since this could be accurately measured in the transient conditions involved using the turbine meter connected to an electronic counter. This is illustrated schematically in Figure 28.

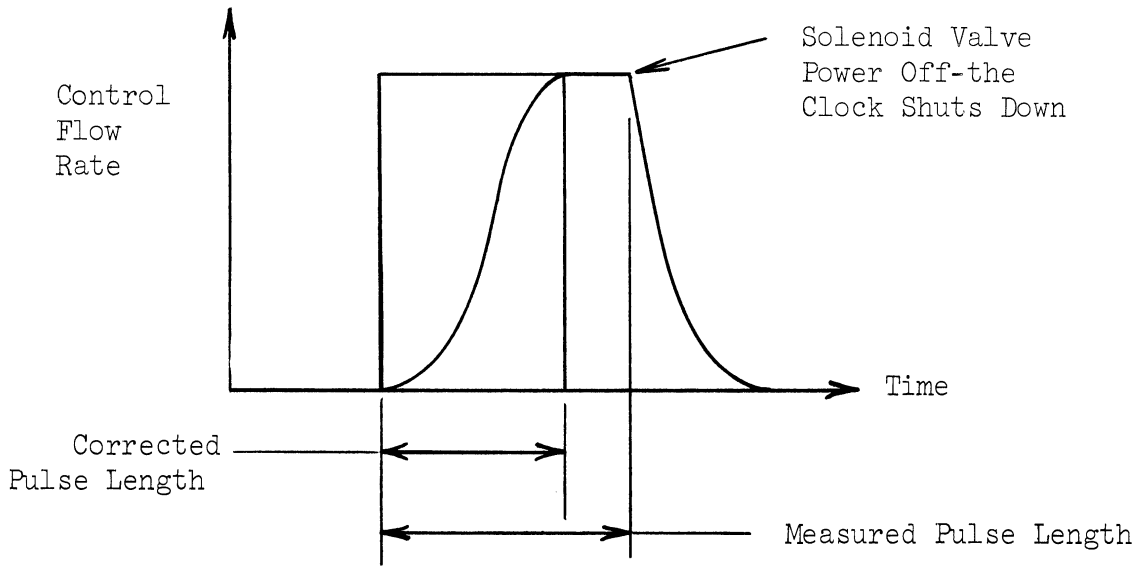

Figure 28. Effect of the Fluid Transients on the Control Pulse.

In order to obtain this correction two sets of experiments were conducted. The first set dealt with determining the time constant of the system for various flow settings for the flow to build up and fall by 90% of the steady state value. These results are shown graphically in Figure 29. Note that both time constants differ by less than 0.06 sec in one second.

The second set of experiments dealt with determining the total mass of fluid injected, for a given pulse length at a given flowrator setting, as registered by the total counts of the turbine flow meter. This is compared with the total counts that should have been obtained had the pulse been a perfect step function. These results are shown in Figure 30. The discrepancy, at least on the basis of total mass, using the worst set of data is less than 8% in a pulse of one second.

The net conclusion to be drawn from Figures 29, and 30 is that there is little need to correct the measured time intervals; this being a result of the "correction" to the total mass injected by the cutoff transient whose time is not recorded by the clock. The above result may be safely extrapolated down to about 0.2 sec., the mechanical limits of the system being about 0.06 sec. While there is little need to correct the τ_1 , τ_a readings, the same does not hold for τ_b where the corrective benefit of the cut off transient, in terms of total mass injected does not come into play. The resulting error is something on the order of +0.4 to 0.5 sec. Despite this, however, no effort to correct the plotted values were made since the error introduced in neglecting the effect is well within the experimental scatter. Moreover, it is to be emphasized that the resulting data are primarily of comparative value and absolute magnitudes have only a limited significance.

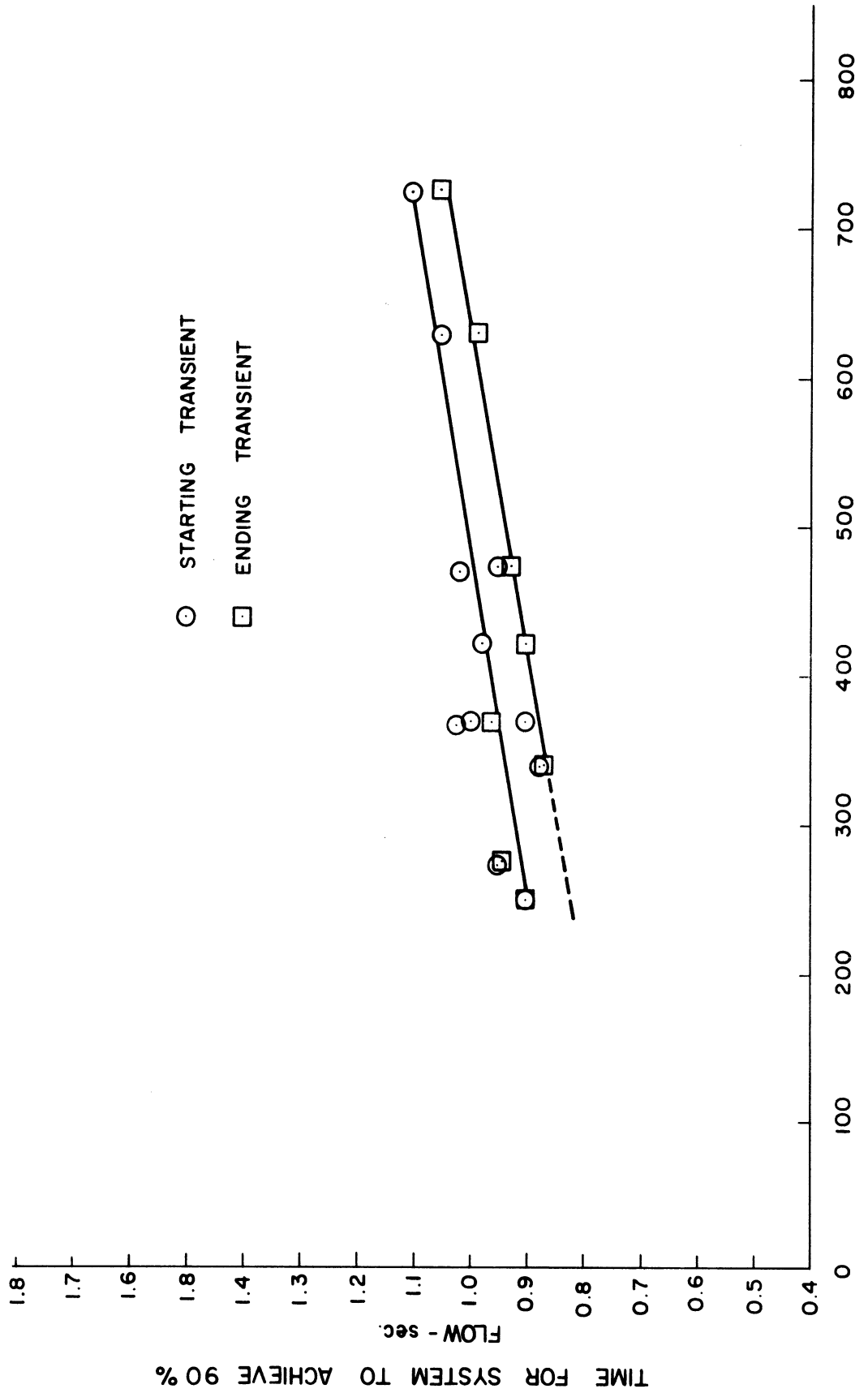

Figure 29. Time Constants for the Control System used for Switching Experiments.

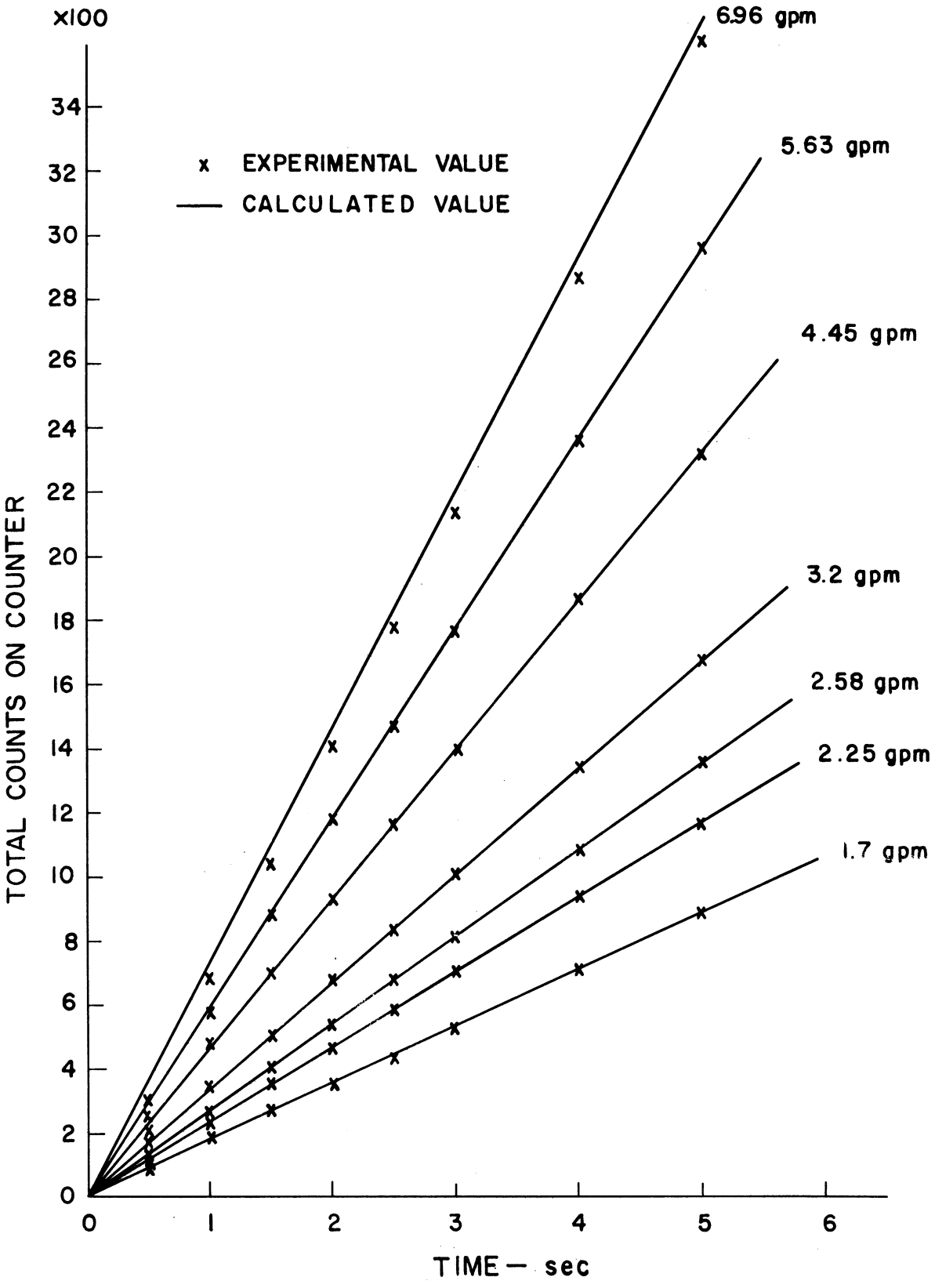

Figure 30. Total Mass of Fluid Injected for Short Pulses.

The two curves shown in Figure 31 and 32 depict the calibration data for the turbine flow meter.

3. Standardization of the Data

Since the data were taken at several different jet settings, in order to generalize the conclusions it was necessary to nondimensionalize the data to yield curves which reflect the influence of geometry and not the jet settings. For this purpose it was found experimentally that plots utilizing the ratio of control to main jet flow rates and a non-dimensionalized time were the most useful. The time was non-dimensionalized with respect to a transport time calculated either with the control or main jet velocity. It was further found that τ_1 and τ_b correlated much better when the reference velocity was that of the control jet while τ_a correlated generally with the main jet exit velocity. In some of the plots it was found that an interesting correlation was obtained by plotting the Euler number (the ratio of the control to main jet momenta) against the non-dimensionalized time. In these cases the data were presented using both types of plots. It is to be noted that the correlations were not based on Reynold's number as the flows involved were essentially free shear turbulent flows with viscosity playing a minimal role.

4. Range of Parameters

The range of parameters investigated in this study are:

Control to main jet nozzle area ratio: 1, 3/4, 1/2, 1/4.

Setback: 0 set back and setback equal to four main jet nozzle widths.

Splitter location: from a location 39 nozzle widths downstream to six nozzle widths downstream from the plane of the control jets.

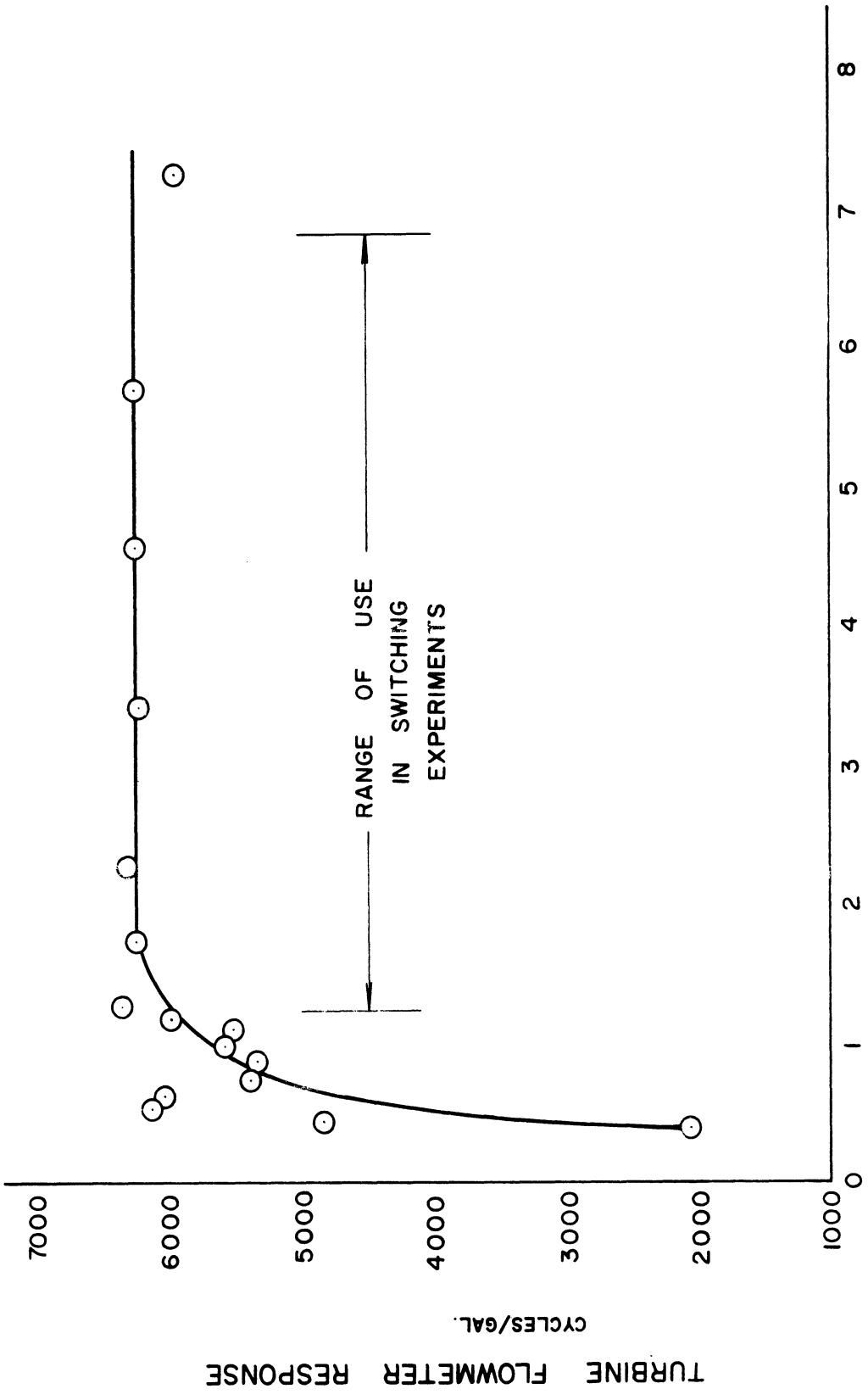

Figure 31. Turbine Flowmeter Linear Response Range.

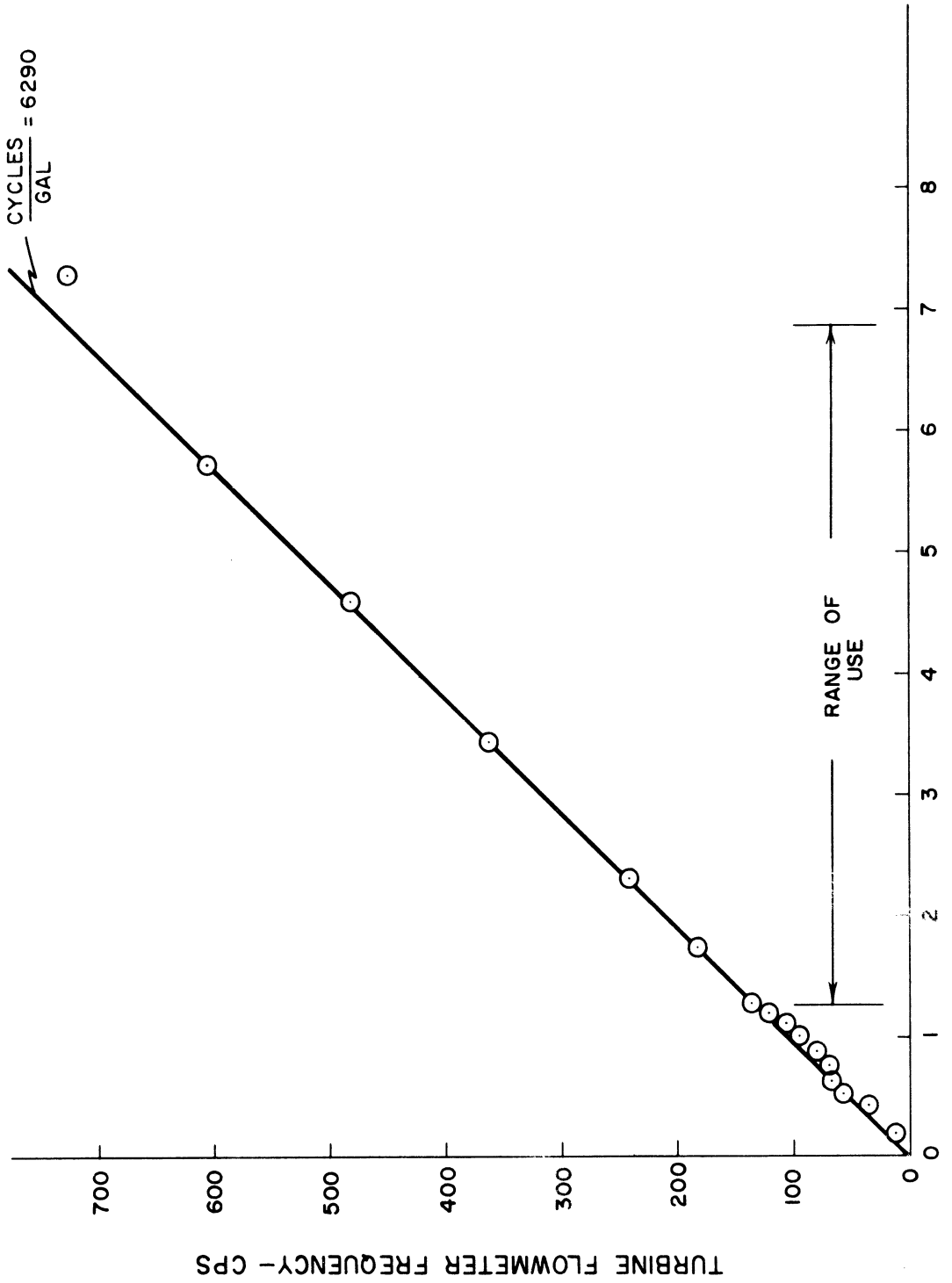

Figure 32. Turbine Flowmeter Calibration Curve.

Offset: values ranging from an offset of one main jet nozzle width to four nozzle widths in increments of half nozzle widths.

5. Test Procedure

At the start of each test, the desired geometry is set up within the water tunnel by adjusting the nozzles to the proper widths and constructing the various sides of the amplifier from plexiglas. With the top plate fastened down and the apparatus checked for leaks, all air is driven out of the test section and nozzles either by forcing it out with high flow rates or by means of an aspirator driven by a jet pump. The desired flow rates are then established in the control and main jet nozzles, their ranges being between 3.5 and 7.0 gpm for the main jet nozzle.

The first piece of data to be determined, knowing the flow rates, is τ_1, the minimum pulse required to initiate switching. τ_1 is located by starting with a very short pulse which does not cause a switch and incrementing the time step by 0.1 sec until a switch is obtained. In order to rule out a chance reading, the above process is repeated by backing down the pulse several increments and starting over again. When a minimum of three to five successive switches are obtained the point is recorded. To ascertain whether indeed a switch has occurred, dye is injected into the main jet and its path traced. After a successful switch the main jet is returned to the active side by the second control jet and then there is a pause of two to five minutes to allow the turbulence level to reach a steady condition, this being necessary to rule out any effect of the previous jet interaction on the following one.

Prior to this the power to the thermistor is turned on with a voltage across the bridge of about 12V. The bridge is then adjusted to obtain a good signal when the main jet is switched over to the inactive side with the thermistor.

Once τ_1 is known, and after a pause to allow the apparatus to settle down, a pulse of length τ_1 is introduced in the control nozzle and the switching process recorded on the visicorder as the signals from the thermistor and turbine meter. τ_a is then measured from the visicorder trace by the time separation between the opening of the control solenoid valve and the thermistor to register a maximum steady velocity signal. This is generally repeated at least five times and the flow rate is monitored in each case by the total count of the turbine meter as registered by the counter. The reading recorded is then the average of the above five readings.

τ_b is then determined in the same fashion as τ_a only now the control jet is maintained on through the whole process, the flow rate being monitored by the rate count of the turbine meter. Once again the trials are generally repeated from four to six times and the average value is then recorded.

For a given geometry, repeated runs are made for different ratios of the control to the main jet flow rates until data sufficient to define a fairly complete curve of τ_1 , τ_b and as much as possible for τ_a are obtained. In the process the lower limiting value of the control flow to main jet flow ratio is determined.

6. Tracer Photographs

To augment the above quantitative studies, tracer photographs of the transient flow patterns were taken. To do this the front silvered mirror was mounted at an angle above the test section and the room darkened except for the narrow beam of light lighting up the central plane of the test section. The desired flow rates were then established in the nozzles and tracer particles injected into the main jet. Then with the control jet turned on (recording essentially τ_b and when convenient τ_a) the various stages of the switching process was recorded using polaroid film. The exposures generally ranged from 1/10 sec to 1 sec.

When it was not possible to photograph the switching sequence during one switch, photographs of the various stages were recorded on different switches until the complete process was photographed.

CHAPTER IV

RESULTS AND DISCUSSION

Unless otherwise mentioned, the time coordinates of the graphs presented in this chapter are non-dimensionalized with respect to a transport time $T = L/U_{ref}$ where U_{ref} is the reference velocity, generally the average control nozzle velocity, and L is a reference length which for general comparative purposes was taken to be one foot. In the other cases the appropriate transport time is defined on the graph or by indicating proper units. The flow gain, μ_Q, is defined as the ratio of the main jet flow rate to the control jet flow rate. The symbols used for the model dimensions are defined in Figure 14. The value of θ in all the results is fixed at 30°.

1. General Relationship Between the Three Switching Times and the Nature of the Switching Process

As was noted in Chapter III, there are three distinct "switching times" associated with the bistable fluid amplifier. τ_1 the minimum pulse to switch and τ_a and τ_b the two complete switching times. Figure 33 is a plot showing the relationship between the three switching times. The plot is shown for a main jet setting corresponding to a Reynolds number for water at 65°F of 6,000.

The data shown in Figure 34 is switching data non-dimensionalized with respect to a transport time defined using the average control nozzle velocity. The data presented are for three different jet settings corresponding to Reynolds number of water at 65°F of 6000, 5000, 3000. On an order of magnitude basis, for the thermistor located about 20 main jet nozzle widths from the main nozzle, it is seen that τ_b^* and τ_a^* are

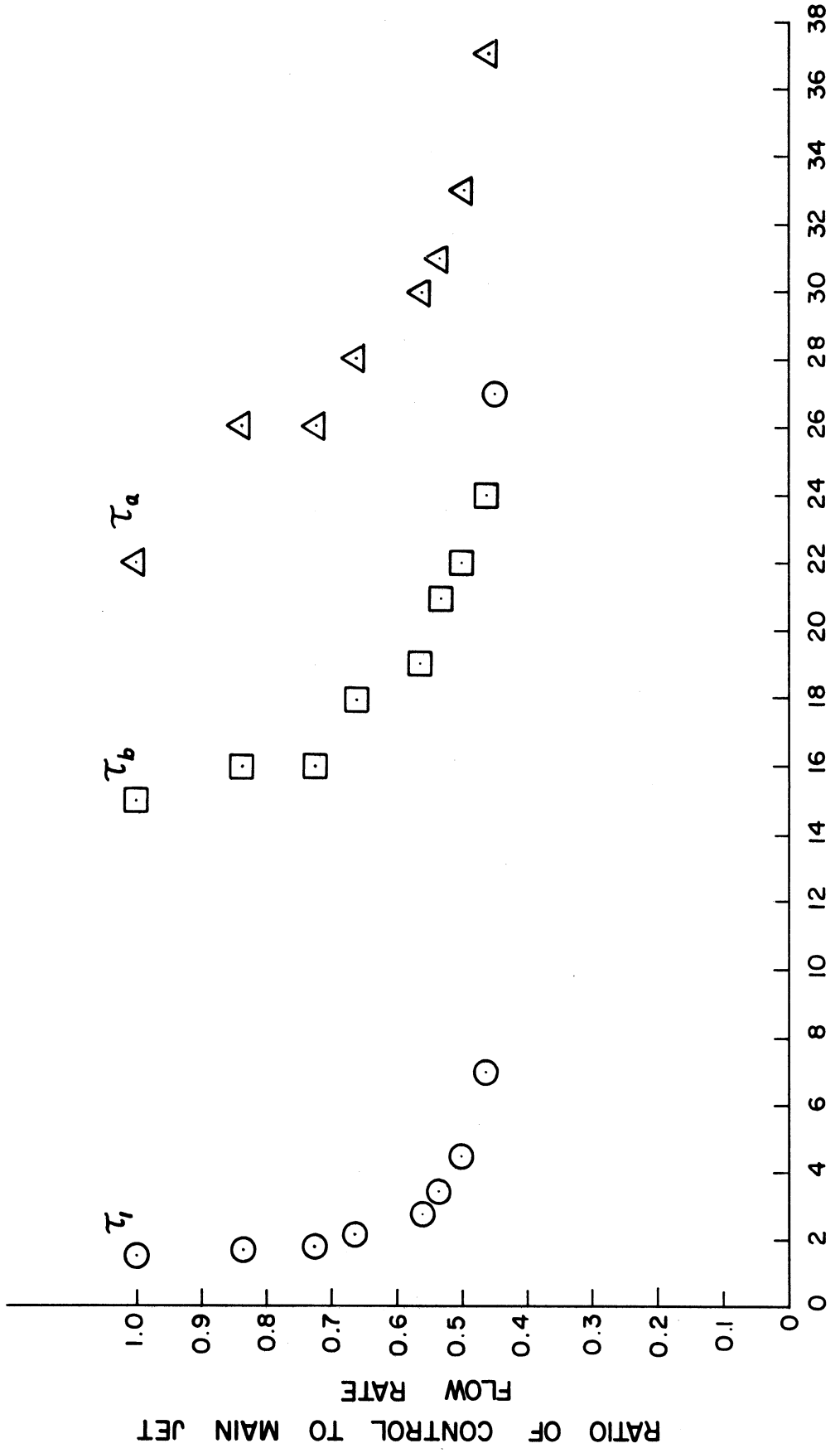

Figure 33. Plot of Switching Times Versus Ratio of Control to Main Jet Flow Rates for $b_c/b_s = 1.$ (Data From Section 1, Appendix E)

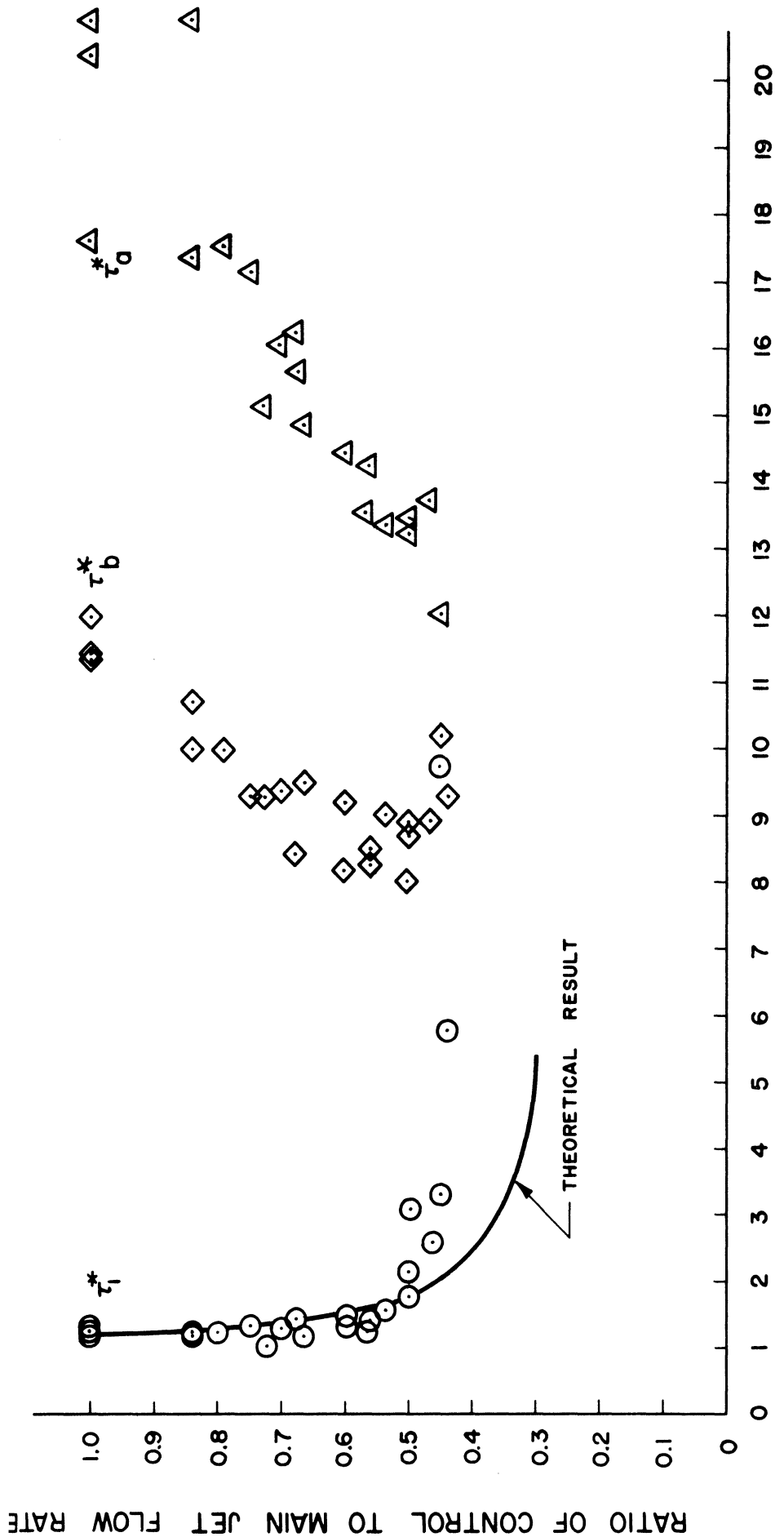

Figure 34. Plot of Switching Times Versus Ratio of Control to Main Jet Flow Rates for $b_c/b_s = 1$. (Data From Section 1, Appendix E)

respectively 10 and 20 multiples of τ_1^* or that τ_a^* is roughly twice τ_b^*. It is to be noted that the magnitudes of τ_a^* and τ_b^* are dependent on the operational definition used and the relations presented here are only of comparitive value.

Figures 35 and 36 present tracer studies of switching in a bistable fluid amplifier. In Figure 35 the tracer was injected into the main jet nozzle while in Figure 36 the tracer was injected into the control nozzle. From a study of these figures and by visual study of dye patterns, the switching process may be qualitatively described as follows: As the control jet is applied, the main jet is deflected causing the angle of reattachment to increase; at the same time the separation bubble volume increases with the input of the control flow and the fluid returned from the stagnation zone formed at the reattachment point. The entrainment rate of the main jet is proportional to the length of the jet up to reattachment, which in turn is approximately proportional to $R\theta$, where θ is the angle of reattachment and R the radius of curvature of the jet. The fluid returned from the reattachment point is proportional to $(1-\cos\theta)$ or θ^2 approximately. Hence, as the control jet is maintained on θ increases and R starts to decrease (as indicated by the drop in the separation bubble pressure, Keto[11] Olson and Stoeffler[12] and Sarpkaya[31]). A point is therefore reached at which the fluid returned to the separation bubble from the reattachment point exceeds the fluid entrained by the main jet by an amount roughly equal to the control jet flow. From this point, which defines τ_1, the control jet may be shut off and the switching process continues on its own. The vortex in the separation bubble grows until it fills the channel walls and then is

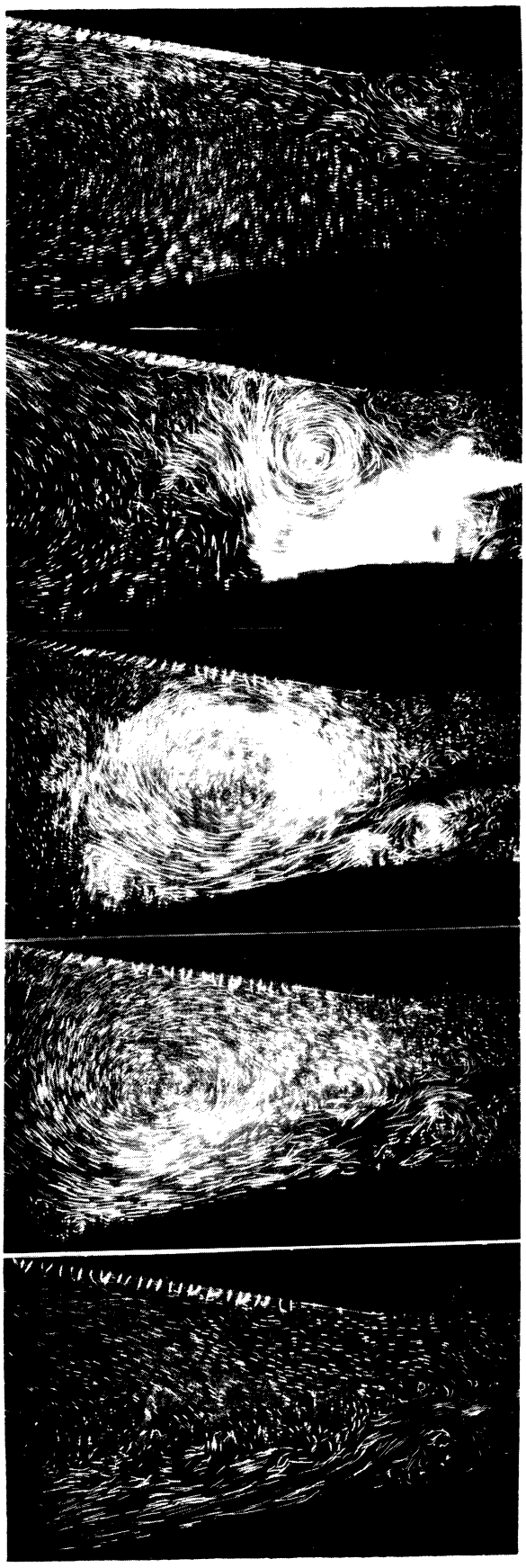

(a)

(b)

(c)

(d)

(e)

Figure 35. Study of a Switching Sequence Using "the Tracer" From Main Jet in a Geometry Without a Splitter.

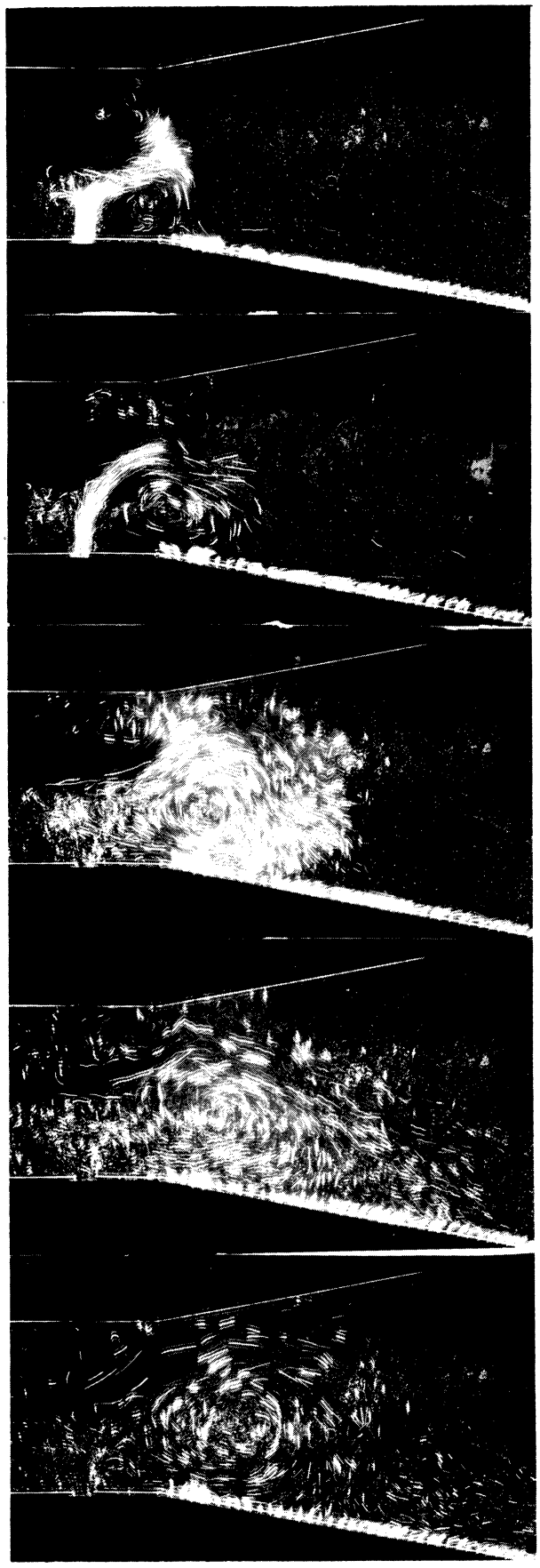

(a)

(b)

(d)

(e)

Figure 36. Study of a Switching Sequence Using Tracer from the Control Nozzle.

swept down the channel leaving the main jet attached to the opposite wall. The photographs clearly show the role played by the two vortices, one of which is in the separation bubble and the second is in the recirculation zone formed on the side of the main jet away from the separation bubble. The role played by these two vortices is further emphasized in the studies with the varying splitter location

2. Effect of Changing the Ratio of Control to Main Jet Nozzle Width on Switching Times

Figures 37, 38, 39 present curves similar to Figure 34 but with the ratio b_c/b_s reduced to 3/4, 1/2, 1/4 respectively. Thus for the same flow rates as in Figure 34 the average momentum of the control jets defined as $\rho A_c U_c^2$, where ρ is the density of water, A_c the area of the control nozzle and U_c the average control jet velocity, is respectively a third greater, doubled and quadrupled. The result of this is that the curves of the three non-dimensionalized switching times shift towards increasing switching times with decreasing control to main jet nozzle width ratio. In terms of actual times, however, switching times are actually decreased. The increase in the non-dimensionalized switching time results from the decrease in transport time, due to the increase in control jet velocity, without a proportionate decrease in actual switching times. This increase shows that a greater amount of fluid must be injected into the separation bubble by the smaller control nozzle. It is to be also noted that for a given main jet setting smaller nozzle dimensions imply higher input impedances and therefore correspondingly require higher control to main jet pressure ratios.

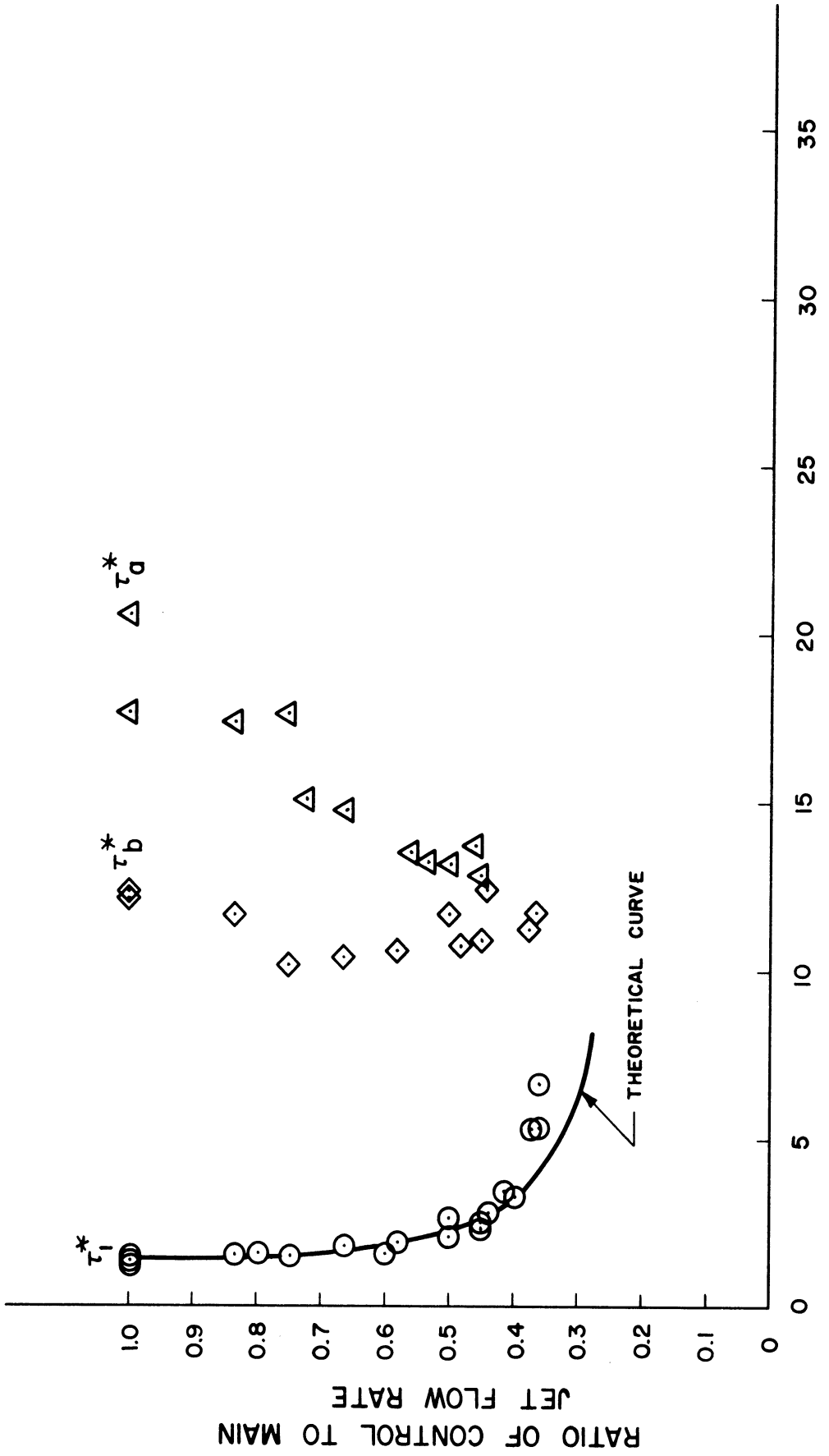

Figure 37. Plot of Switching Times Versus Ratio of Control to Main Jet Flow Rates for $b_c/b_s = 3/4$. (Data From Section 1, Appendix E)

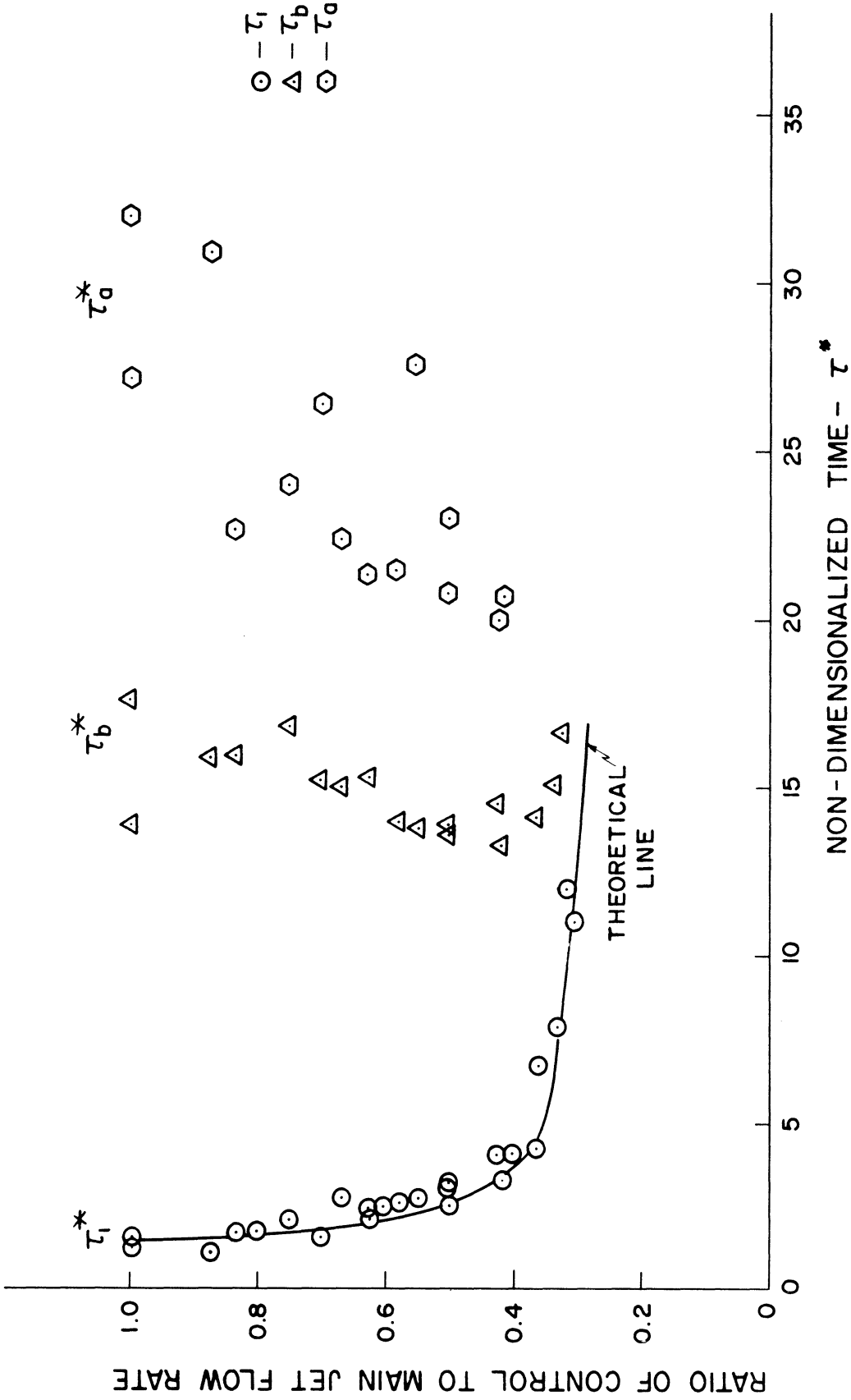

Figure 38. Plot of Switching Times Versus Ratio of Control to Main Jet Flow Rates for $b_c/b_s = 1/2$. (Data From Section 1, Appendix E)

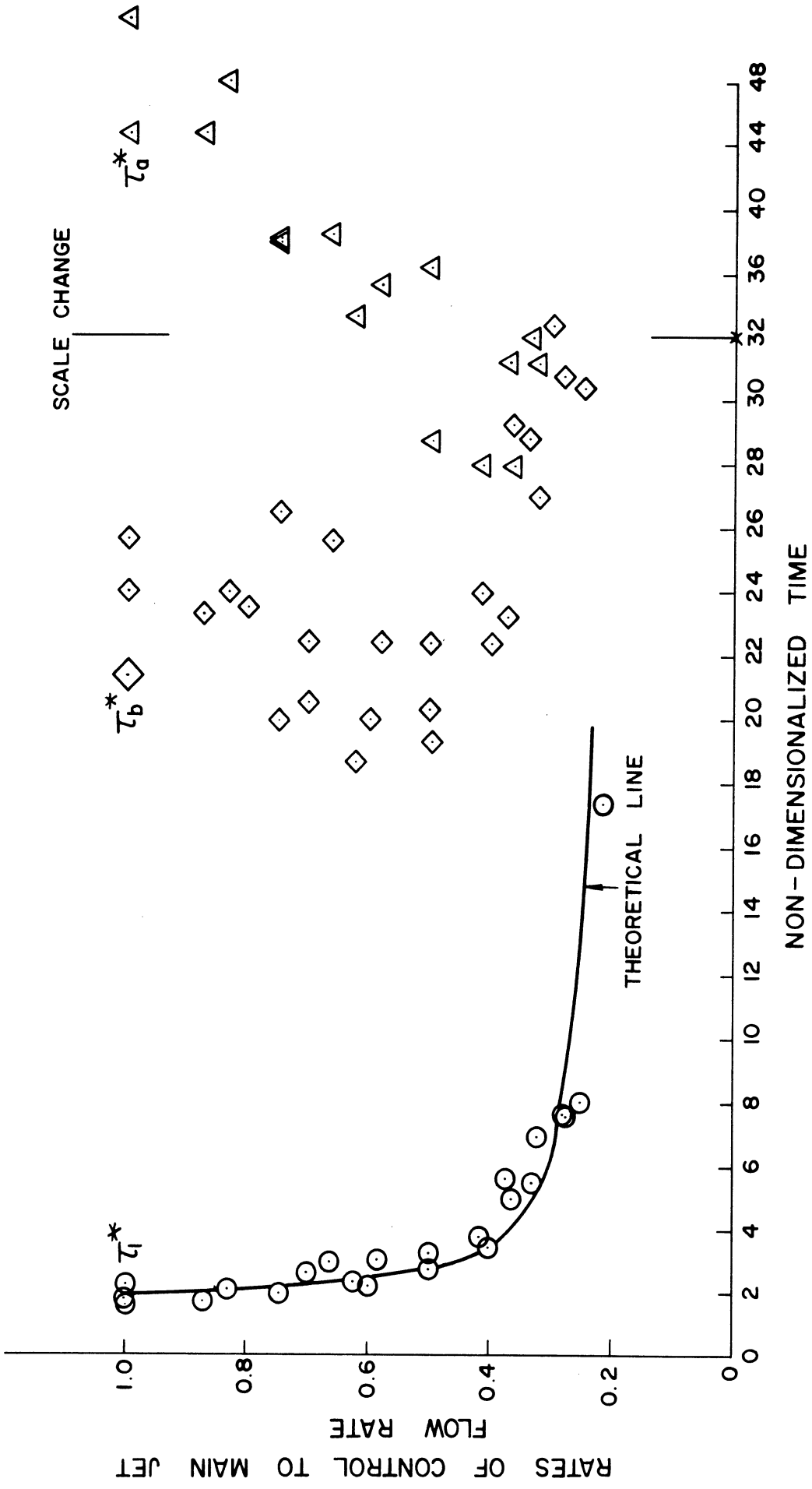

Figure 39. Plot of Switching Times Versus Ratio of Control to Main Jet Flow Rates for $b_c/b_s = 1/4$. (Data From Section 1, Appendix E)

Note that the maximum flow gain, obtained by considering th value of the flow gain as τ_1 becomes indefinitely large, increased from about 2.5 for $b_c/b_s = 1$ to about 4.5 or 5 for $b_c/b_s = 1/4$.

The above discussed increases in non-dimensionalized switching times indicate that mass flow rate is not the only factor in switching and that the momenta of the interacting jets is an equally important factor. This is seen more clearly in Figure 40 where the minimum pulse to switch is plotted against the Euler number or the ratio of the control to main jet momenta. Interestingly, all the curves asymptote to the lines Euler number equal to 0.2 and the line τ_1^* equal to 1.1. The near hyperbolic nature of the curves suggests a model to fit the curves of the type $(E-E_o)\ (\tau_1^* - \tau_{1O}^*) = K$, where E is the Euler number, τ_1^* , the minimum pulse to switch and K , E_o , τ_{1O}^* are constants representing respectively the total impulse, and the two asymptotes. The resulting theoretical curves are seen as broken lines in Figure 40. The values of the constants corresponding to the curves are:

$E_o = 0.2$	$\tau_{1O}^* = 1.1$
b_c/b_s	K
1	0.08
3/4	0.2
1/2	0.63
1/4	1.6

These values yield the best general representation of the experimental data, although it is possible to obtain a much closer fit over a limited range by adjusting the value of K . The significance of E_o is that for a given main jet setting it represents the minimum level of control jet momentum below which switching is not possible and that this value

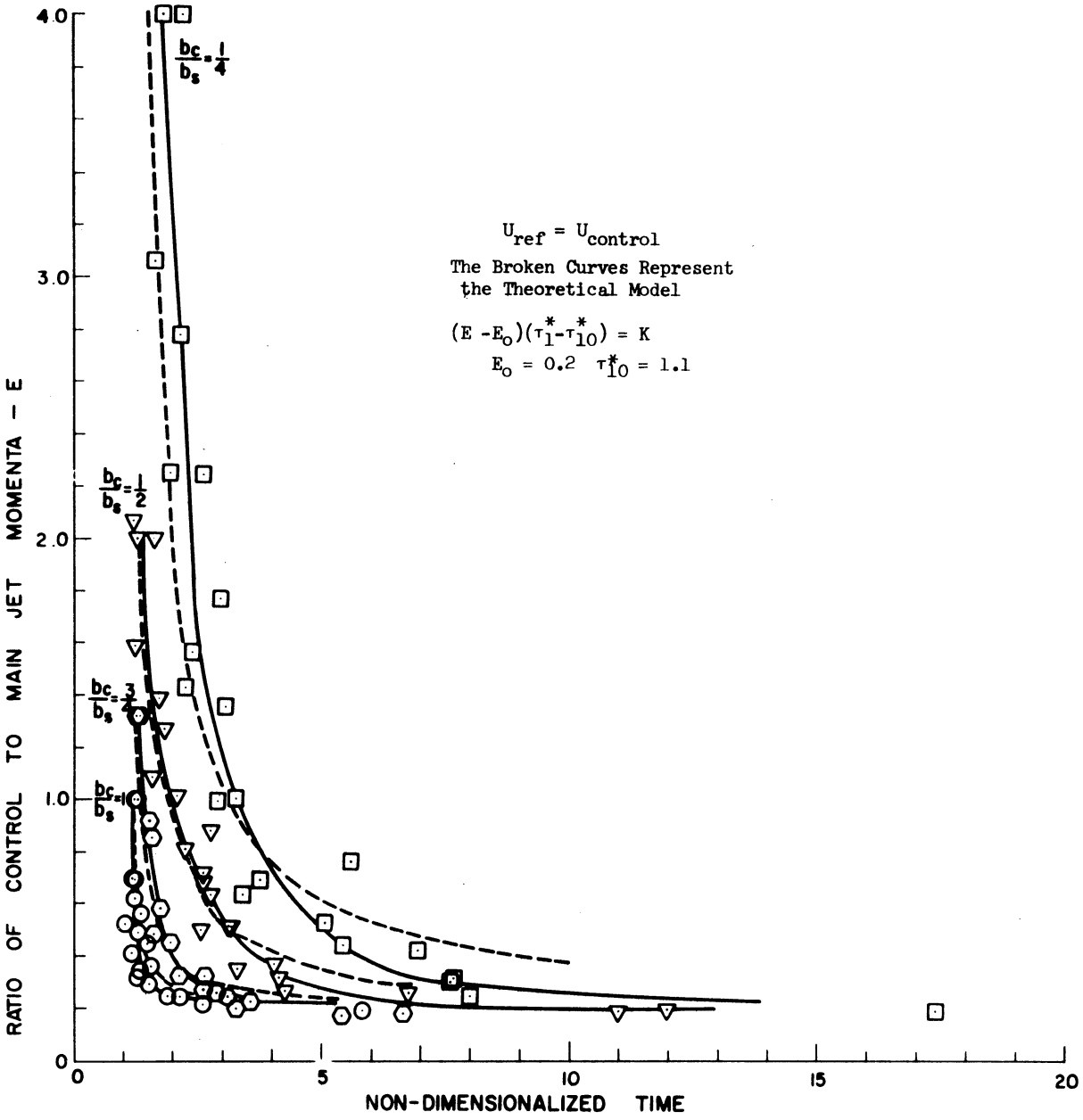

Figure 40. Plots of Minimum Pulse to Switch Versus Ratio of Control to Main Jet Momentum Ratio. (Data From Section 1, Appendix E)

appears to remain constant for the range of control to main jet nozzle width ratios tested. As the overall geometry is changed, including the addition of a splitter, changing the offset, the value of E_o is changed.

While the model discussed above is based on the notion of constant total impulse, Appendix D presents a model which is essentially a modified version of the model developed by Johnston.[17] Johnston's model was based on continuity and the assumption of a constant cross-sectional area of the separation bubble as the factor determining the τ_1 curve. The theoretical curves that result from this model are shown as solid lines in Figures 34, 37, 38 and 39. By way of comparison, it is seen that the two models best represent the data at the opposite ends of the spectrum of b_c/b_s values. The first model represents the experimental data for $b_c/b_s = 1, 3/4$ better than the second, the second model better represents the data for $b_c/b_s = 1/2, 1/4$. Despite the ability of both models to represent selected data, the second model based on the model of Johnston is preferable since it requires only two experimentally determined constants as opposed to the three required by the constant total impulse model.

Figure 41 shows τ_a curves non-dimensionalized with respect to the main jet velocity. Comparison of these curves with those of Muller[19] shown in Figure 13, where the transport time was defined using a reference length L equal to one nozzle width and the main jet nozzle velocity, shows an order of magnitude agreement if the τ_a times in Figure 41 are multiplied by 12, the factor by which the reference length in Figure 41 differs from Figure 13. It is to be noted that Muller's model had a nozzle width of 5mm. with the angle θ

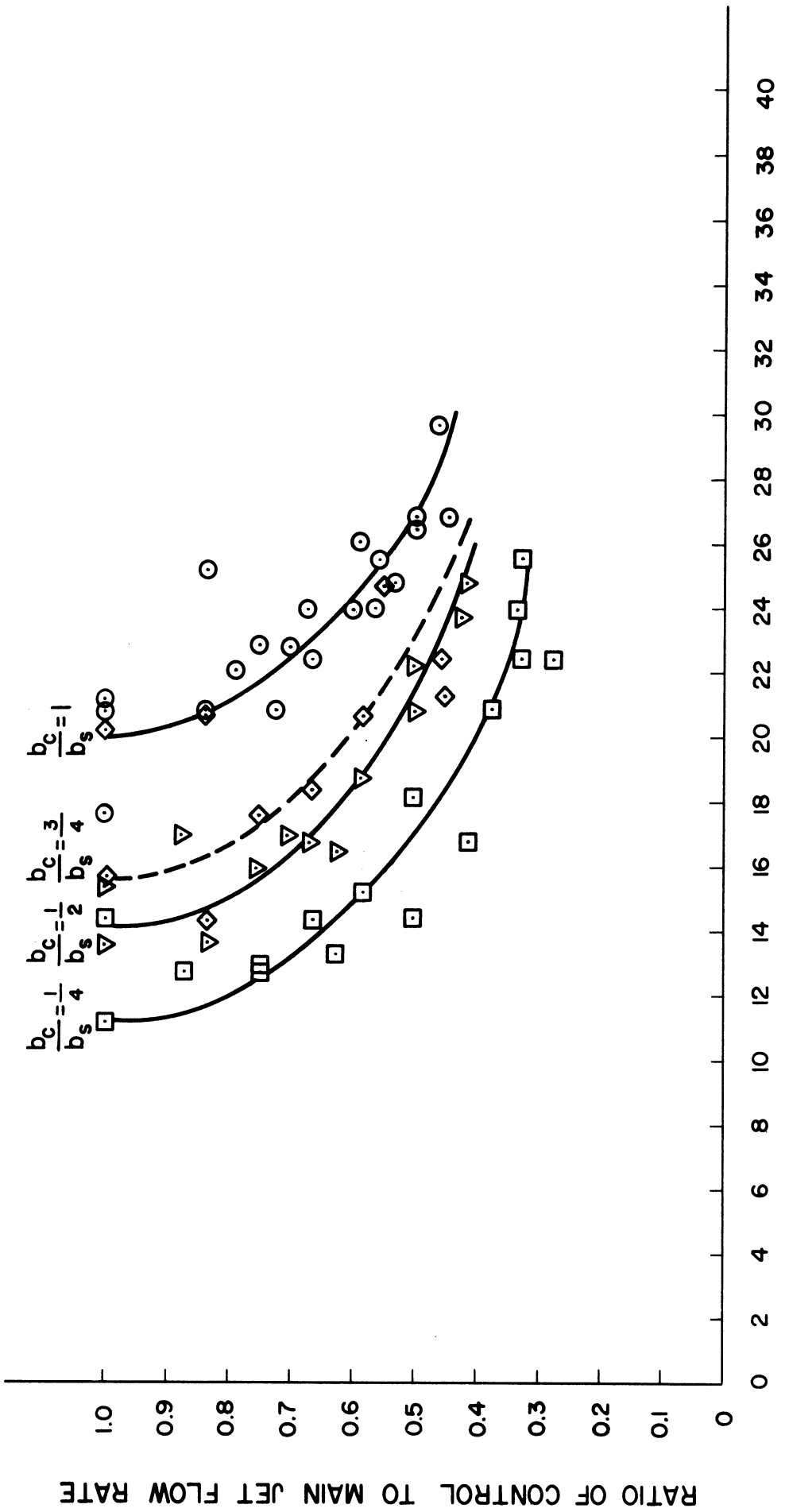

Figure 41. Effect of Varying the Ratio of Control to Main Jet Nozzle Width on τ_a.

contained by the side walls of 30° and $b_c/b_s = 1$. Thus while the relative size of his model compared to that in the present study was about 1/5 the other parameters were similar.

Order of magnitude agreement is also seen with Muller's results in Figure 12 of the curve for an amplifier with an offset of 0.2 nozzle widths (L for this model is 14 nozzle widths).

It has already been noted that τ_a and τ_b bear a relationship to τ_1 . Figure 42 shows this relationship. In this figure the ratio τ_b/τ_1 is plotted against the ratio of the control to main jet flow rate. The primary use of this plot is in interpreting the data obtained by varying splitter locations.

3. Effect of the Splitter Location on Switching Times

The effect of the location of the splitter on the switching times is shown in Figures 43 through 50. The experimental data presented are shown for two values of the flow gain $\mu_Q = 1$ and $\mu_Q = 2$.

The curves for τ_1 and τ_b/τ_1 shown in Figures 43, 46, and 47 clearly show the existence of two distinct regions of operation. The two regions are marked by the abrupt change in nature of the τ_1 and τ_b/τ_1 curves when the splitter location is about 20 nozzle widths from the main jet nozzle (16 nozzle widths from the control nozzle). An explanation for the behavior seen in Figure 43 may be given in terms of vortex interaction. As the splitter is moved upstream, the separation, r , between the two vortices, one in the separation bubble, which is fixed, and the other in the recirculation zone, decreases. The influence of the recirculation vortex on the separation bubble varies roughly as $\frac{1}{r}$.

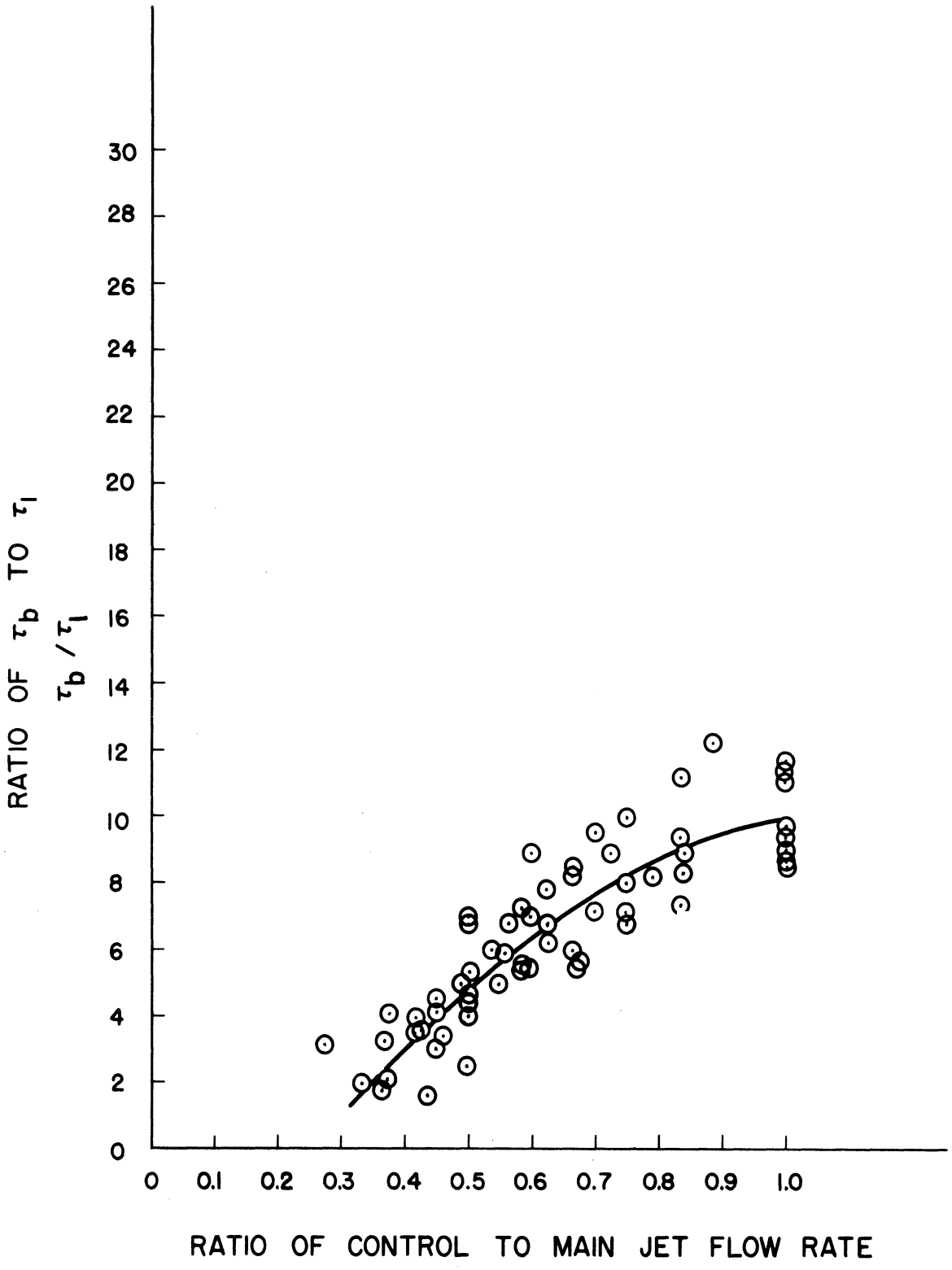

Figure 42. Plot Showing the Ratio of Control to Main Jet Flow Rates Versus the Ratio of τ_b to τ_l .

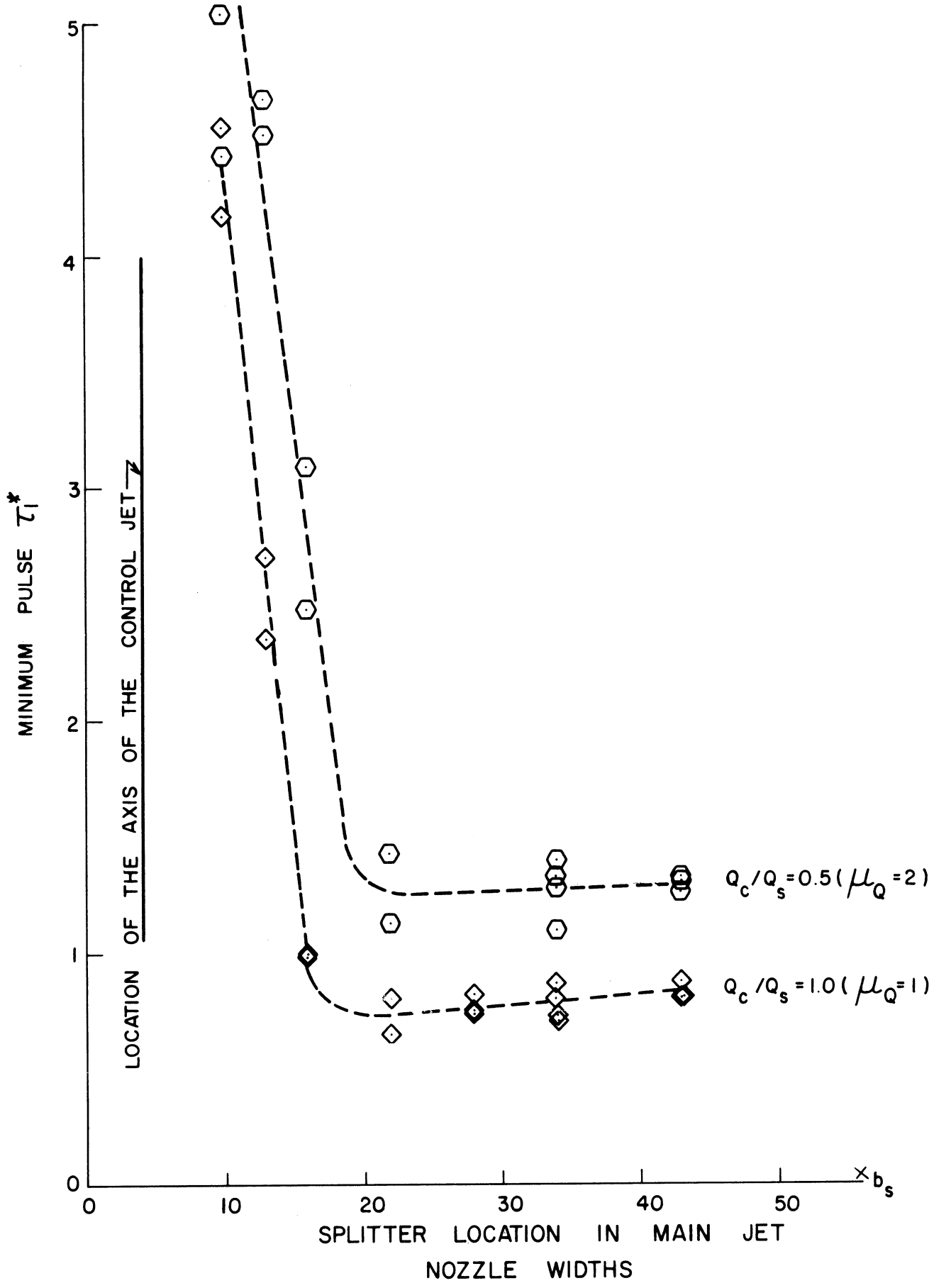

Figure 43. Effect of Splitter Location on the Minimum Pulse to Switch $U_{ref} = U_C$. (Data From Section 3, Appendix E)

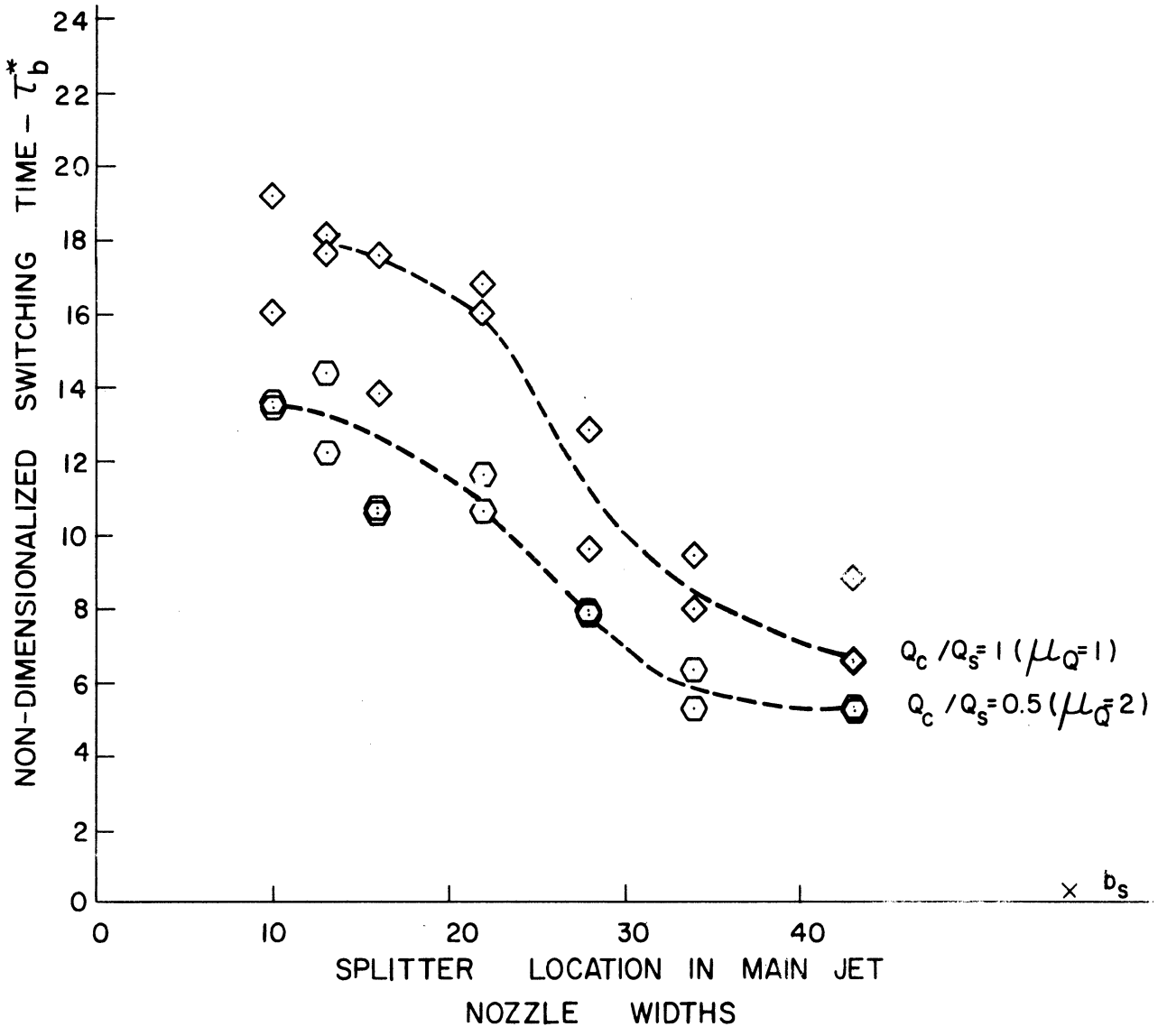

Figure 44. Effect of Splitter Location on τ_b^*, $U_{ref} = U_{control}$. (Data From Section 3, Appendix E)

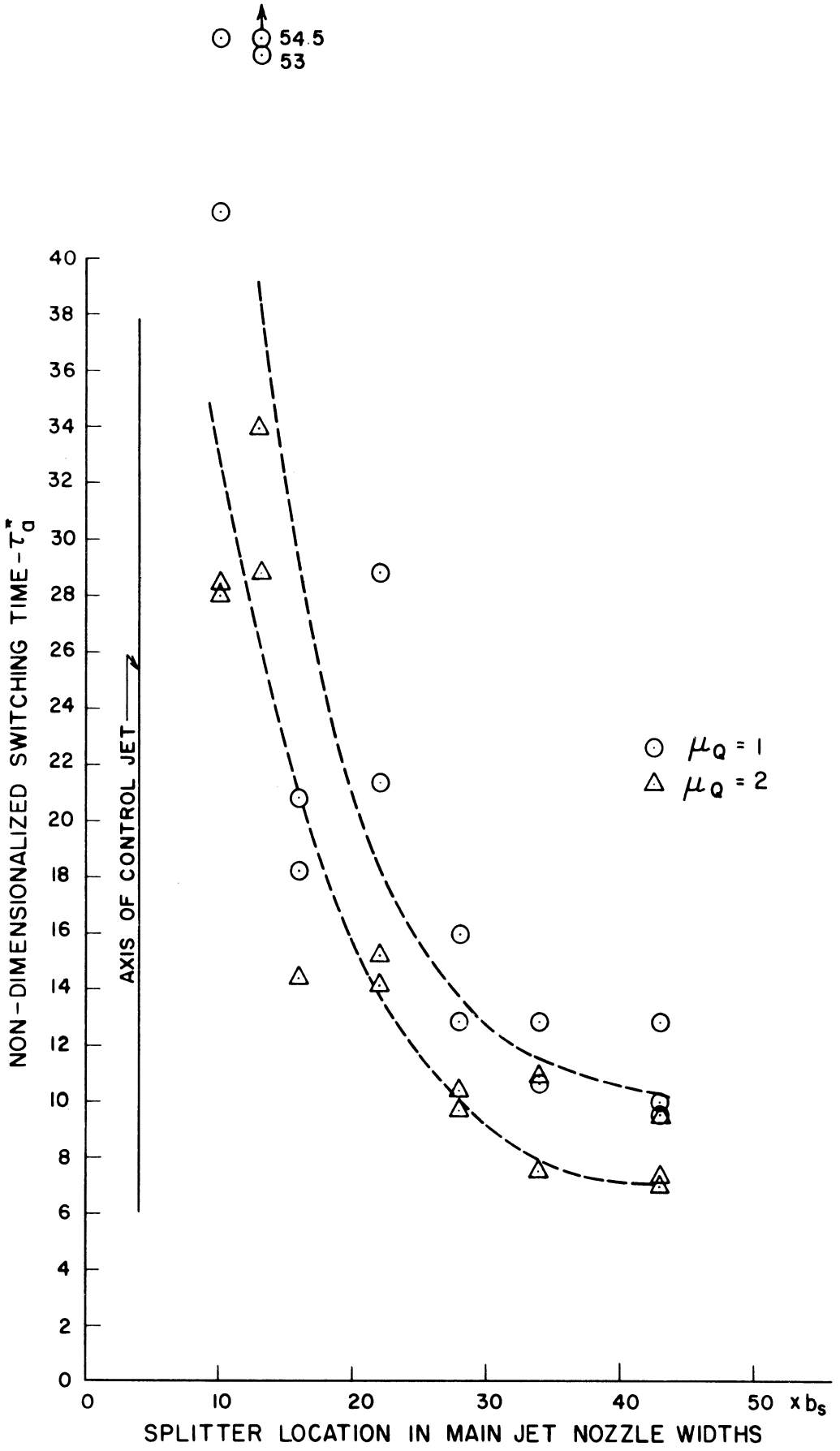

Figure 45. Effect of Splitter Location on τ_a^*, $U_{ref} = U_{control}$. (Data From Section 3, Appendix E)

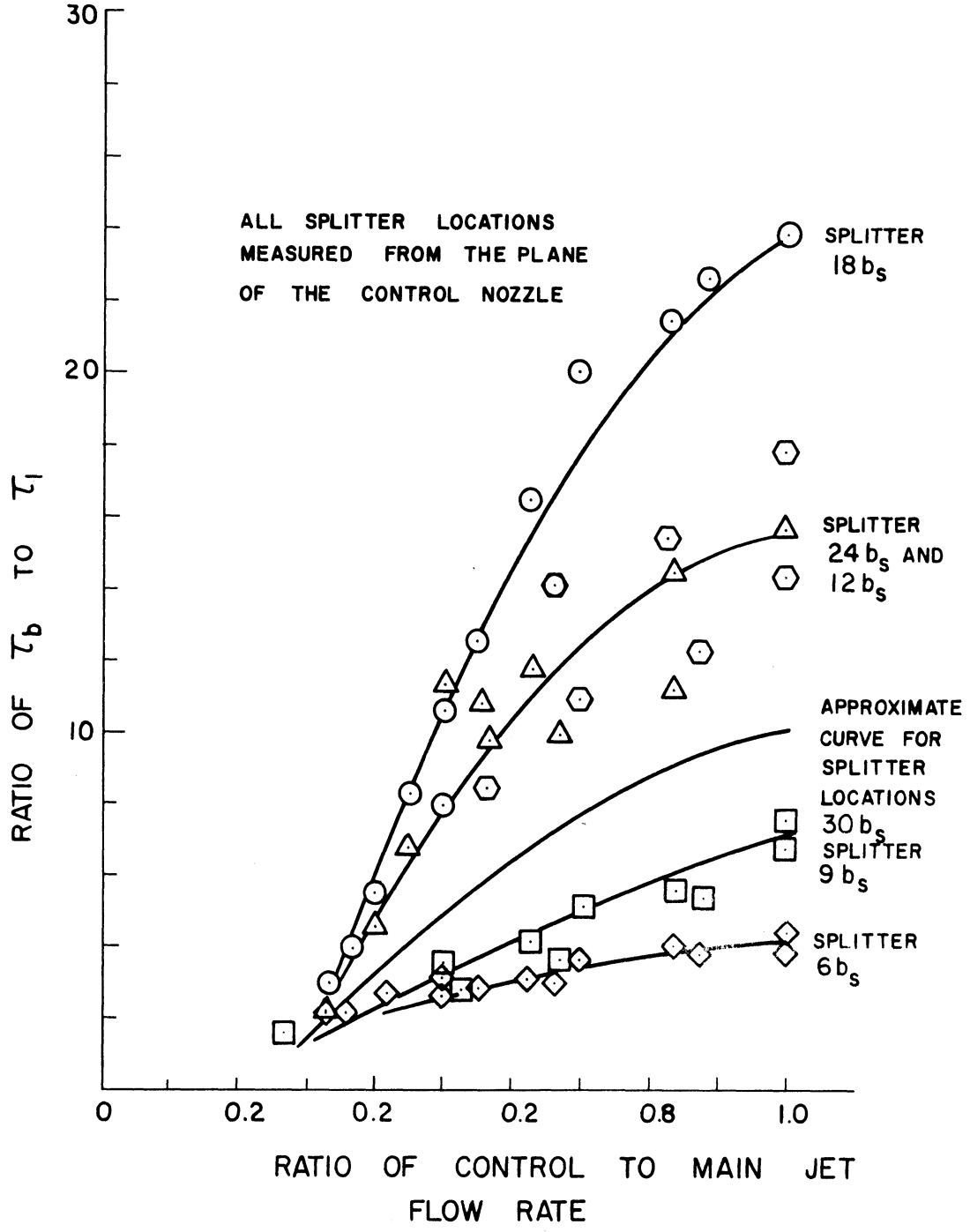

Figure 46. Plots of Ratio of Control to Main Jet Flow Rate Versus (τ_b/τ_1) . (Data From Section 3, Appendix E)

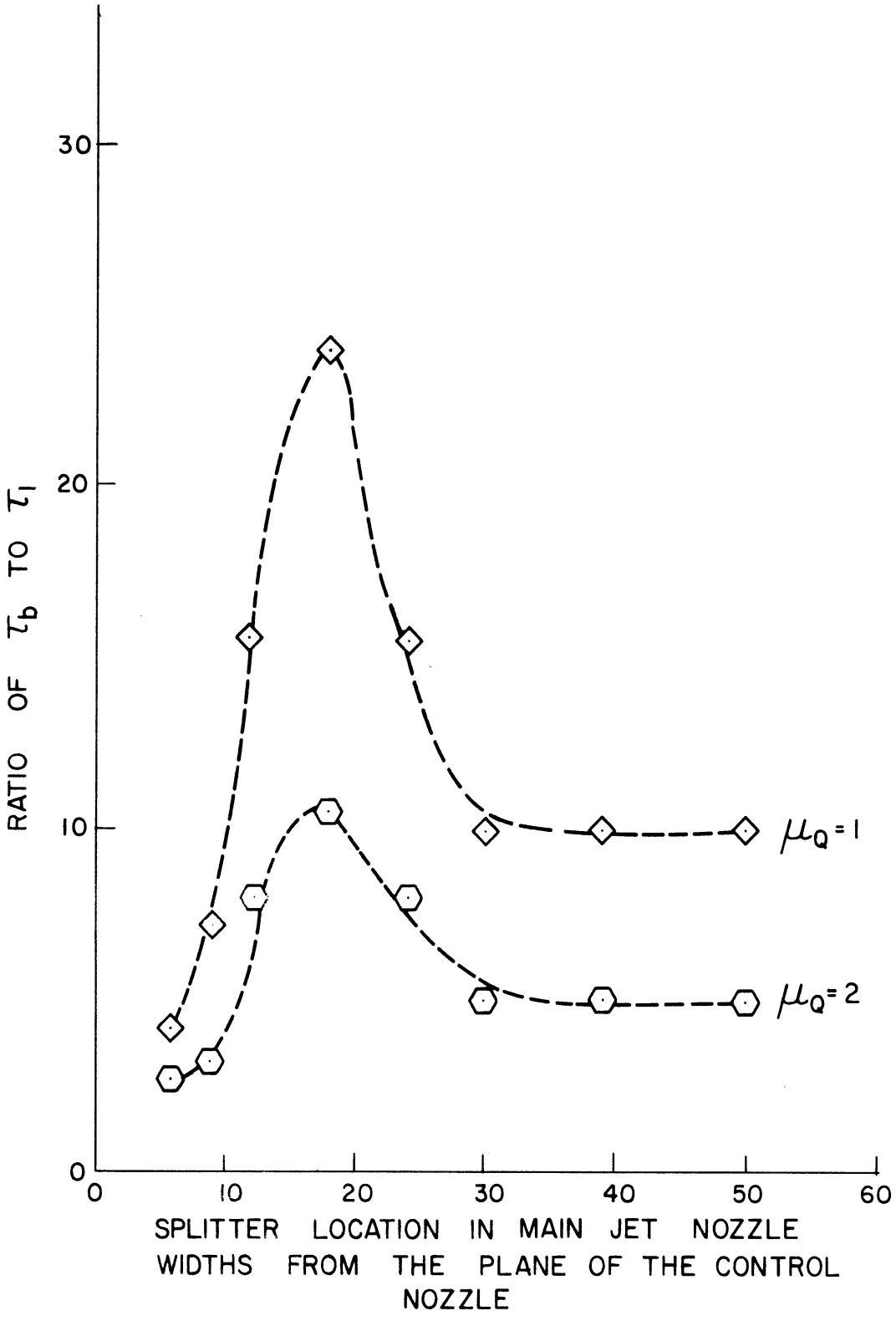

Figure 47. Effect of the Splitter Location on τ_b/τ_1 .

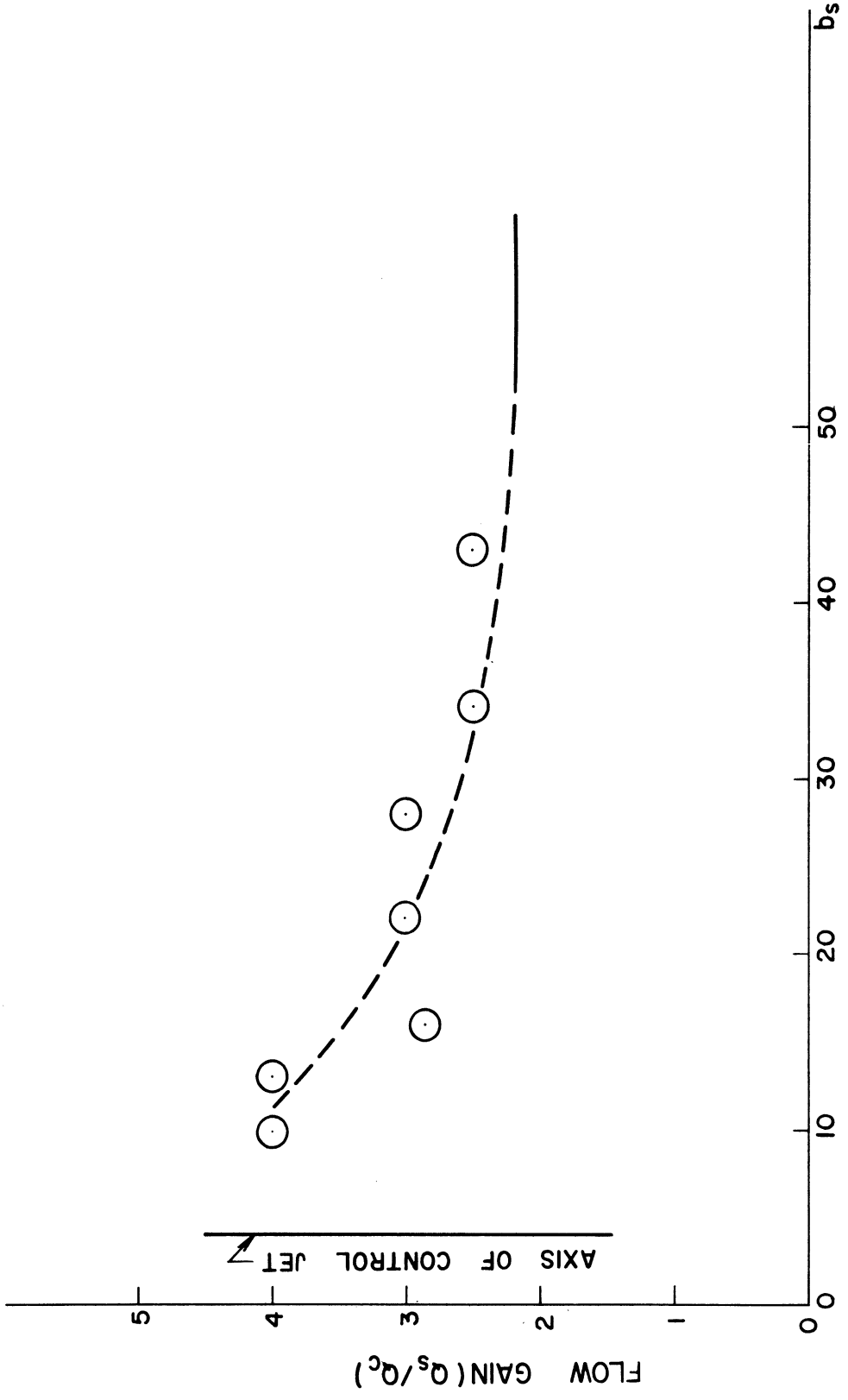

Figure 48. Effect of the Splitter Location on Maximum Dynamic Flow Gain.

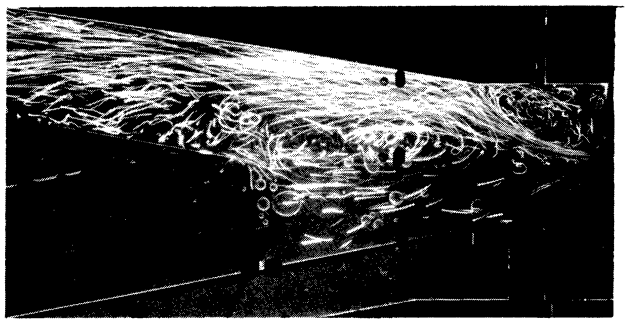

(a)

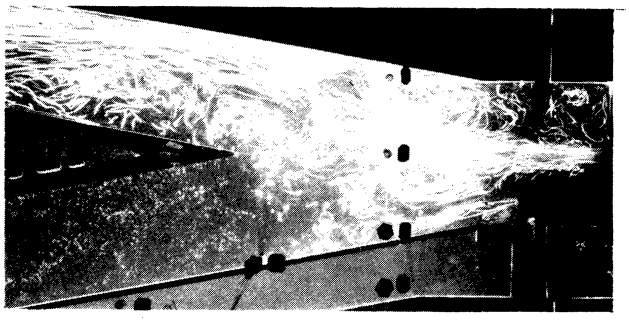

(b)

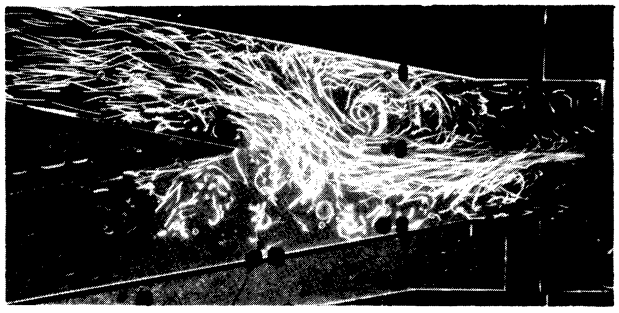

(c)

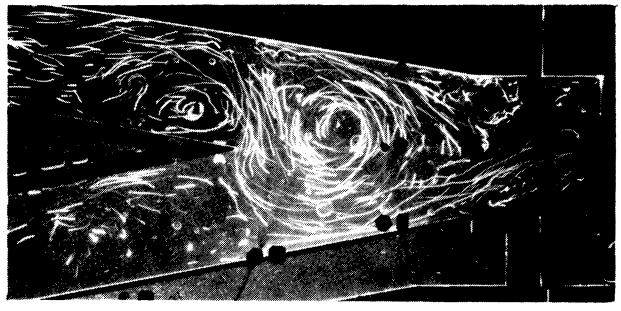

(d)

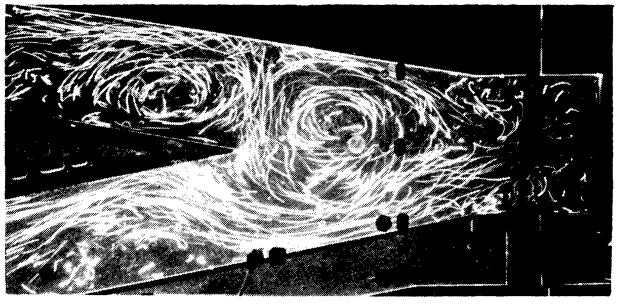

(e)

Figure 49. A Tracer Switching Sequence with the Splitter 18 Main Jet Nozzle Widths From the Control Nozzles.

(Note the Way the Main Jet After Reattachment Fills Up the Receiver Port.)

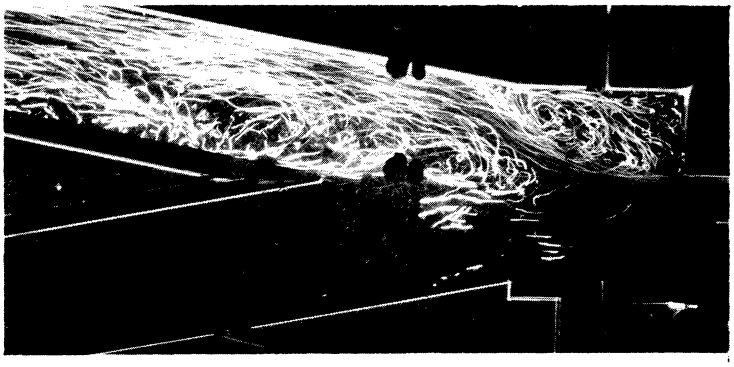

(a)

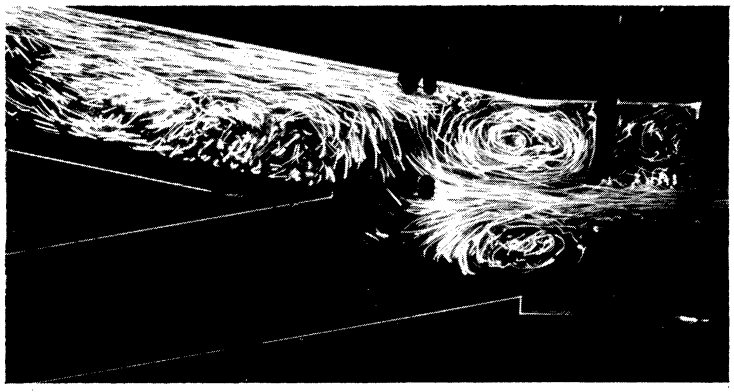

(b)

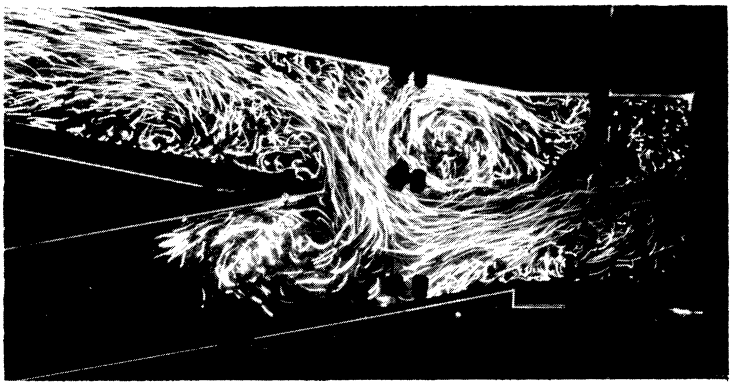

(c)

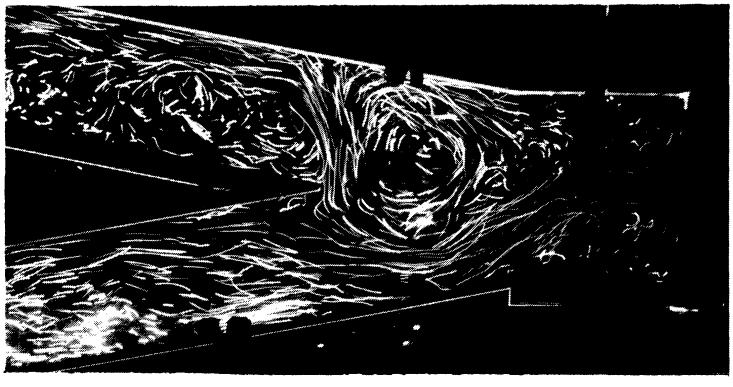

(d)

Figure 50. A Tracer Switching Sequence with the Splitter 12 Main Jet Nozzle Widths from the Axis of the Control Jets.

(e)

Figure 50. (Continued)

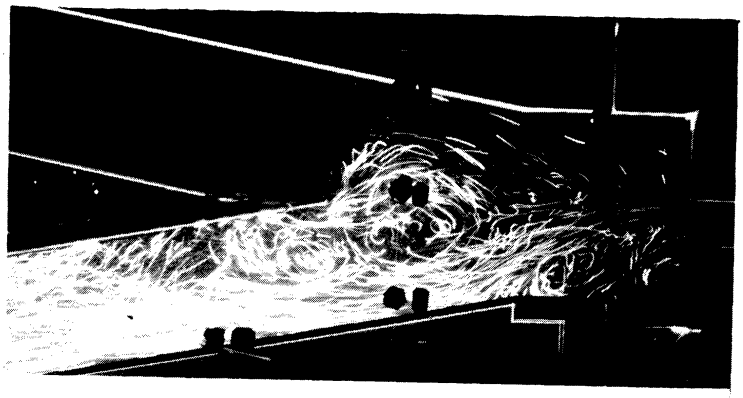

(f)

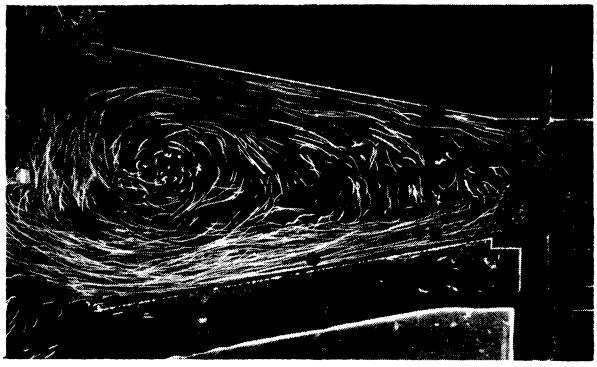

(a) Separator 43 Main Jet Nozzle Widths from the Main Jet

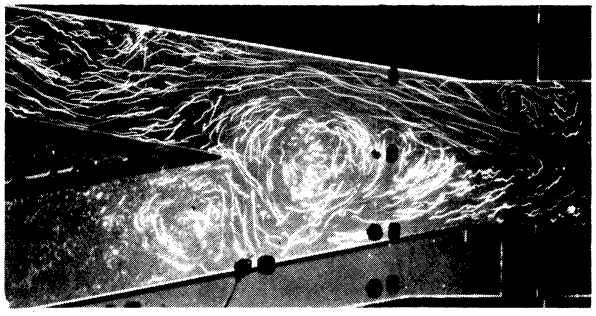

(b) Splitter 22 Main Jet Nozzle Widths from the Main Jet

(c) Splitter 14 Main Jet Nozzle Widths from the Main Jet

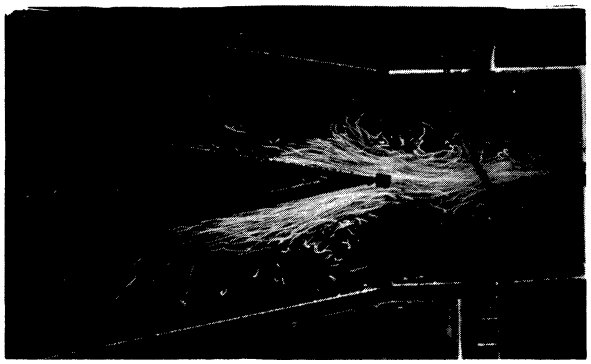

(d) Splitter 8 Main Jet Nozzle Widths from the Main Jet

Figure 51. Nature of the Recirculation Vortices.

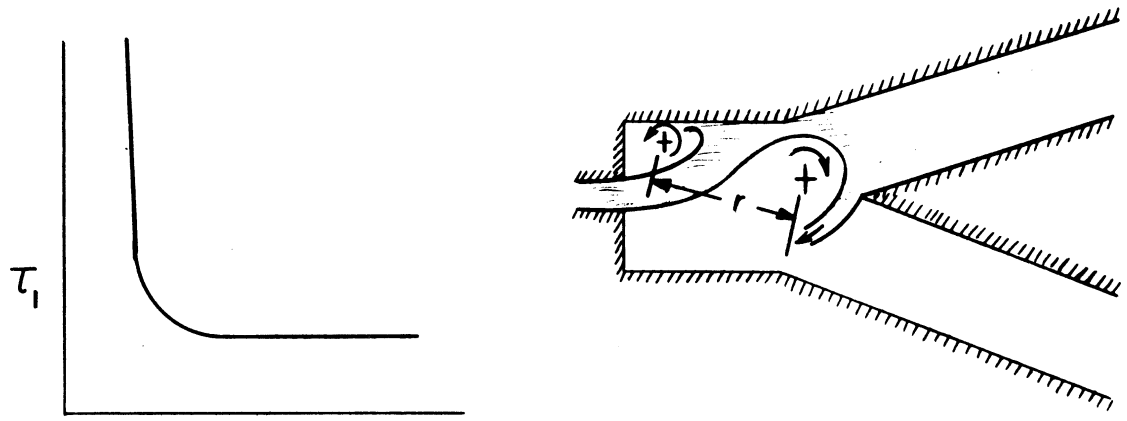

Figure 52. Effect of the Splitter on the Recirculation Vortex.

Thus, the control pulse required to make the vortex in the separation bubble strong enough to destroy the recirculation vortex to bring about switching varies as some function of $\frac{1}{r}$ yielding the curves seen in Figure 43. These vortices and their interaction can be seen clearly in the tracer photographs of the switching sequences presented in Figures 35, 36, 49 and 50. The photographs show switching for a geometry without a splitter and geometries with the splitter located at 18 and 12 nozzle widths from the axis of the control jet. These photographs together with those in Figure 51 clearly show the decrease in the dimensions of the recirculation vortex with an increasing concentration of vorticity as the splitter is moved upstream.

The recirculation vortex also strongly affects the nature of the entrance flow into the receiver ports. In Figure 51-a the vortex has caused the wall jet to attach to the channel separator placed about 40 nozzle widths downstream of the control jets. Photographs in Figures 51-b and 51-c show how the vortex causes the expansion of the reattached

jet to fill the receiver channel giving rise to an adverse pressure gradient in the entrance region of the receiver port. As the splitter is brought upstream, the main jet no longer reattaches and flows down the centerline of the amplifier as seen in Figure 51-d.

From the previously discussed critical point of the experimentally studied amplifier, 16 nozzle widths from the control jets the main jet develops an increasing tendency to oscillate about the centerline of the amplifier before reattaching, if the jet is pushed over to the centerline. Finally about two nozzle widths from the control jets, the main jet definitely ceases to reattach as already mentioned.

Figure 43 also indicates that, as the splitter location is increased beyond the critical point, τ_1 ' shows a slight increase, but it is not absolutely certain that this trend is true.

Figures 44 and 45 show the effect of the splitter location on τ_b and τ_a. While τ_b seems to level off as the splitter is brought closer than 16 nozzle widths from the control nozzle, τ_a is seen to continually increase, a trend that can be clearly discerned despite the scatter in the data.

Even as the switching times increased as the splitter was moved upstream, maximum gain also increased from a value of about 2.5 at a splitter location 39 nozzle widths from the control jet to four at a splitter location of six nozzle widths from the control jets. This increase in maximum gain also means a decrease in the E_o value already discussed. The results for the maximum flow gain are shown in Figure 47.

4. Effect of the Setback on Switching Times

Figures 53 and 54 show plots of τ_1^*, τ_a^* and τ_b^* versus ratio of control to main jet flow rates for data obtained from a limited study of the effect of setback. The data represents two setbacks of zero and four main jet nozzle widths. The data reveals that within the scope of the study the setback does not affect switching times of the bistable fluid amplifier. The reason for this can be given by interpreting the tracer photographs in Figures 35, 36, 49, 50 and 51. It can be seen that the vortex within the separation bubble is largely confined in the zone between the control nozzles and the reattachment point. It is to be emphasized, however, that this result may be restricted to the particular overall geometry chosen for the experimental studies.

5. Effect of the Offset on Switching Times

On the basis of the static characteristics discussed by Bourque and Newman,[7] Levin and Manion[13] and the quasi-steady study of Olson and Stoeffler[12] it would seem that the offset would be one of the critical parameters. This is indeed what is borne out by the present dynamic response studies. Figures 55 through 59 present the data obtained. Due to the magnitude of scatter in the data for τ_a and τ_b the data was not non-dimensionalized and presented in the dimensional form in Figures 58 and 59.

The data for the minimum pulse to initiate switching, τ_1^*, is presented in Figures 55 and 56. The two curves seen represent flow gains μ_Q of 1 and 2. τ_1^* is seen to change very nearly in a linear fashion and decreases as the offset is decreased. Oddly enough the slope

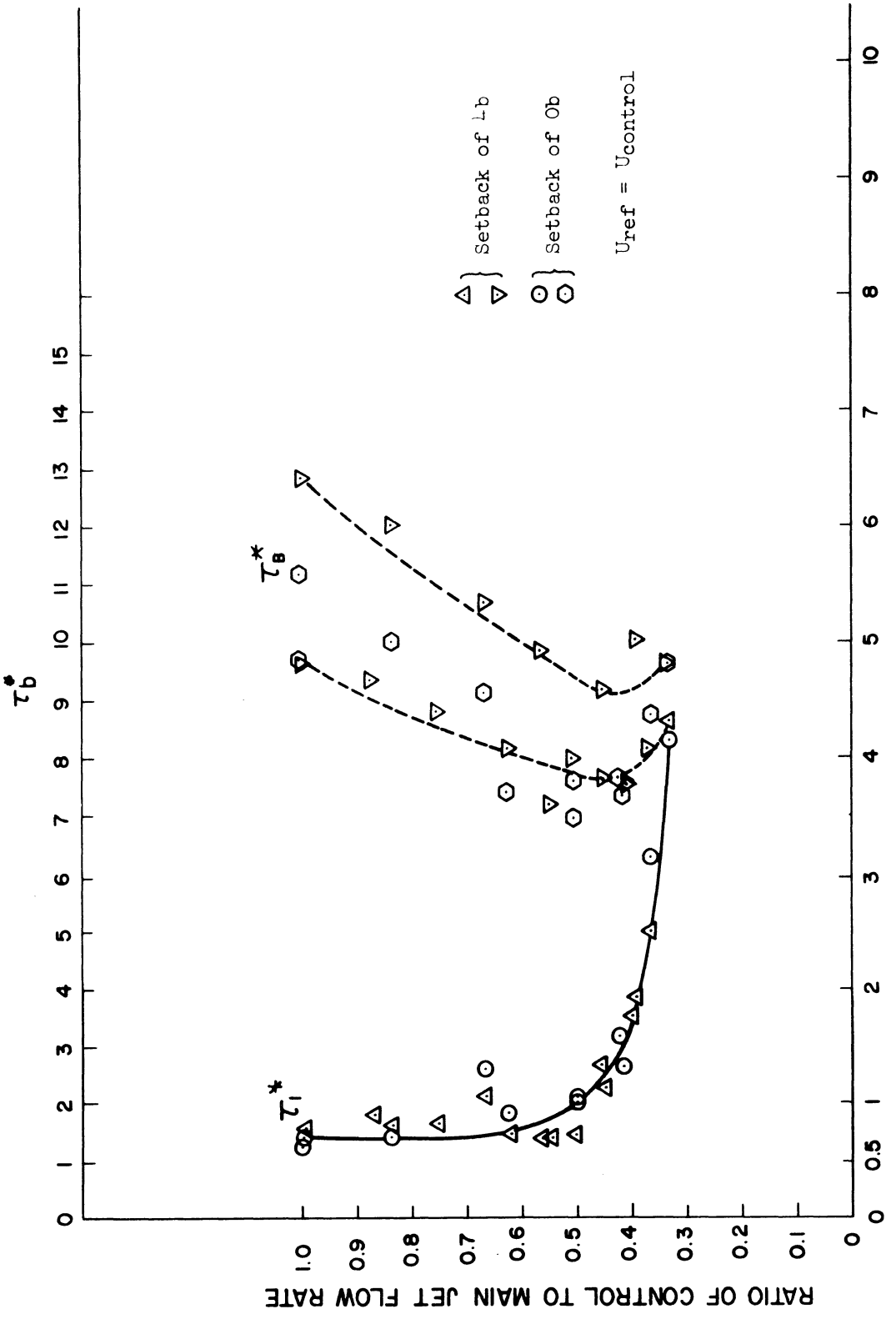

Figure 53. Effect of Setback on Switching Times.

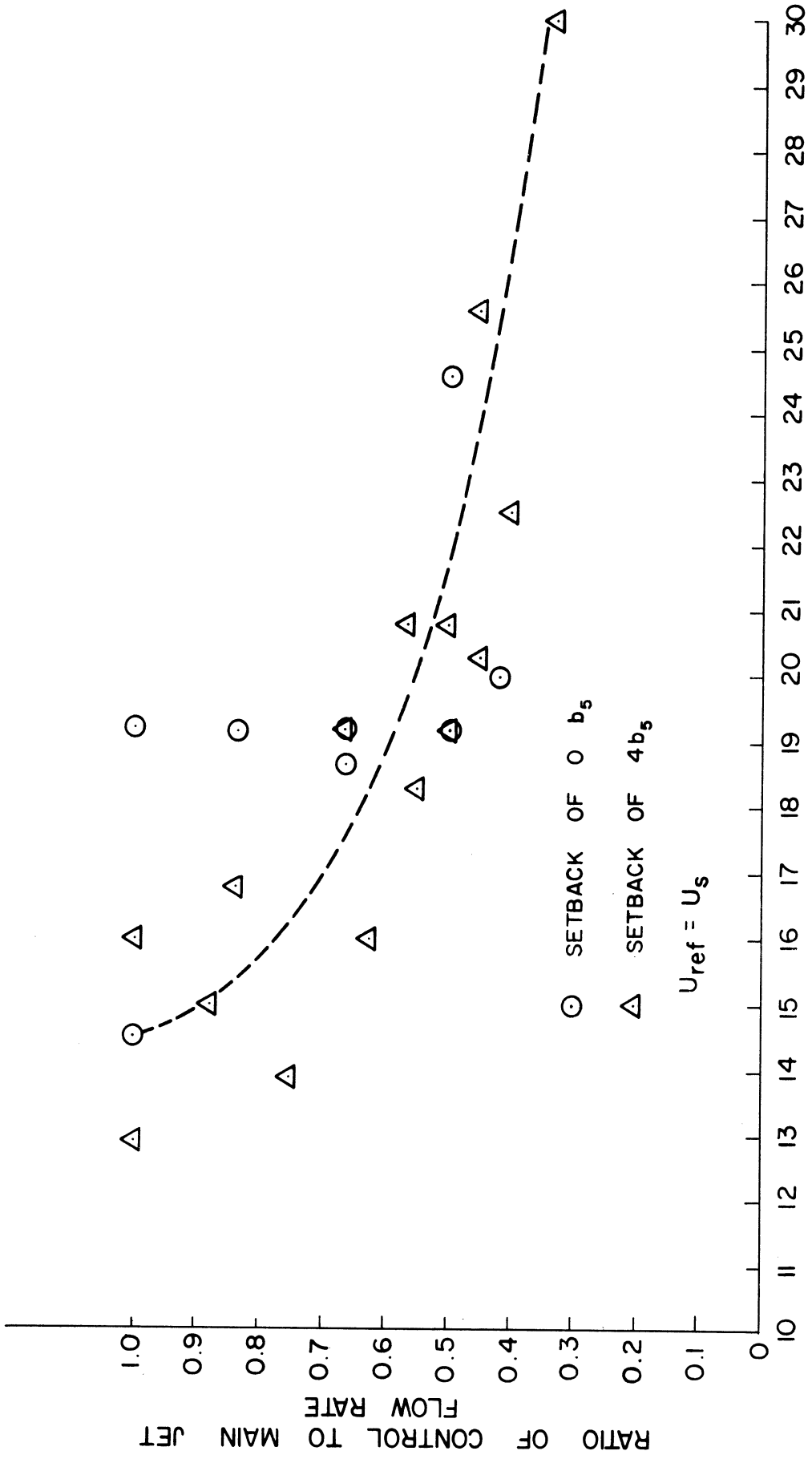

Figure 54. Effect of the Setback on Switching Time τ_a^*.

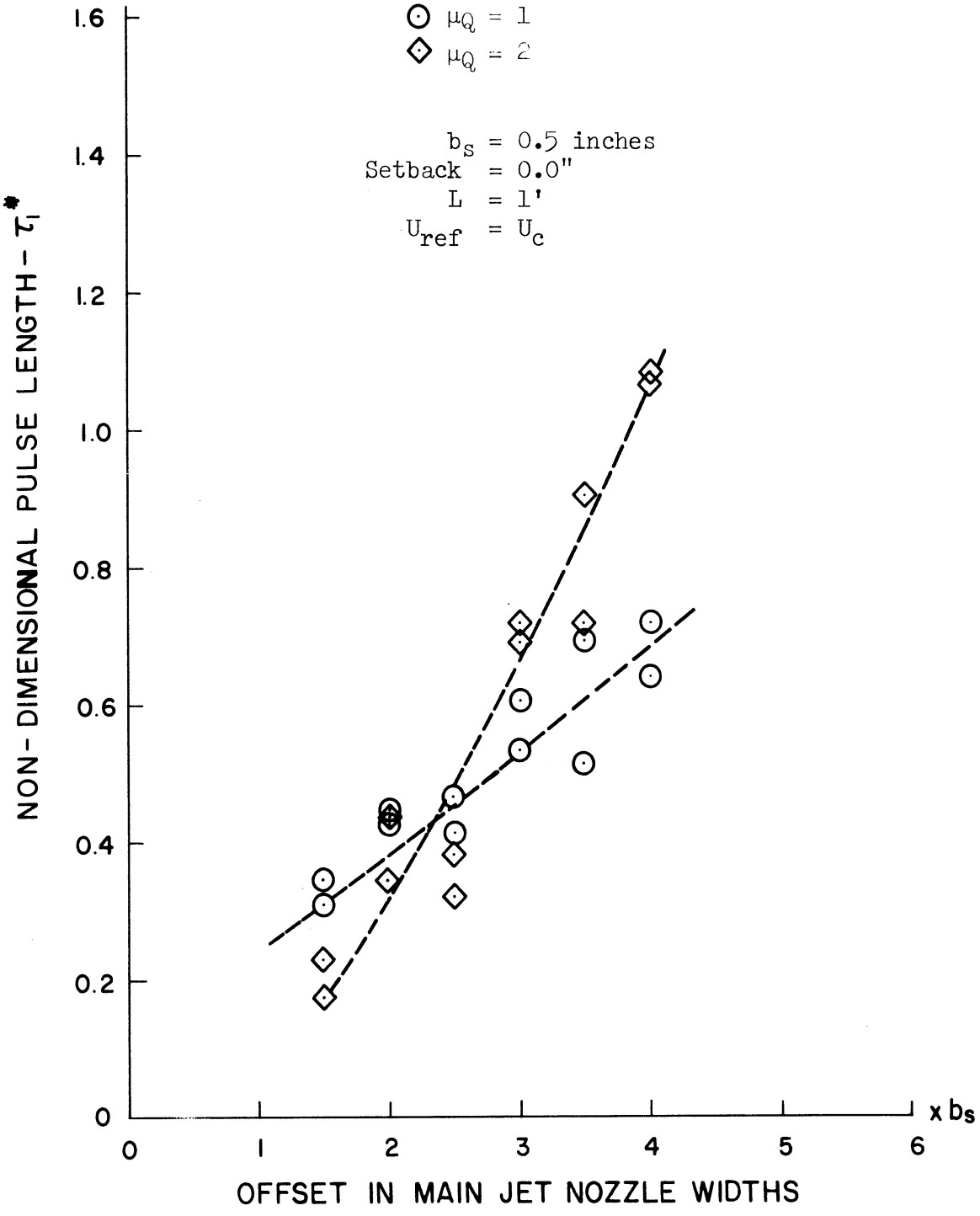

Figure 55. Effect of the Offset on the Non-Dimensional Pulse Length τ_1^* .

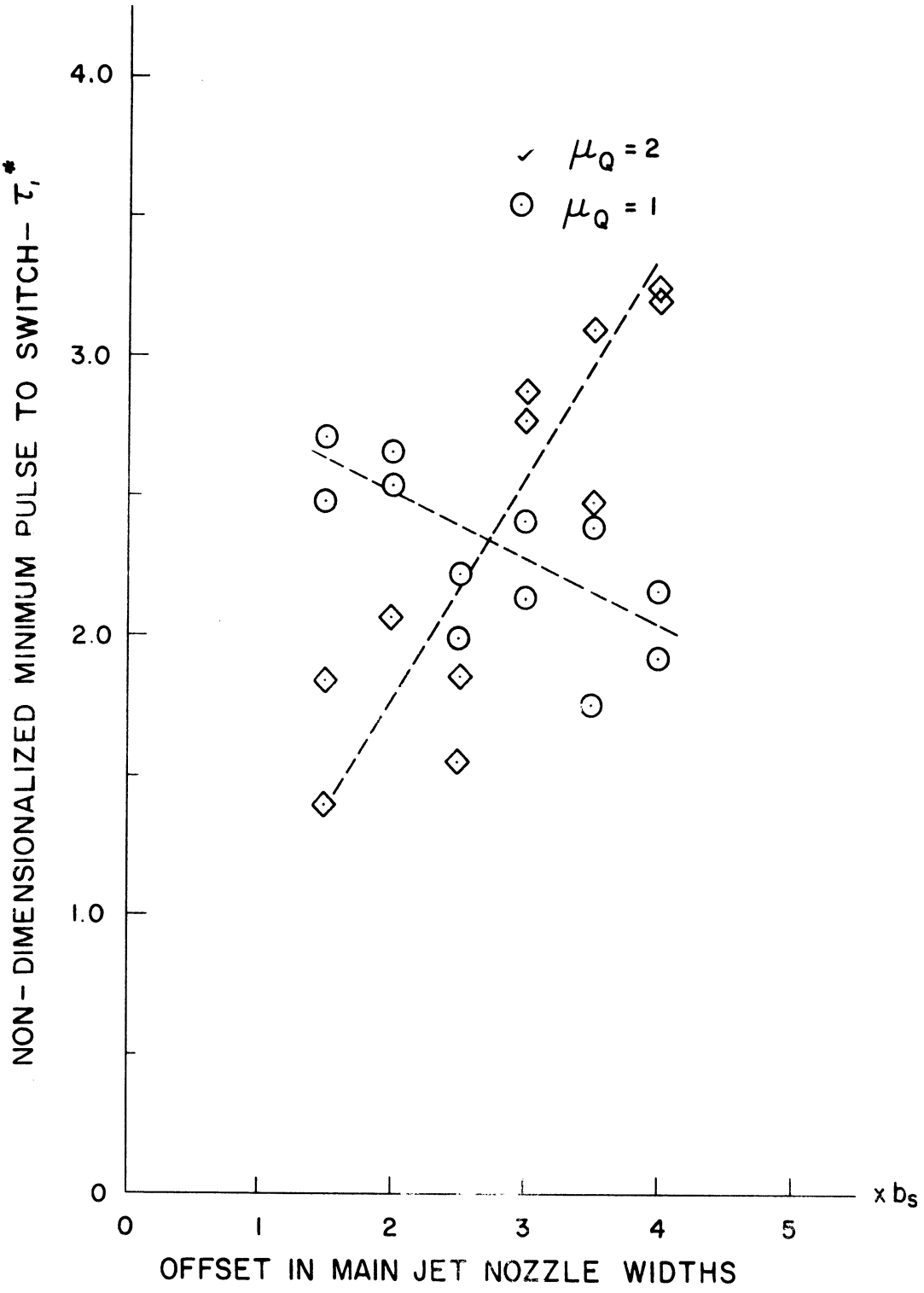

Figure 56. Effect of the Offset on the Non-Dimensional Pulse Length τ_1^* Using L = 2x Offset in Inches $U_{ref} = U_c$.

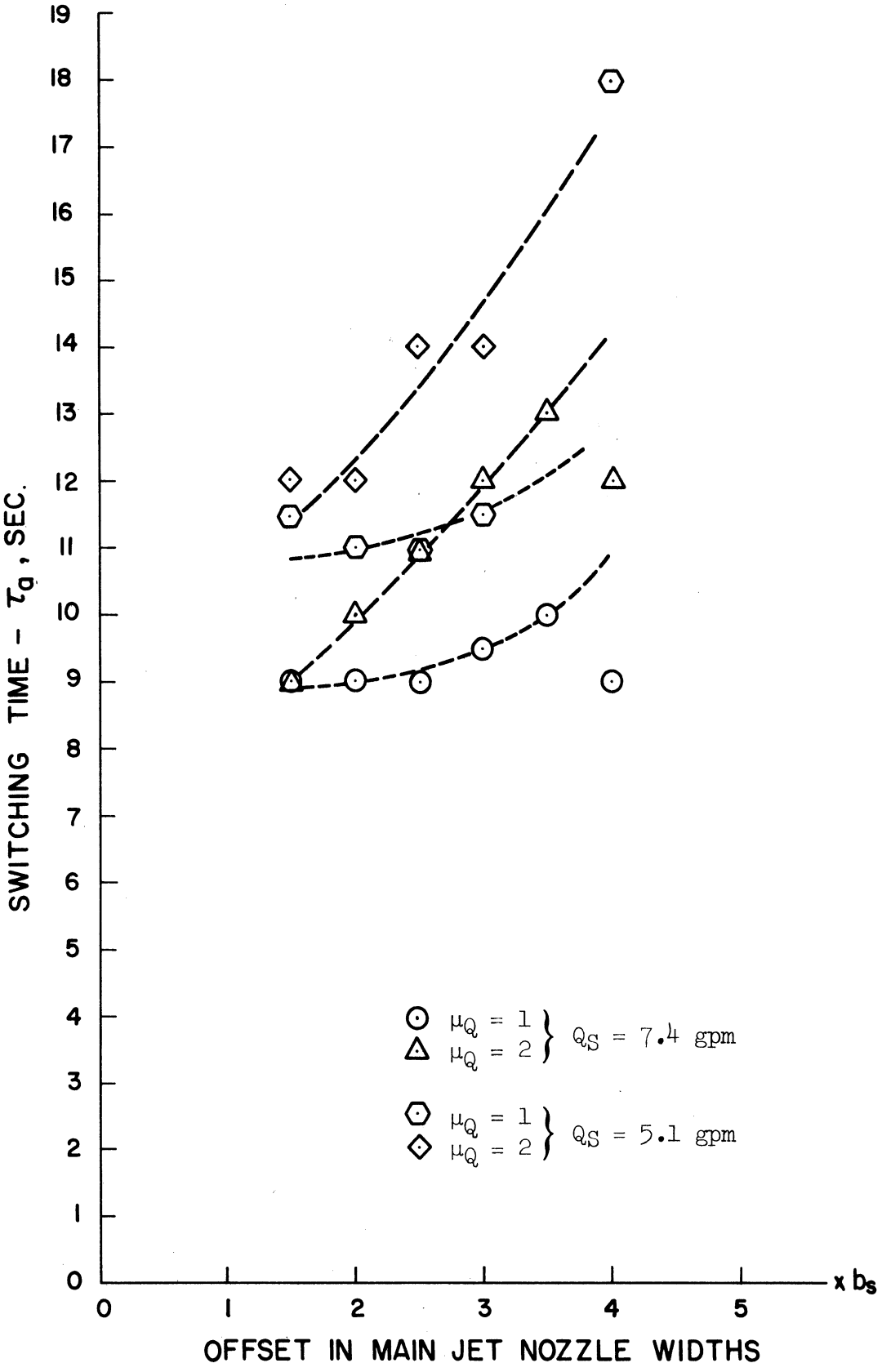

Figure 57. Effect of the Offset On τ_a. (Data From Section 4, Appendix E)

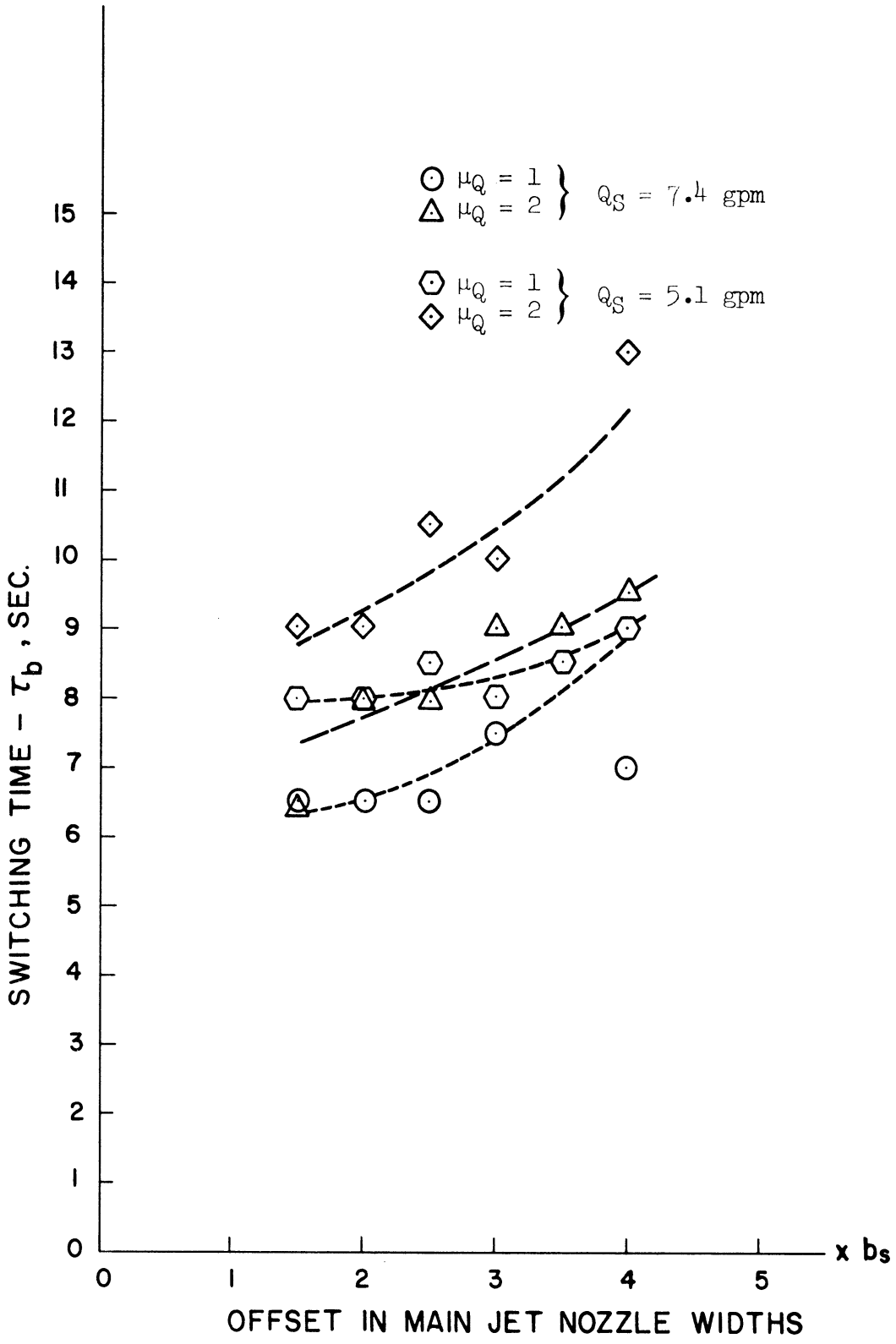

Figure 58. Effect of the Offset on τ_b . (Data From Section 4, Appendix E)

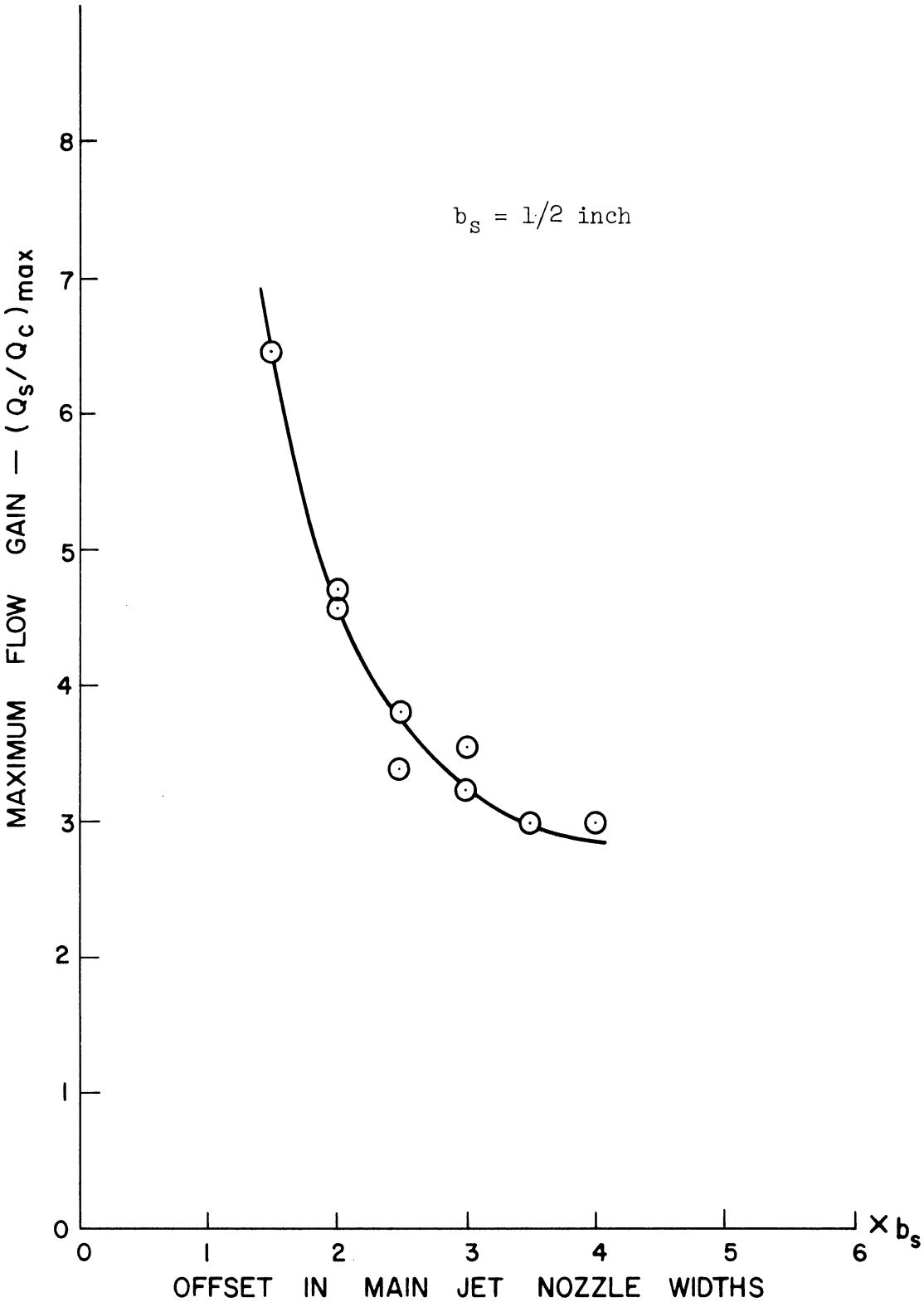

Figure 59. Maximum Dynamic Flow Gain of a Bistable Fluid Amplifier in Relation to the Offset.

of the line $\mu_Q = 2$ is greater than the slope of the line for $\mu_Q = 1$ and the two lines cross in the vicinity of the offset of 2.5 nozzle widths. The chief purpose of Figure 56 was to test a logical choice for L by setting L equal to the width of the interaction zone (twice the offset). The figure shows that the transport time based on the interaction zone is no more useful than if it were based some arbitrary length as in Figure 55. Thus it seems that it is not possible to pick out any one given geometric parameter in a bistable fluid amplifier as being the key parameter.

Figures 57 and 58 depict the effect of reducing the offset on τ_a and τ_b. As with τ_1, both τ_a and τ_b are seen to decrease as the offset is reduced. Also evident is that the slopes of the curves for $\mu_Q = 2$ are greater than the curves for $\mu_Q = 1$. Hence, the switching times for both flow gains tend to become equal in the vicinity of the offset of one nozzle width.

The effect of reducing the offset on the maximum dynamic flow gain is seen in Figure 59. The maximum flow gain is seen to increase from a value of about 3 to 6.5 as the offset is reduced from 4 to 1.5 main jet nozzle widths. Interpretation of these results in terms of E_o shows how the reduced offset decreases E_o, pointing up once again the interaction of the various geometric parameters.

These results seem to concur with the predictions made using static characteristics in that reducing the offset tends to increase the effectiveness of the control flow.

6. Results of a Limited Study in Changing Scales

In order to check out the non-dimensionalization parameters chosen, a limited study of effect of changing scale was conducted. Three models

were tested, full scale model of one inch main jet nozzle width, three quarter scale model of 3/4 inch main jet nozzle and half scale model with 1/2 inch main jet nozzle. These data are presented in Figures 60, 61 and 62. It is seen that the definition of the transport time used to non-dimensionalize τ_1 seems to work quite well, whereas transport times based on either the control or the main nozzle velocities seem to correlate τ_a and τ_b. The scatter in the data although considerable seems to bear this out except for the square boxed data with crosses in it. These data points correspond to a main jet setting of a Reynolds number of 6000 at 65°F. These points while retaining the general trend seem to be translated by 4 units. Aside from this anomaly, further confidence in the data can be had by an order of magnitude comparison with the data of Muller presented in Figures 12 and 13. These latter data taken in a model 1/5 the size of the model in the present study correspond to Reynolds numbers of 5,500 and 10,000 respectively; however, a direct comparison cannot be made as Muller's data is correlated with the ratio of control to main jet pressures and not the flow rates.

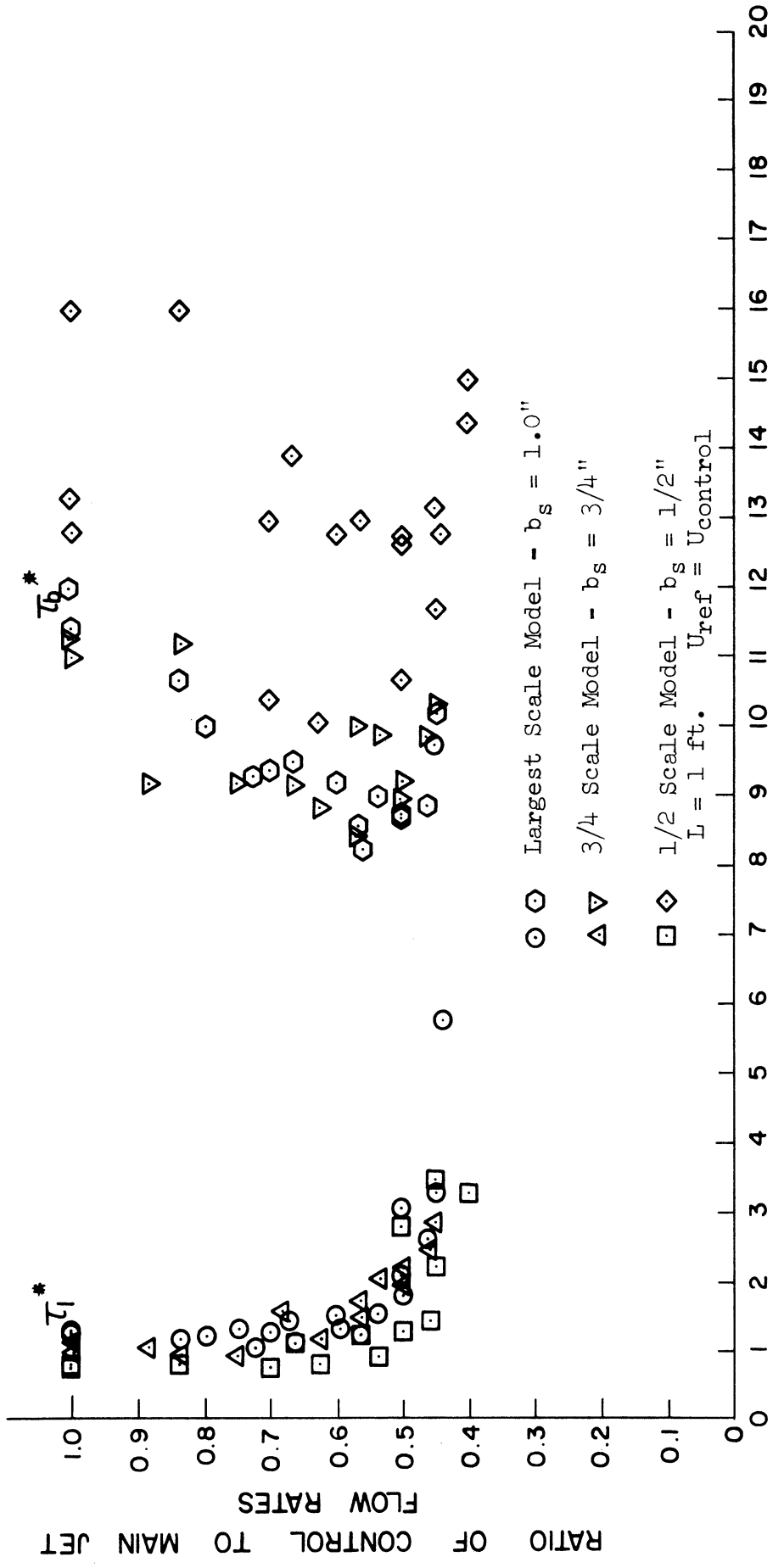

Figure 60. Effect of Changing Model Scale On τ_1^* and τ_b^*.

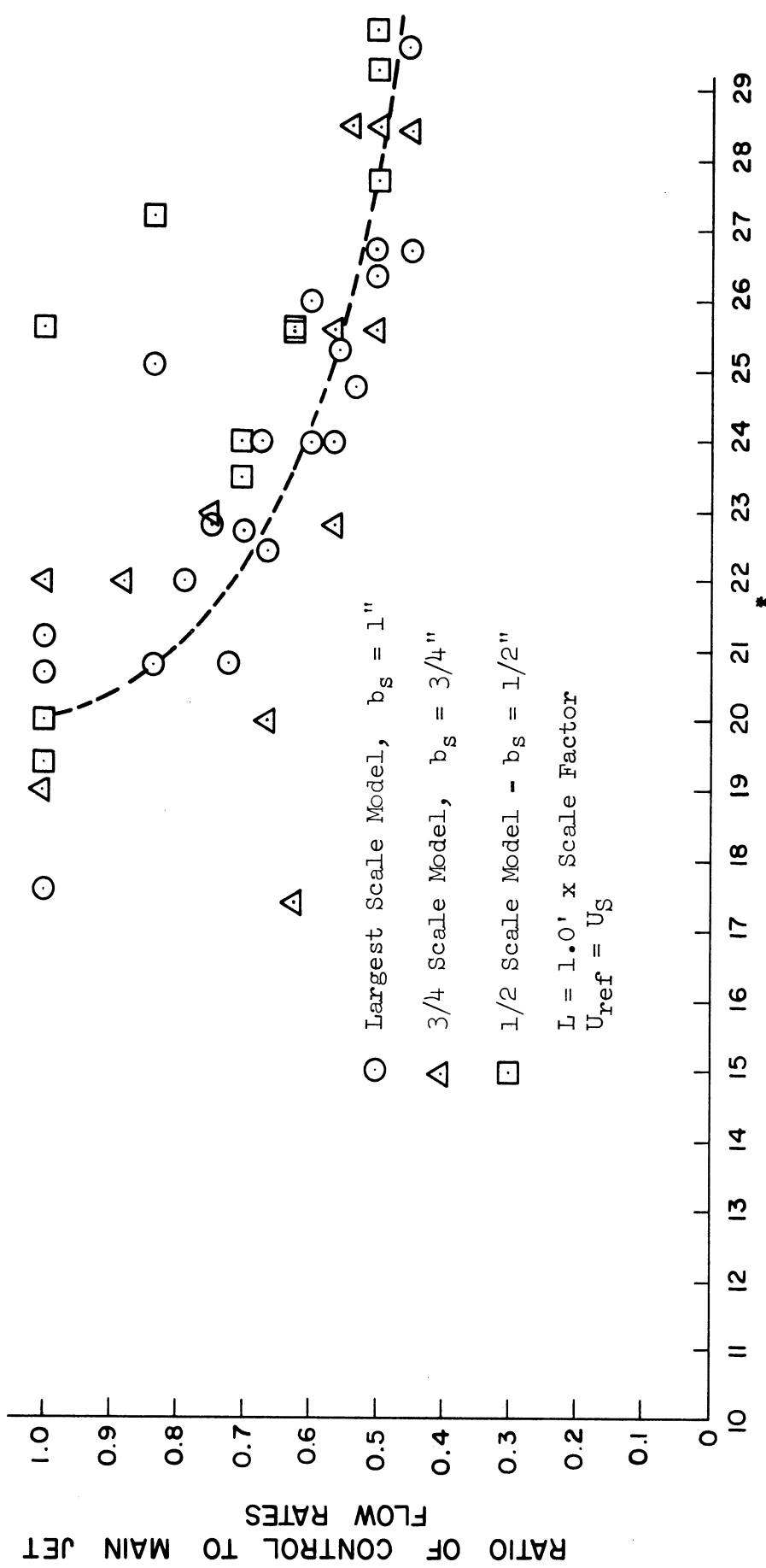

Figure 61. Effect of Changing Model Scale On τ_a^*.

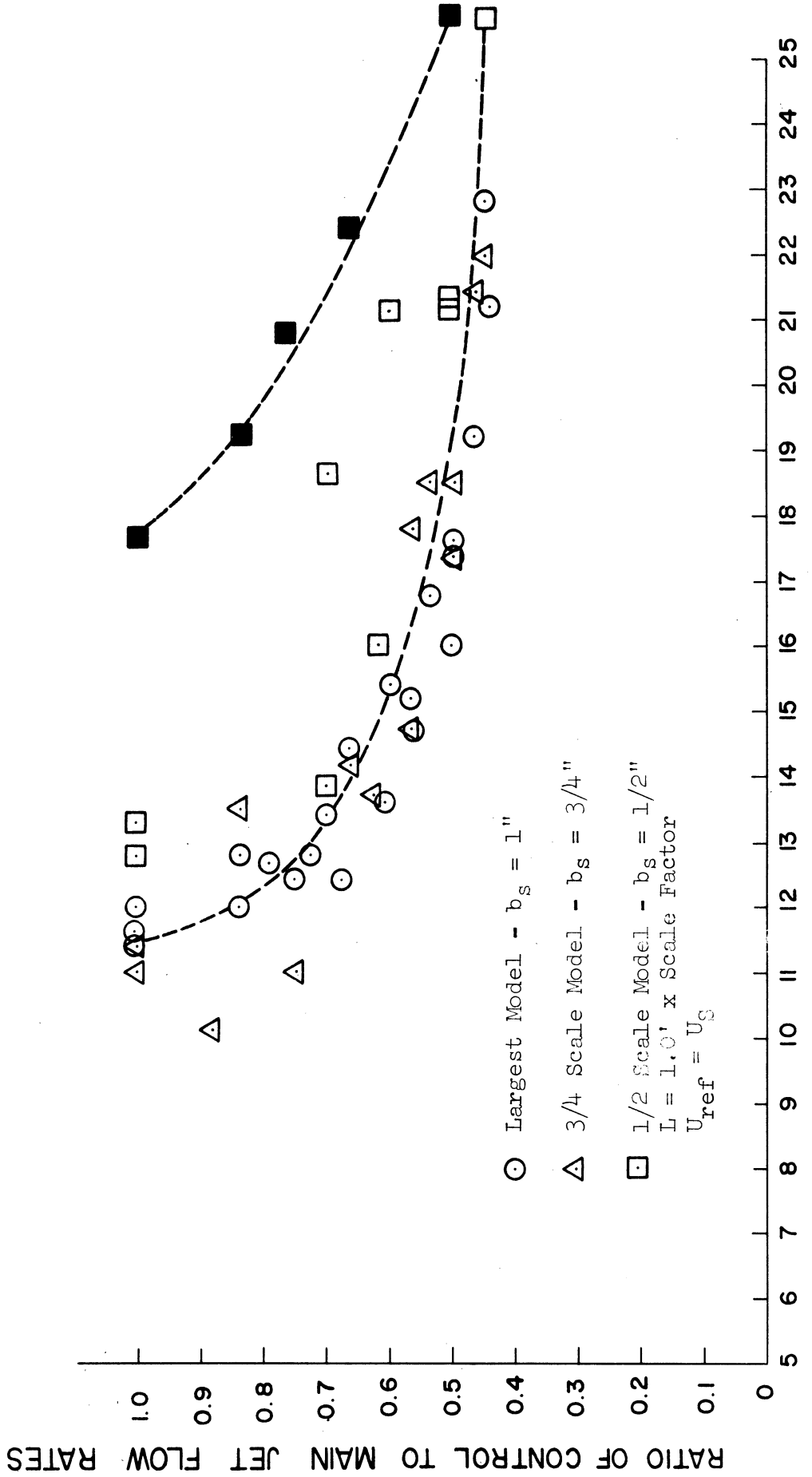

Figure 32. Effect of Changing Model Scale On τ_b .

CHAPTER V

CONCLUSIONS

Presented in this chapter is a summary of the conclusions drawn from the experimental results and discussion in Chapter IV:

1. Switching time is a function of the control pulse length and varies inversely to it.
2. Associated with a given overall geometry, all of whose parameters are fixed except the ratio of control to main jet nozzle width, is the minimum level of control to main jet momentum ratio E_o below which switching is not possible. For the experimental model without a splitter the E_o value was 0.2.
3. Switching times increase as the splitter is moved closer to the control jet (main jet) nozzles.
4. The minimum pulse to switch and the ratio τ_b/τ_1 change abruptly as the splitter is moved closer than 16 main jet nozzles widths to the control jets and the main jet shows an increasing tendency to oscillate about the splitter from about this point.
5. The main jet ceases to reattach when the splitter is about two main jet nozzle widths from the control jets.
6. Reducing the offset results in a near linear decrease in the minimum pulse to switch together with a decrease in switching times.
7. Reducing the offset significantly increased the maximum dynamic flow gain of the amplifier.
8. Setback had a negligible effect on the switching performance.

9. The qualitative studies clearly show the importance of the interaction between the vortices in the separation bubble and the recirculation region.

10. The qualitative studies also show that switching is not a separation phenomena but rather the growth of the vortex in the separation bubble and that the role of the control jet is to augment the vortex in the separation bubble until the vortex reaches a threshold strength from which its growth is self-sustaining.

APPENDICES

APPENDIX A

A METHOD OF REDUCING THE PROBLEM OF A CURVED FREE JET TO THAT OF A STRAIGHT JET

Introduction

Recently, due to the impact of the fluid jet amplifiers, considerable effort has been expended in studying reattaching jets. In such phenomena one necessarily has to deal with a curved jet or jet boundary and although Prandtl, as early as 1929, had argued that there should be a considerable effect of curvature on the entrainment rate of the jet, up to now most of the studies conducted have had the tendency to either ignore or not adequately take this effect into account. A notable exception to this is the attempt by Sawyer[9] who carried out a modification to the Bourque-Newman[7] analysis of the attached jet by a semiempirical means.

Sawyer in 1962 conducted several studies dealing with turbulent wall jets flowing over specially constructed surfaces designed to maintain the ratio of the jet thickness b to the radius of curvature R at a constant value along the length of the jet. Sawyer's data revealed that, for b/R of the order of 0.05, the rate of spread of the curved jet was increased or decreased by approximately 50% as compared with a plane wall jet for a convex or concave surface respectively.

In light of this, it was somewhat surprising that the curved submerged jet had seemingly the same rate of spread as the plane, straight jet and seemed to exhibit a symmetry. Sawyer, therefore, concluded that there must be a flow across the centerline in order to obtain the seeming symmetry of the velocity profile.

The object of this brief study is to present, using an adaptation of Prandtl's mixing length hypothesis, a method of analyzing in the boundary layer sense, turbulent, curved free shear flow whose axis is curved along the arc of a circle of a radius R .

Theory for a Curved Jet of Radius R

Consider the Navier-Stokes and Continuity equations in polar coordinates for steady, incompressible flow field, neglecting body forces:

With u = tangential component and v = radial component of velocity, equations of motion are

$$\frac{\partial v}{\partial r} + \frac{v}{r} + \frac{1}{r}\frac{\partial u}{\partial \theta} = 0 \tag{1}$$

$$\rho\left(\frac{u}{r}\frac{\partial u}{\partial \theta} + v\frac{\partial u}{\partial r} + \frac{uv}{r}\right) = -\frac{1}{r}\frac{\partial p}{\partial \theta} + \mu \nabla^2 u \tag{2}$$

$$\rho\left(\frac{u}{r}\frac{\partial v}{\partial \theta} + v\frac{\partial v}{\partial r} - \frac{u^2}{r}\right) = -\frac{\partial p}{\partial r} + \mu \nabla^2 v \tag{3}$$

Consider now the following transformations

$$r = R + y \qquad R\theta = x$$

where R is the radius of curvature of the axis of the free shear layer flow, and thus obtain

$$\frac{R}{R+y}\frac{\partial u}{\partial x} + \frac{\partial v}{\partial y} + \frac{v}{R+y} = 0 \tag{4}$$

$$\begin{aligned}\frac{R}{R+y}u\frac{\partial u}{\partial x} + v\frac{\partial u}{\partial y} + \frac{uv}{R+y} = &-\frac{R}{R+y}\frac{1}{\rho}\frac{\partial p}{\partial x} + \nu\frac{R^2}{(R+y)^2}\frac{\partial^2 u}{\partial x^2} \\ &+ \frac{\partial^2 u}{\partial y^2} + \frac{1}{R+y}\frac{\partial u}{\partial y} - \frac{u}{(R+y)^2} + \frac{2R}{(R+y)^2}\frac{\partial v}{\partial x} \\ &- \frac{R}{(R+y)^3}\frac{dR}{dx}v + \frac{Ry}{(R+y)^3}\frac{dR}{dx}\frac{\partial u}{\partial x}\end{aligned} \tag{5}$$

$$\frac{R}{R+y} u \frac{\partial v}{\partial x} + v \frac{\partial v}{\partial y} - \frac{u^2}{R+y} = - \frac{1}{\rho} \frac{\partial p}{\partial y} + \nu \{...\} \tag{6}$$

Making the substitution

$$W = \frac{Ru}{R+y}$$

and considering for the time being the case of a turbulent jet, where R is at best a function of time ($R=R(t)$ only). Having assumed a turbulent free shear flow (that is the region of interest is devoid of solid boundaries and associated laminar sublayer) the effect of viscosity may be neglected (as a result of which the characteristics of the flow are independent of the effects of Reynolds number over a very broad range). Further, if R is sufficiently large the pressure gradient in the x direction maybe neglected (See Appendix C).

The equations of motion are reduced to:

$$W \frac{\partial W}{\partial x} + v \frac{\partial W}{\partial y} + \frac{Wv}{R+y} = - \frac{Wv}{R+y} \tag{8}$$

$$W \frac{\partial v}{\partial x} + v \frac{\partial v}{\partial y} - \frac{W^2(R+y)}{R^2} = - \frac{1}{\rho} \frac{\partial p}{\partial y} \tag{9}$$

$$\frac{\partial W}{\partial x} + \frac{\partial v}{\partial y} + \frac{v}{R+y} = 0 \tag{10}$$

Retaining only the terms of significance to the jet boundary layer, Equations 8 through 10 are reduced to

$$W \frac{\partial W}{\partial x} + v \frac{\partial W}{\partial y} = 0 \tag{11}$$

$$\frac{\partial p}{\partial y} = \frac{\rho W^2(R+y)}{R^2} \tag{12}$$

$$\frac{\partial W}{\partial x} + \frac{\partial v}{\partial y} = 0 \tag{13}$$

The assumption of large R compared to the boundary layer thickness is therefore further emphasized.

Multiplication of (13) by W and manipulation of the resulting equation results in

$$\frac{\partial W^2}{\partial x} + \frac{\partial Wv}{\partial y} = W \frac{\partial W}{\partial x} + v \frac{\partial W}{\partial y} \tag{14}$$

Hence by noting Equation 11, Equation 14 is reduced to

$$\frac{\partial W^2}{\partial x} + \frac{\partial Wv}{\partial y} = 0 \tag{15}$$

Decomposing the turbulent velocity components into mean and fluctuating parts

$$W = \overline{W} + W' \tag{16}$$

$$v = \overline{v} + v' \tag{17}$$

and introducing these into (12), (13), (15) and neglecting the higher order terms and considering averages with respect to time it is seen that

$$\overline{W}' = 0$$

$$\overline{v}' = 0$$

Hence the equations of motion become

$$\frac{\partial \overline{W}^2}{\partial x} + \frac{\partial \overline{W}\overline{v}}{\partial y} + \frac{\partial \overline{W'v'}}{\partial y} = 0 \tag{18}$$

$$\frac{\partial p}{\partial y} = \rho \overline{W}^2 \frac{R+y}{R^2} \tag{19}$$

$$\frac{\partial \overline{W}}{\partial x} + \frac{\partial \overline{v}}{\partial y} = 0 \tag{20}$$

Thus (16) and (17) identically satisfy continuity.

Equation 18 may be transformed back again to

$$W \frac{\partial W}{\partial x} + v \frac{\partial W}{\partial y} = - \frac{\partial \overline{W'v'}}{\partial y} \tag{21}$$

(the bars representing average values for W,v have been dropped).

Again, two dimensional, steady, incompressible isobaric flow may be represented by

$$W \frac{\partial W}{\partial x} + v \frac{\partial W}{\partial y} = \frac{1}{\rho} \frac{\partial \tau_{xy}}{\partial y} \tag{22}$$

where τ_{xy} is the shear stress in the plane $\perp$ to the z-axis.

As in the theory of Prandtl $\rho\overline{W'v'}$ may be identified with the shear stress τ_{xy}. Hence by analogy to Prandtl's mixing length theory Equation (22) may be written as

$$W \frac{\partial W}{\partial x} + v \frac{\partial W}{\partial y} = \pm 2cx^2 \frac{\partial W}{\partial y} \frac{\partial^2 W}{\partial y^2} \tag{23}$$

as in Prandtl's first theory or as

$$W \frac{\partial W}{\partial x} + v \frac{\partial W}{\partial y} = \epsilon \frac{\partial^2 W}{\partial y^2} \tag{24}$$

as in Prandtl's second theory. ϵ is the eddy kinematic viscosity in terms of the transformed velocity components. Noting how Equation (24) is similar to Goertler's equation, a theoretical distribution for the curved jet velocity profile may be obtained by assuming that the W profile is symmetrical about the x axis. That is:

$$\frac{\partial W}{\partial y} = 0 \qquad @ \qquad y = 0, \quad v = 0 \tag{25}$$

and it is known that $W = 0$ at $y = \infty$ (26)

If now it is assumed that the virtual kinematic viscosity is given by

$$\epsilon = \alpha b U \tag{27}$$

where α is a constant, b jet width $\sim x$

U = velocity of the jet along the x axis.

If the centerline velocity and the width of the jet a fixed characteristic distance s from the orifice are denoted by U_s and b_s

$$\begin{aligned} U &= U_s (x/s)^{1/2} \\ b &= b_s \, x/s \\ \epsilon &= \epsilon \, (x/s)^{1/2} \\ \text{or} \quad \epsilon_s &= \alpha_1 \, b_s \, U_s \end{aligned} \tag{28}$$

Further, if the similarity parameter η is defined as $\eta = \sigma \, y/x$ where as per plane jet theory σ denotes a free parameter to be specified experimentally. Equation (24) may be reduced to an ordinary differential equation by assuming that the stream function ψ is

$$\begin{aligned} \psi &= \sigma^{-1} \, U_s \, s^{1/3} \, x^{1/3} \, F(\eta) \\ \text{and} \quad W &= U_s \, (x/s)^{-1/2} \, F'(\eta) \\ v &= \sigma^{-1} \, U_s \, s^{1/2} \, x^{-1/2} \, (\eta \, F' - 1/2 \, F) \end{aligned} \tag{29}$$

Thus Equation 24 becomes

$$1/2 \, F' + 1/2 \, FF'' + \frac{\epsilon_s}{U_s S} \, \sigma^2 \, F''' = 0 \tag{30}$$

subject to the boundary conditions

$$F = 0 , \quad F' = 1 \quad @ \quad \eta = 0$$

$$F' = 0 \quad @ \quad \eta = \infty$$

Since σ is a free constant it may be defined as

$$\sigma = 1/2 \quad \frac{U_s s}{\epsilon_s} \tag{31}$$

Double integration of (30) yields

$$F^2 + F' = 1 \tag{32}$$

whose solution is $F = \tanh \eta$

$$\therefore \quad W = U_s (x/s)^{-1/2} \ (1-\tanh^2\eta) \tag{33}$$

If J the momentum of the jet is

$$J = \rho \int_{-\infty}^{\infty} W^2 \, dy = \text{constant}$$

or $J/\rho = K$

Then $$W = \frac{1}{2}\sqrt{\frac{3K\sigma}{x}} \quad \{1-\tanh^2\eta\} \tag{34}$$

$$v = \frac{1}{4}\sqrt{\frac{3K}{\sigma x}} \quad \{2\eta(1-\tanh^2\eta) - \tanh\eta\} \tag{35}$$

$$\eta = \sigma y/x$$

Now $$u = \frac{(R+y)}{R} \ W \tag{36}$$

or a maximum of u occurs at

$$\frac{\partial u}{\partial y} = 0, \quad \frac{W}{R} + \frac{R+y}{R} \ \frac{\partial W}{\partial y} = 0 \tag{37}$$

Indicating that maximum value of u is not on the curved x-axis but is shifted in the positive y direction or the direction of the region with the smaller curvature where $\frac{\partial W}{\partial y}$ is negative.

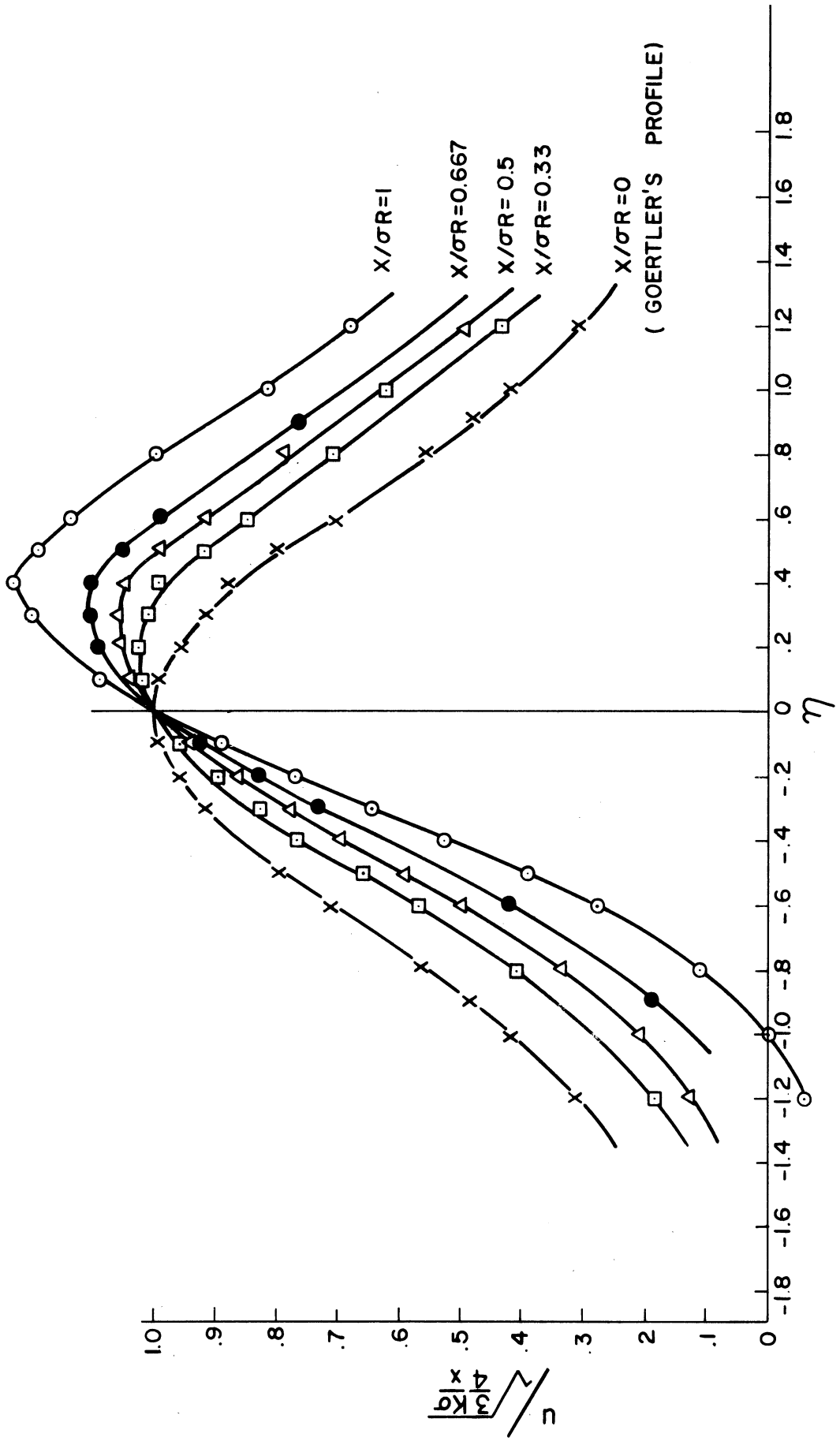

Figure 63. Dimensionless Velocity Profiles in the Curved Jet.

The velocity distribution

$$u\Big/\sqrt{\frac{3K\sigma}{4x}} = (1+y/R)\left\{1-\tanh^2\eta\right\}$$

$$\eta = \frac{(y/R)}{(x/\sigma R)}$$

is plotted in Figure 63. The figure shows both the shift towards positive y of the maximum value of u and also that the maximum velocity in the curved jet is higher than in the case of the corresponding straight jet. This increase in the maximum velocity, although only on the order of 3 to 5% for curved jets which could be experimentally devised, could, with some very careful hot wire studies, provide a verification for this theory. The difficulty of conducting such measurements should nevertheless be emphasized, as the magnitude of the increase in the maximum velocity is on the order or magnitude of the turbulent velocity fluctuations found in the central region of a fully developed turbulent jet.

APPENDIX B

SOLUTION FOR THE NORMAL PRESSURE DISTRIBUTION IN A CURVED FREE JET

If the axial pressure gradient is neglected, Equation (12) for the normal pressure may be integrated to obtain

$$\frac{dp}{dy} = \frac{R+y}{R^2}\,\rho W^2$$

or for fixed x station

$$p = \frac{-\rho}{R^2}\left(\frac{3K\sigma}{4x}\right)\int_y^\infty (R+z)\left(1-\tanh^2\frac{\sigma z}{x}\right)^2 dz$$

The negative sign results from the assumption of $p = 0$ at $+\infty$. It can be seen that the integrand is well behaved over the range of integration and should present few difficulties during evaluation.

APPENDIX C

AN ESTIMATE OF THE AXIAL PRESSURE GRADIENT IN THE CURVED FREE JET

From Equation (12) Appendix A it is seen

$$\frac{\partial p}{\partial y} = \rho W^2 \frac{(R+y)}{R^2}$$

$$\therefore \frac{\partial^2 p}{\partial y \partial x} = \frac{2\rho(R+y)}{R^2} W \frac{\partial W}{\partial x}$$

If it is assumed that W can be approximately represented as

$$W = W_{max}\, e^{-y^2/b^2}$$

where $W_{max} \sim C\sqrt{x}$, $b \sim Dx$ (C and D being constants)

$$\frac{\partial^2 p}{\partial x \partial y} \sim 2 \frac{\rho(R+y)}{R^2} W_{max}\, e^{-y^2/b^2} \left\{ \frac{\partial W_{max}}{\partial x}\, e^{-y^2/b^2} + 2 \frac{W_{max}}{b^3} y^2 \frac{db}{dx} \right\}$$

$$\therefore \frac{\partial p}{\partial x} \sim 2\rho \left[W_{max} \frac{\partial W_{max}}{\partial x} \int_{-\infty}^{\infty} \frac{R+y}{R^2}\, e^{-2y^2/b^2}\, dy + 2 \frac{W^2_{max}}{b^3} D \int_{-\infty}^{\infty} \frac{R+y}{R^2}\, y^2 \cdot e^{-y^2/b^2}\, dy \right]$$

$$\sim 0$$

Thus if both R is large and the flow field is not examined near the source (an assumption already incorporated in the similarity transformation) the pressure gradient is not too severe and may be neglected as is done in Appendix A.

APPENDIX D

A MODEL FOR THE MINIMUM PULSE TO SWITCH

The following is a rough analysis adopted from the model proposed by Johnston.[17] The basic assumption is that during the separation process, the main jet acts as a flexible boundary for the changing vortex bubble. Thus, if dv is the change in the vortex bubble volume and dt the elapsed time, conservation of mass may be expressed as

$$dv = (Q_c + Q_r - Q_e)\, dt \tag{1}$$

where

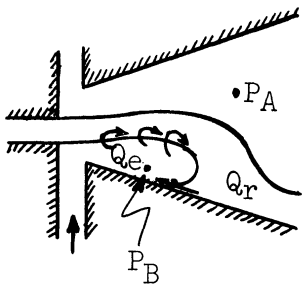

Q_c is the control flow rate

Q_r is the fluid returned to the separation bubble at the re-attachment point.

Q_e is the fluid entrained.

Thus $(Q_r - Q_e)$ is the net excess fluid returned to the separation bubble and is related to the volume in that Q_e is related to the length of the inner side of the main jet and Q_r is proportional to the angle of impingement and the pressure differential $(P_A - P_B)$. Hence, if $(Q_r - Q_e)$ is expressed as Q_n

$$dv = Q_c\, dt + Q_n\, dt \tag{2}$$

Integration of (2) yields

$$\Delta v = Q_c \tau_1 + \int_o^{\tau_1} Q_n \, dt \qquad (3)$$

If the remaining integral on the right hand side is replaced by an average value defined as follows,

$$Q_{n_{average}} = \tilde{Q}_n = \frac{1}{\tau_1} \int_o^{\tau_1} Q_n \, dt$$

(3) becomes

$$\Delta v = \tau_1 (Q_c + \tilde{Q}_n) \qquad (4)$$

If both sides are divided by $Q_s \cdot T$ where Q_s is the Main jet flow rate and T is the transport time calculated with respect to the control jet velocity. (4) becomes

$$\frac{Q_c}{Q_c} \frac{\Delta V}{Q_s \cdot T} = \frac{\tau_1}{T} \left(\frac{Q_c}{Q_s} + \frac{\tilde{Q}_n}{Q_s} \right) \qquad (5)$$

Writing μ_Q for Q_s/Q_c as the flow gain, τ_1^* for τ_1/T, ΔV^* for $\Delta V/Q_c T$ and $\tilde{Q}_n^*$ for $\tilde{Q}_n/Q_s$, (5) becomes

$$\tau_1^* = \Delta V^* / (1 + \tilde{Q}_n^* \mu_Q)$$

Following the procedure of Johnston (17) it may be assumed that ΔV^* and $\tilde{Q}_n^*$ are constants to be determined experimentally. Thus, if τ_1^* and μ_Q are known for two separate readings denoted by the added subscripts

$$Q_n = \frac{\tau_{12}^* - \tau_{11}^*}{\tau_{11}^* \mu_{Q_1} - \tau_{12}^* \mu_{Q_2}}$$

$$\Delta V^* = (1 + \tilde{Q}_n^* \mu_Q) \tau_1^*$$

and

$$\mu_{Q_{max}} = \tilde{Q}_n^{*\,-1} \, .$$

This model would at least be useful over a limited range. The difference between this model and Johnston's is in the inclusion of the term Q_r but the difference is a minor one as a comparison with Johnston's thesis would show, hence little originality can be claimed for this model.

APPENDIX E

SUMMARY OF EXPERIMENTAL DATA

The tables below include a summary of all experimental data used in this study. Besides the shorthand notation defined in Figure 14 following additional notation is used in this section.

Run:	The first number designates the data set and the second number the reading number.
t/b_s:	Aspect ratio of the main nozzle (ratio of nozzle depth to width)
x:	The dimension being varied in that set of data
R:	Equivalent Reynolds number based on viscosity of water at 65°F
Q_s:	Main jet flow rate - gpm
Q_c:	Control jet flow rate - gpm
θ:	Angular separation of the receiver ports; for all the data presented θ is held constant at 30°.
FP:	List of parameters held fixed
VP:	List of variable parameters
T/b_s:	Distance to the thermistor from the control nozzle

The units of the switching time are seconds

1. Effect of Decreasing b_c/b_s .

FP: b_s = 1 in. t/b_s = 3 D/b_s = 4

l_b/b_s = 4 l_w/b_s = 7.6 l_s/b_s = ∞

T/b_s = 16

VP: Q_s=7.4 gpm R=6000 $x=b_c/b_s$

RUN	X	Q_c/Q_s	τ_l	τ_a	τ_b
1-1	1	1.000	1.60	22.0	15.0
1-2	1	0.838	1.80	26.0	16.0
1-3	1	0.725	1.83	26.0	16.0
1-4	1	0.663	2.20	28.0	18.0
1-5	1	0.563	2.80	30.0	19.0
1-6	1	0.537	3.50	31.0	21.0
1-7	1	0.500	4.50	33.0	22.0
1-8	1	0.462	7.00	37.0	24.0
2-1	0.75	1.000	1.30	25.2	11.5
2-2	0.75	0.833	1.75	26.0	13.0
2-3	0.75	0.667	2.50	23.0	14.7
2-4	0.75	0.583	3.10	25.8	17.0
2-5	0.75	0.500	5.00	26.0	22.0
2-6	0.75	0.450	5.40	28.0	22.0
2-7	0.75	0.417	8.00		28.0
2-8	0.75	0.367	17.00		30.0
3-1	0.50	1.000	1.00	17.0	11.0
3-2	0.50	0.833	1.30	17.0	12.0
3-3	0.50	0.750	1.75	20.0	14.0
3-4	0.50	0.670	2.60	21.0	14.0

Run	X	Q_c/Q_s	τ_1	τ_a	τ_b
3-5	0.50	0.583	2.80	23.0	15.0
3-6	0.50	0.500	3.20	26.0	17.0
3-7	0.50	0.417	5.00	31.0	20.0
3-8	0.50	0.367	7.20		24.0
3-9	0.50	0.333	15.00		30.0
3-10	0.50	0.300	23.0		
4-1	-.25	1.000	0.70	14.0	8.0
4-2	0.25	0.833	0.80	18.0	9.0
4-3	0.25	0.750	1.10	16.0	11.0
4-4	0.25	0.667	1.40	18.0	12.0
4-5	0.25	0.583	1.65	19.0	12.0
4-6	0.25	0.500	2.05	18.0	14.0
4-7	0.25	0.416	2.80	21.0	18.0
4-8	0.25	0.333	5.10	30.0	27.0
4-9	0.25	0.250	10.00		38.0
4-10	0.25	0.367	4.30	23.0	25.0
4-11	0.25	0.283	8.50		34.0
4-12	0.25	0.217	25.0		40.0
VP	Q_s=6.3 gpm		R=5000		$x=b_c/b_s$
5-1	1	1.000	1.98	31.0	17.0
5-2	1	0.790	2.30	33.0	19.0
5-3	1	0.700	2.80	34.0	20.0
5-4	1	0.600	3.30	39.0	23.0
5-5	1	0.560	3.70	38.0	22.0

Run	X	Q_C/Q_S	τ_1	τ_a	τ_b
5-6	1	0.500	6.50	40.0	26.0
5-7	1	0.450	11.00	40.0	34.0
6-1	0.75	1.000	1.50		
6-2	0.75	0.800	2.25		
6-3	0.75	0.600	3.00		
6-4	0.75	0.500	4.80		
6-5	0.75	0.440	7.00		
6-6	0.75	0.400	9.00		
6-7	0.75	0.360	18.00		
7-1	0.50	1.000	1.00		
7-2	0.50	0.800	1.70		
7-3	0.50	0.600	3.20		
7-4	0.50	0.500	4.80		
7-5	0.50	0.400	7.70		
7-6	0.50	0.360	14.00		
7-7	0.50	0.320	30.00		
8-1	0.25	1.000	0.60		9.0
8-2	0.25	0.800			11.0
8-3	0.25	0.700			12.0
8-4	0.25	0.600	1.40		12.5
8-5	0.25	0.500			14.5
8-6	0.25	0.400	3.20		21.0
8-7	0.25	0.300			41.0

VP	Q_s=3.7 gpm		R=3000		X=b_c/b_s
9-1	1	1.000	3.00	53.0	29.0
9-2	1	0.838	3.60	63.0	30.0
RUN	X	Q_c/Q_s	τ_1	τ_a	τ_b
9-3	1	0.675	5.50	60.0	31.0
9-4	1	0.675	5.50	60.0	31.0
9-5	1	0.600	6.30	60.0	34.0
9-6	1	0.500	15.50		40.0
9-7	1	0.437	33.0		53.0
10-1	0.75	1.000	2.00	29.0	17.0
10-2	0.75	0.750	2.80	33.0	19.0
10-3	0.75	0.450	7.50	40.0	34.0
10-4	0.75	0.375	20.0		42.0
11-1	0.50	1.000	1.15	30.0	13.0
11-2	0.50	0.876	1.30	33.0	17.0
11-3	0.50	0.700	2.00	33.0	19.0
11-4	0.50	0.625	3.70	32.0	23.0
11-5	0.50	0.550	4.65	46.0	23.0
11-6	0.50	0.500	5.90	43.0	26.0
11-7	0.50	0.425	8.90	44.0	32.0
11-8	0.50	0.375			
11-9	0.50	0.325			48.0
12-1	0.25	1.000	0.85	27.0	10.0
12-2	0.25	0.875	0.90	24.0	11.0

Run	X	Q_C/Q_S	τ_l	τ_a	τ_b
12-3	0.25	0.750	1.23	24.0	12.5
12-4	0.25	0.625	1.80	25.0	14.0
12-5	0.25	0.500	2.70	31.0	19.0
12-6	0.25	0.375	7.00	39.0	29.0
12-7	0.25	0.325	10.00	42.0	39.0
12-8	0.25	0.275	13.00	42.0	42.0

2. Effect of Changing Scales

FP	b_s=3/4 in.		t/b_s=4	D/b_s=4
	l_b/b_s = 4		l_w/b_s=7.6	l_s/b_s=∞
	b_c/b_s = 1		T/b_s= 16	
VP	Q_S=7.4 gpm		R=6000	
13-1		1.000	1.05	13.3	8.0
13-2		0.838	1.10	21.0	9.5
13-3		0.663	2.10	14.0	10.0
13-4		0.563	2.50	16.0	12.5
13-5		0.537	3.60	20.0	13.0
13-6		0.500	3.60	20.0	13.0
13-7		0.462	5.0	23.0	15.0
VP	Q_S=5.1 gpm		R=4000		
14-1		1.000	1.50	24.0	12.0
14-2		0.883	1.70	24.0	11.0
14-3		0.750	1.75	25.0	12.0
14-4		0.625	2.65	19.0	15.0
14-5		0.563	4.30	28.0	16.0

Run	X	Q_C/Q_S	τ_l	τ_a	τ_b
14-6		0.507	6.10	28.0	19.0
14-7		0.450	9.00	31.0	24.0
FP	b_s = 1/2 in.		t/b_s = 6		D/b_s = 4
	l_b/b_s = 4		l_w/b_s = 7.6		l_s/b_s =43
	b_c/b_s = 1		T/b_s = 16		
VP	Q_S=7.4 gpm		R=6000		
Run	X	Q_C/Q_S	τ_l	τ_a	τ_b
15-1		1.000	0.55	8.0	5.5
15-2		0.838	0.65	8.5	6.0
15-3		0.663	1.05	10.0	6.5
15-4		0.563	1.35	11.0	7.0
15-5		0.537	1.10	12.0	
15-6		0.500	1.60	12.0	8.0
15-7		0.457	2.00	15.0	9.0
15-8		0.500	3.5		9.0
15-9		0.457	4.75		10.0
15-10		0.333	27.00		40.0
VP	Q_S=5.1 gpm		R=4000		
16-1		1.000	0.75	9.0	6.0
16-2		0.700	0.95	11.0	6.5
16-3		0.625	1.20	12.0	7.5
16-4		0.500	2.35	13.0	10.0
16-5		0.450	4.60	17.0	12.0
16-6		0.400	7.30	18.0	16.0

VP	Q_S=6.3 gpm		R=5000		
Run	X	Q_C/Q_S	τ_1	τ_a	τ_b
17-1		1.000	0.60	7.5	5.0
17-2		0.700	1.00	9.0	7.0
17-3		0.600	1.45	13.0	8.0
17-4		0.500	2.00	11.0	8.0
17-5		0.440	2.40	13.0	11.0
17-6		0.400	6.00	15.0	14.0
17-7		0.360	12.00	21.0	22.0

3. Effect of Moving the Splitter Upstream

FP	b_s = 1/2 in.	t/b_s = 6	D/b_s = 4
	l_b/b_s = 4	l_w/b_s = 7.6	b_c/b_s = 1
		T/b_s = 16	

VP	Q_S=7.4 gpm		R=6000		$x=l_s/b_s$
18-1	34	1.000	0.52	8.0	5.0
18-2	34	0.838	0.50	10.0	6.0
18-3	34	0.663	0.90	10.0	7.0
18-4	34	0.563	1.20	9.7	8.0
18-5	34	0.500	1.60	13.5	8.0
18-6	34	0.457	2.00	12.0	9.0
19-1	28	1.000	0.51	10.0	8.0
19-2	28	0.838	0.62	10.5	9.0
19-3	28	0.663	1.00	12.0	10.0

Run	X	Q_C/Q_S	τ_1	τ_a	τ_b
19-4	28	0.563	0.75	13.0	10.5
19-5	28	0.500	0.90	13.0	10.0
19-6	28	0.457	1.85	16.0	12.5
19-7	28	0.367	4.30	17.0	14.0
19-8	28	0.333	8.10	18.5	18.0
20-1	22	1.000	0.50	18.0	10.5
20-2	22	0.838	0.60	16.0	13.0
20-3	22	0.663	0.92	17.5	13.0
20-4	22	0.500	1.80	19.0	14.5
20-5	22	0.367	4.70	21.0	18.5
20-6	22	0.416	3.90	21.0	18.0
20-7	22	0.563	1.35	17.5	15.0
20-8	22	0.333	5.10	22.0	18.0
21-1	16	1.000	0.62	13.0	11.0
21-2	16	0.838	0.72	14.0	11.0
21-3	16	0.663	1.43	16.0	12.0
21-4	16	0.563	1.55	17.0	13.0
21-5	16	0.500	3.10	18.0	13.5
21-6	16	0.416	6.60	25.0	17.5
21-7	16	0.367	8.40	27.0	20.0
22-1	13	1.000	1.65	33.0	11.0
22-2	13	0.838	2.20	33.0	12.0
22-3	13	0.663	3.70	33.0	13.0
22-4	13	0.500	5.80		

Run	X	Q_C/Q_S	τ_l	τ_a	τ_b
22-5	13	0.416	8.50	40.0	21.0
22-6	13	0.367	10.50		
22-7	13	0.333	11.00	39.0	23.0
22-8	13	0.302	12.50	40.0	25.0
22-9	13	0.281	14.00	44	27.0
22-10	13	0.265	16.50		29.0
23-1	10	1.000	2.85	30.0	12.0
23-2	10	0.838	3.40	31.5	13.5
23-3	10	0.663	4.60	33.0	14.0
23-4	10	0.500	6.30	35.0	17.0
23-5	10	0.416	7.60	36.5	21.0
23-6	10	0.267	9.50	35.0	22.0
23-7	10	0.333	11.20	26.0	24.0
23-8	10	0.302	12.00		25.0
23-9	10	0.281	17.00		31.0
23-10	10	0.265	18.00		32.0
VP	Q_S=5.1 gpm		R=4000		$X=l_s/b_s$
24-1	34	1.000	0.60	10.0	7.0
24-2	34	0.700	1.10	12.0	9.0
24-3	34	0.625	1.20	12.0	8.0
24-4	34	0.500	2.05	14.0	10.0
24-5	34	0.450	3.60	15.0	12.0
24-6	34	0.400	4.10	16.0	13.0
25-1	28	1.000	0.70	12.0	9.0

Run	X	Q_C/Q_S	τ_1	τ_a	τ_b
25-2	28	0.874	1.00	14.0	10.0
25-3	28	0.75	1.05	13.0	11.0
25-4	28	0.625	1.10	15.0	13.0
25-5	28	0.550	1.20	17.0	13.0
25-6	28	0.500	1.35	18.0	15.0
25-7	28	0.450	2.35	19.0	16.0
25-8	28	0.400	3.90	21.0	17.0
25-9	28	1.000	0.70	12.5	9.0
25-10	28	0.289	4.60	17.0	24.0
26-1	22	1.000	0.63	20.0	15.0
26-2	22	0.874	0.75	21.0	17.0
26-3	22	0.700	0.85	21.0	17.0
26-4	22	0.625	1.10	23.5	18.0
26-5	22	0.547	1.50	24.5	19.0
26-6	22	0.500	1.90	26.5	20.0
26-7	22	0.450	2.55	27.5	21.0
26-8	22	0.407	4.40	27.0	24.0
27-1	16	1.000	0.92	17.0	13.0
27-2	16	0.874	1.03	18.0	12.5
27.3	16	0.700	1.25	19.0	13.5
27-4	16	0.625	1.70	22.0	15.0
27-5	16	0.547	2.75	23.0	16.5
27-6	16	0.500	4.55	36.0	20.0
27-7	16	0.450	9.00	52.0	22.0
28-1	13	1.000	2.20	51.0	17.0

Run	X	Q_C/Q_S	τ_l	τ_a	τ_b
28-2	13	0.874	3.00	49.0	16.0
28-3	13	0.700	3.20	53.0	16.5
28-4	13	0.625	4.30	51.0	17.5
28-5	13	0.547	7.50	55.0	20.0
28-6	13	0.500	8.50	64.0	23.0
29-1	10	1.000	3.90	39.0	15.0
29-2	10	0.874	4.40	48.0	17.0
29-3	10	0.700	5.00	45.0	18.0
29-4	10	0.625	6.30	52.0	20.0
29-5	10	0.547	7.60	52.0	22.0
29-6	10	0.500	8.30	53.0	25.0
29-7	10	0.450	9.80	53.0	26.0
29-8	10	0.420	10.90		29.0
29-9	10	0.360	13.00		29.0

4. Effect of Reducing the Setback

FP	b_s = 1/2 in.	t/b_s = 6	D/b_s = 4
	l_b/b_s = 0	l_w/b_s = 3.4	l_s/b_s = 25
	b_c/b_s = 1	T/b_s = 12	

VP	Q_S=7.4 gpm		R=6000		
30-1		1.000	0.45	9.0	7.0
30-2		0.838	0.53	12.0	7.5
30-3		0.663	1.10	12.0	8.5
30-4		0.500	1.35	12.0	9.5
30-5		0.416	2.00	12.5	11.0

Run	X	Q_C/Q_S	τ_1	τ_a	τ_b
30-6		0.367	5.40		15.0
30-7		0.333	8.00		18.0
VP	Q_S=5.1 gpm		R=4000		
31-1		1.000	0.60	18.0	9.0
31-2		0.625	1.40	17.5	11.0
31-3		0.500	2.00	23.0	13.0
31-4		0.420	3.50	18.0	17.0

5. Effect of Decreasing the Offset

In this data set $(Q_C/Q_S)_{min}$ is the lowest ratio of the control to power flow rate for which switching is possible. The following parameters are fixed through the remainder of the study.

b_s = 1/2 in. $\quad t/b_s = 6 \quad l_b/b_s = 0$

$l_w/b_s = 3.4 \quad l_s/b_s = 25$

$T/b_s = 12$

VP	Q = 7.5 gpm		R=6000			x = D/b_s
Run	X	Q_C/Q_S	$(Q_C/Q_S)_{min}$	τ_1	τ_a	τ_b
32-1	3.5	1.000		0.32	10.0	8.5
32-2	3.5	0.500		0.90	13.0	9.0
32-3	3.5		0.320			
32-4	3.0	1.000		0.38	9.5	7.5
32-5	3.0	0.500		0.90	12.0	9.0
32-6	3.0		0.281			
32-7	2.5	1.000		0.26	9.0	6.5

Run	X	Q_C/Q_S	$(Q_C/Q_S)_{min}$	τ_1	τ_a	τ_b
32-8	2.5	0.500		0.40	11.0	8.0
32-9	2.5		0.263			
32-10	2.0	1.000		0.28	9.0	6.5
32-11	2.0	0.500		0.55	10.0	8.0
32-12	2.0		0.239			
32-13	1.5	1.000		0.29		6.5
32-14	1.5	0.500		0.40		6.5
VP	Q_S=6.3 gpm		R=5000			
33-1	1.5	1.000		0.26	9.5	7.5
33-2	1.5	0.500		0.26	9.5	8.0
VP	Q_S=5.1 gpm		R=4000			
34-1	3.5	1.000		0.65		
34-2	3.5	0.500		1.70		
34-3	3.0	1.000		0.50	11.5	8.0
34-4	3.0	0.500		1.30	14.0	10.0
34-5	3.0		0.309			
34-6	2.5	1.000		0.44	11.0	8.5
34-7	2.5	0.500		0.72	14.0	10.5
34-8	2.5		0.295			
34-9	2.0	1.000		0.40	11.0	8.0
34-10	2.0	0.500		0.65	12.0	9.0
34-11	2.0		0.239			
34-12	1.5	1.000		0.29	11.5	8.0
34-13	1.5	0.500		0.43	12.0	9.0
34-14	1.5		0.157			

REFERENCES

1. Schlichting, H., Boundary Layer Theory, Fourth Edition, McGraw Hill, 1960.

2. Birkhoff, G. and E. H. Zarantonello, Jets, Wakes and Cavities, Academic Press, New York, 1957.

3. Lachmann, G. V., (Ed.), Boundary Layer and Flow Control, Vol. 1, Pergamon Press, New York, 1961.

4. Rouse, H. (Ed.) Advanced Mechanics of Fluids, J. Wiley and Sons, Inc., New York, 1959.

5. Abramovich, G. N., The Theory of Turbulent Jets, M.I.T. Press, 1963.

6. Rouse, H., "On the Role of Eddies in Fluid Motion", American Scientist, Vol. 51, September 1963, pp. 285.

7. Bourque, C. and B. G. Newman, "Reattachment of a Two-Dimensional, Incompressible Jet to an Adjacent Flat Plate", The Aeronautical Quarterly, Vol. XI, August 1960.

8. Muller, H. R., "A Study of the Dynamic Features of a Wall-Reattachment Fluid Amplifier", ASME Publication, Paper No. 64-FE-10.

9. Sawyer, R. A., "Two Dimensional Reattaching Jet Flows Including the Effects of Curvature on Entrainment," Journal of Fluid Mechanics, Vol. 17, Part 4, December 1963.

10. Moynihan, F. A. and R. J. Reilly, "Deflection and Relative Flow of Three Interacting Jets," Proceedings of the Fluid Amplification Symposium, Vol. 1, May 1964.

11. Keto, J. R., "Transient Behavior of Bistable Fluid Elements", Proceedings of the Fluid Amplification Symposium, Vol. III, May 1964.

12. Olson, R. E. and R. C. Stoeffler, "A Study of Factors Affect the Time Response of Bistable Fluid Amplifiers," United Aircraft Research Laboratories Report.

13. Levin, S. G. and F. M. Manion, "Jet Attachment Distance as a Function of Adjacent Wall Offset and Angle." HDL TR-1087, December 31, 1962.

14. Brown, F. T., "A Combined Analytical and Experimental Approach to the Development of Fluid Jet Amplifiers," ASME Paper No. 62-WA-154.

15. Comparin, R. A., et al, "On the Limitations and Special Effects in Fluid Jet Amplifiers," ASME Symposium on Fluid Jet Control Devices, November 1962.

16. Warren, R. W., "Some Parameters Affecting the Design of Bistable Fluid Amplifier," ASME Symposium on Fluid Jet Control Devices, November 1962.

17. Johnston, R. P., "Dynamic Studies of Turbulent Reattachment Fluid Amplifiers" MS Thesis, University of Pittsburgh, 1963.

18. Katz, S., et al, "The Response of a Bistable Fluid Amplifier to a Step Input," Proceedings of the Fluid Amplification Symposium, Vol. I, pp. 321, May 1964.

19. Muller, H. R., "Wall Reattachment Device with Pulsed Control Flow", Proceedings of the Fluid Amplification Symposium, Vol. I, pp. 179, May 1964.

20. Glaettli, H. H., et al, "Remarks on the Limitation of Pure Fluid Elements", Proceedings of the Fluid Amplification Symposium, Vol. I, May 1964.

21. Hrubecky, H. F. and L. N. Pearce, "The Effects of Geometric Changes Upon the Switching Point in a Model Bi-stable Fluid Amplifier," Proceedings of the Fluid Amplification Symposium, Vol. I, May 1964.

22. Sher, N. C., "Jet Attachment and Switching in Bistable Fluid Amplifiers", Paper No. 64-FE-19, ASME Publication.

23. Lane, R. S., "A Thermistor Velocity-Meter for Low Velocity Flows," Unpublished paper, was presented in partial fulfillment of ME 600, December 1965, Department of Mechanical Engineering, The University of Michigan.

24. DISA Information, "Electronic Measurements of Mechanical Events, No. 1, January 1965.

25. Brown, F. T., "On the Future of Dynamic Analysis of Fluid Systems," Proceedings of the Fluid Amplification Symposium, Vol. I, October 1965.

26. Korst, H. H., R. H. Page and M. E. Childs, "A Theory for Base Pressures in Transonic and Supersonic Flow". University of Illinois, ME-TN-392-2, March 1955.

27. Albertson, M. L., Y. B. Dai, R. A. Jensen, Junter Rouse, "Diffusion of Submerged Jets," Proceedings American Society of Civil Engineers, 74, 1751 (1948).

28. Gurski, R. J., "Static and Dynamic Modeling of a Pressure Controlled Subsonic Fluid Modulator," Thesis (ScD) Dept. of Mech. Engr., M.I.T., May 1965.

29. Warren, R. W. and S. J. Peperone, "Fluid Amplification, Basic Principles," DOFL Report No. TR-1039.

30. Fluid Amplifier State of the Art, Vol. 1, Research and Development-ment-Fluid Amplifiers and Logic, NASA Contractor Report, NASA CR-101.

31. Sarpkaya, T., "Steady and Transient Behavior of a Bistable Amplifier a Latching Vortex," Proceedings of the Fluid Amplification Symposium, Vol. II, October 1965.

32. Harvey, D. W., "Transient Theory of Switching in a Bistable Valve," Proceedings of the Fluid Amplification Symposium, Vol. IV, October 1965.

33. Symposium on Measurement in Unsteady Flow, ASME Hydracelic Division Conference, May 1962.

34. Allen, M. and A. J. Yerman, "Visualizing Three Dimensional Flow," Instruments and Control Systems, March 1966.

35. Pope, A., Wind Tunnel Testing, John Wiley and Sons, Inc. New York, 2nd Ed., 1954, page 110.

36. Booth, W. A., A. C. Fluidic Systems, Lecture Notes presented at M.I.T. Fluid Control Summer Seminar, July 1966.

37. Kirshner, J. M. Fluirics, Where Do We Go From Here, Lecture presented at M.I.T. Fluid Controls Summer Session July 1966.

38. Belsterling, C. A., "Development of Techniques for the Static and Dynamic Analysis of Fluid State Components and Systems," USAAVLABS TR.66-16, Giannini Controls Corp., February, 1966.

39. Greber, Issac, "Bubble Pressures Under Reattaching Laminar Jets and Boundary Layers", Fluid Jet Control Devices, ASME Publication, November, 1962.

40. Gartshore, I. S., "The Streamwise Development of Certain Two Dimensional Turbulent Shear Flows", Report 65-3, ME Research Labs. McGill University.

41. Lee, S. Y. and H. H. Richardson, "Basic Applied Research in Fluid Power Control", Technical Report AFFDL-TR-65-229.

42. Mueller, T. J., H. H. Korst and W. L. Chow, "On the Separation Reattachment and Redevelopment of Incompressible Turbulent Shear Flow," ASME Paper No. 63-AHGT-5.

43. Norwood, R. E., "A Performance Criterion for Fluid Jet Amplifiers," Fluid Jet Control Devices, ASME Publication November, 1962.

44. Yih, O. T. and H. Cohen, "A Theoretical Model for Separation in the Fluid Jet Amplifier," IBM Journal, October 1963.